Localization and transport of ribosomes in axons of the mammalian PNS and CNS

Dissertation

zur Erlangung des Grades

„Doktor der Naturwissenschaften“

am Fachbereich Biologie

der Johannes Gutenberg-Universität in Mainz

Kerstin Müller

geb. am 06. April 1986 in Würzburg

Mainz, 2016

The present PhD thesis was conducted at the Institute of Microanatomy and Neurobiology, University Medical Center of the Johannes-Gutenberg University Mainz, from May 1st, 2011 until June 30th, 2016.

Dekan:
1. Berichterstatter:
2. Berichterstatter:

Tag der mündlichen Prüfung: 24.10.2016

Declaration

“I hereby declare that I wrote the dissertation submitted without any unauthorized external assistance and used only sources acknowledged in the work. All textual passages which are appropriated verbatim or para-phrased from published and unpublished texts as well as all information obtained from oral sources are duly indicated and listed in accordance with bibliographical rules. Moreover, I declare that this is a true copy of my thesis, and that this thesis has not been submitted for a higher degree to any other University or Institution. In carrying out this research, I complied with the rules of standard scientific practice as formulated in the statutes of Johannes Gutenberg-University Mainz to insure standard scientific practice.”

Mainz, 05.07.2016

(Kerstin Müller)

Abstract

In recent years, many studies have indicated that some neuronal cell types produce proteins not only in the cell body, but also locally in dendrites, especially at synaptic sites, and in the axon. Local axonal translation seems to be important for the maintenance and growth of the axon, for retrograde signaling, and for the regeneration of peripheral nervous system (PNS) axons after injury. It was shown that messenger RNAs (mRNAs) are transported in ribonucleoprotein particles (RNPs) and there is increasing evidence that their axonal localization is selective for specific mRNAs. Additionally, the presence of ribosomes in the axonal compartment has been reported and many studies assumed that they are likewise transported in RNPs from the neuronal cell body. Recently, however, glial cells were proposed as an alternative source of axonal ribosomes. Such a glia-to-axon transfer is believed to account for the increased ribosomal levels observed in PNS axons after injury and to support local protein synthesis for regeneration.

The aim of the present study was to show that axonally localized ribosomes originate from the neuronal cell body *in vivo*, also upon injury. To visualize ribosomes, the ribosomal protein L4 (RPL4), a component of the large 60S subunit of the ribosomal complex, was labeled in a transgenic mouse line. 'RiboTracker' mice contained the fusion construct of RPL4 tagged with tandem dimer protein Tomato (tdTomato) downstream of a floxed stop cassette in the *ROSA26* locus. Crossbreeding with mice expressing Cre recombinase under the calcium/calmodulin-dependent protein kinase II alpha (CamKIIα) or Advillin promoter led to the neuron-specific expression of L4-tdTomato as shown for central nervous system (CNS) hippocampal and cortical neurons (CamKIIα), as well as dorsal root ganglia (DRG) neurons (CamKIIα, Advillin). However, when focusing on axons, L4-tdTomato was neither detected *in vitro* nor *in vivo*, even though the staining with an antibody against the ribosomal protein L26 (RPL26) confirmed the presence of axonal ribosomes. In the case of PNS injury, increased axonal levels of RPL26-stained ribosomes were observed, but again, L4-tdTomato signals were not found in the sciatic nerve fibers. These findings led to the conclusion that ribosomes are not transported from the neuronal cell body to the axon. Paralleling experiments with recombinant adeno-associated virus (rAAV) that express RPL4 fused to enhanced green fluorescence protein (eGFP) in a neuron-specific way supported the *in vitro* data from neuronal RiboTracker-Cre mice. Based on the prior *in vivo* results, however, studies with rAAVs were not continued.

Next, glial cells were reconsidered as an alternative source of axonal ribosomes. To investigate this hypothesis, RiboTracker mice were crossed with a glial Cre line driven by the 2',3'-cyclic-nucleotide 3'-phosphodiesterase (CNP) promoter. Satellite glia cells and Schwann cells in the PNS showed strong expression of the transgene, but some DRG neurons also contained L4-tdTomato. These neuronal subpopulations were similar to those in the neuron-

specific RiboTracker-Cre mice, therefore, axonal ribosomes were unlikely to originate from the neuronal cell body. In the sciatic nerve, occasional L4-tdTomato signals were detected in uninjured axons of the RiboTracker-CNP-Cre mice. Upon injury, a massive increase of axonally localized tagged ribosomes was observed, paralleling the findings of immunostaining with the anti-RPL26 antibody. Since increased axonal levels of L4-tdTomato were also observed distally to the lesion site, glial cells represent the only possible source of axonal ribosomes. This is the first study investigating the origin of axonal ribosomes in transgenic mice *in vivo*.

Taken together, the results from the present work strongly support the hypothesis of a glia-to-axon transfer of ribosomes, and go even beyond this by providing evidence for Schwann cells being the exclusive source of axonal ribosomes in the peripheral nervous system.

Zusammenfassung

In den letzten Jahren haben viele Studien gezeigt, dass einige neuronale Zelltypen Proteine nicht nur in ihrem Zellkörper, sondern auch lokal in Dendriten, vor allem an Synapsen, und im Axon produzieren. Lokale Proteintranslation scheint für die Versorgung und das Wachstum des Axons, für retrograde Signalübertragung und für die Regeneration der Axone des peripheren Nervensystems (PNS) nach Verletzung wichtig zu sein. Es ist gezeigt worden, dass messenger RNAs (mRNAs) in Ribonukleoprotein-Partikeln (RNPs) transportiert werden und es gibt immer mehr Hinweise darauf, dass deren axonale Lokalisation für spezifische mRNAs selektiv ist. Zusätzlich ist berichtet worden, dass Ribosomen im axonalen Kompartiment vorhanden sind, und es wird angenommen, dass sie ebenfalls in RNPs vom neuronalen Zellkörper ausgehend transportiert werden. Kürzlich jedoch wurden Gliazellen als alternativer Ursprung axonaler Ribosomen vorgeschlagen. Man vermutet, dass dieser Glia- Axon Transfer für die erhöhten Ribosomenmengen, die in Axonen des PNS nach Verletzung beobachtet wurden, verantwortlich ist und dass er die lokale Proteinsynthese zur Regeneration unterstützt.

Ziel dieser Studie war es zu zeigen, dass axonal vorkommende Ribosomen dem neuronalen Zellkörper *in vivo* entstammen, auch nach einer Verletzung. Um Ribosomen zu visualisieren wurde das ribosomale Protein L4 (RPL4), eine Komponente der großen 60S Untereinheit des ribosomalen Komplexes, in einer transgenen Mauslinie markiert. „RiboTracker“ Mäuse beinhalten das Fusionskonstrukt, bestehend aus dem mit dem Tandemdimer-Protein Tomato (tdTomato) markierten RPL4, hinter einer gefloxten Stopkassette im *ROSA26*Lokus. Kreuzung mit Mäusen, die die Cre-Rekombinase unter dem Promoter der Kalzium/Kalmodulin-abhängigen Kinase II alpha (CamKIIα) oder dem Advillin-Promoter exprimieren, führte zu einer neuronspezifischen Expression des L4-tdTomato, wie für hippokampale und kortikale Neurone des zentralen Nervensystems (CamKIIα) und für Neurone der dorsalen Wurzelganglien (engl. dorsal root ganglia, DRG; CamKIIα, Advillin) gezeigt wurde. Als jedoch die Axone näher betrachtet wurden, konnte L4-tdTomato weder *in vitro* noch *in vivo* detektiert werden, obwohl die Färbung mit dem Antikörper gegen das ribosomale Protein L26 (RPL26) das Vorhandensein axonaler Ribosomen bestätigt hatte. Bei einer Verletzung des PNS wurden erhöhte, axonale Mengen RPL26-gefärbter Ribosomen beobachten, jedoch wurden auch hier keine Signale des L4-tdTomatos in den Fasern des Ischiasnervs gefunden. Diese Ergebnisse führten zu der Schlussfolgerung, dass Ribosomen nicht vom neuronalen Zellkörper zum Axon transportiert werden. Parallelexperimente mit einem rekombinanten Adeno-assoziierten Virus (rAAV), welcher RPL4, das mit dem verstärkt grün fluoreszierendem Protein (engl. enhanced green fluorescent protein, eGFP) fusioniert ist, neuron-spezifisch exprimiert, unterstützen die *in vitro*-Daten der neuronalen RiboTracker-

Cre-Mäuse. Basierend auf den vorausgehenden *in vivo*-Ergebnissen, wurden die Studien mit rAAVs jedoch nicht weiterverfolgt.

Als nächstes wurden die Gliazellen als alternativer Ursprung axonaler Ribosomen erneut in Betracht gezogen. Um dieser Hypothese nachzugehen, wurden RiboTracker-Mäuse mit der glialen Cre-Linie, die den Promoter der 2‘,3’-zyklisches Nukleotid 3‘-Phosphodiesterase (CNP) besitzt, verpaart. Mantelzellen und Schwannzellen des PNS zeigten eine starke Expression des Transgens, aber auch einige DRG-Neurone beinhalteten L4-tdTomato. Diese neuronalen Subpopulationen waren vergleichbar mit denen der neuronspezifischen RiboTracker-Cre-Mäuse. Daher ist es sehr unwahrscheinlich, dass axonale Ribosomen dem neuronalen Zellkörper entstammen. Im Ischiasnerv wurden vereinzelte L4-tdTomato Signale in unverletzten Axonen der RiboTracker-CNP-Cre-Mäuse entdeckt. Nach Verletzung wurde ein massiver Anstieg axonal-lokalisierter, markierter Ribosomen beobachtet, was den Ergebnissen der Immunfärbung mit dem anti-RPL26 Antikörper entsprach. Da erhöhte axonale Menge an L4-tdTomato auch distal zur Läsionsseite bemerkt wurden, kommen Gliazellen als einziger möglicher Ursprung dieser axonalen Ribosomen in Frage. Diese Studie ist die erste, die die Herkunft axonaler Ribosomen in transgenen Mäusen *in vivo* untersucht.

Zusammenfassend bestätigen die Ergebnisse dieser Arbeit die Hypothese des Ribosomentransfers von der Glia zum Axon und gehen sogar darüber hinaus, in dem sie Hinweise dafür liefern, dass Schwannzellen der alleinige Ursprung axonaler Ribosomen im peripheren Nervensystem sind.

Table of contents

Figures

Tables

Abbreviations

°C	degree Celsius
µ	micro
µFD	micro Faraday
µg	microgram
µl	microliter
µm	micrometer
AAV	adeno-associated virus
ALS	amyotrophic lateral sclerosis
AmpR	ampicillin resistance
APS	ammonium peroxydisulphate
ATP	adenosine triphosphate
BAC	bacterial artificial chromosome
BC	boundary cap
BDNF	brain-derived neurotrophic factor
bGHpA	bovine growth hormone polyadenylation signal
bHLH	basic helix-loop-helix
bp	base pair
BrU	bromouridine
BSA	bovine serum albumin
CA1	cornu ammonis 1
Ca^{2+}	calcium
CA3	cornu ammonis 3
$CaCl_2$	calcium chloride
CAG	cytomegalovirus early enhancer/chicken-beta actin
CAMKII□	calcium/calmodulin-dependent protein kinase II alpha
cAMP	cyclic adenosine monophosphate
CGRP	calcitonin gene-related protein
Ci	Curie
cm	centimeter
cm^2	square centimeter
CMT	Charcot-Marie-Tooth
CMV	cytomegalovirus
CNP	2′,3′-cyclic nucleotide 3′-phosphodiesterase
CNS	central nervous system
CO_2	carbon dioxide
CPEB1	cytoplasmic polyadenylation element-binding protein-1
cps	counts per second
CRE	cAMP-responsive element
CREB	CRE-binding protein
CST	corticospinal tract
DAPI	4′,6-Diamidino-2-phenylindole dihydrochloride
DC	dorsal columns
dCTP	deoxycytidine triphosphate
DG	dentate gyrus
dH_2O	distilled water
DIC	differential interference contrast

DIV	days *in vitro*
DMEM	Dulbecco’s modified eagle medium
DMSO	dimethyl sulfoxide
DNA	deoxyribonucleic acid
dNTP	deoxynucleoside triphosphate
DPBS	Dulbecco’s phosphate buffered saline
dpo	days post operation
DRG	dorsal root ganglia
DTT	dithiothreitol
E	embryonic day
E.coli	*Escherichia coli*
e.g.	exempli gratia
EAE	experimental autoimmune encephalomyelitis
EDTA	ethylenediamine tetraacetic acid
EF	embryonic feeder
eGFP	enhanced green fluorescent protein
EGTA	Triethylene glycol diamine tetraacetic acid
EM	electron microscopic
ER	endoplasmic reticulum
ES	embryonic stem
ESI	electron spectroscopic imaging
FBS	fetal bovine serum
FD	fast digest
FISH	fluorescence *in situ* hybridization
FMRP	fragile x mental retardation protein
g	gram
g	gravity
GAP-43	growth associated protein-43
GDP	guanosine diphosphate
GFAP	glial fibrillary acidic protein
GFP	green fluorescent protein
GLT	germline transmission
GTP	guanosine triphosphate
h	hour
H	hydrogen
HA	hemagglutinin
HA	Hibernate A
HBSS	Hank’s balanced salt solution
HCl	hydrochloric acid
HEK	human embryonic kidney
HEPES	4-(2-hydroxyethyl)-1-piperazineethanesulfonic acid
het	heterozygous
hnRNP R	heterogeneous nuclear ribonucleoprotein R
HS	horse serum
i.t.	intrathecal
i.v.	intravenous
IB4	isolectin B4
ICC	immunocytochemistry
IgG	immunoglobulin G

IHC	immunohistochemistry
ISH	*in situ* hybridization
ITR	inverted terminal repeats
KanR	kanamycin resistance
kb	kilobase
KCl	potassium chloride
kDa	kilodalton
kg	kilogram
L	liter
L	lumbar level
LA ROASA26	long arm of homologous sequence of *ROSA26*
LB2	lamin B2
LIF	leukemia inhibitory factor
MAP2	microtubule-associated protein 2
MBP	myelin basic protein
MEM	minimum essential medium
mg	milligram
$MgCl_2$	magnesium chloride
min	minute
ml	milliliter
mM	millimolar
MMC	Mytomycin C
mmol	millimole
mRNA	messenger RNA
ms	millisecond
MS	multiple sclerosis
MT	microtubule
mTOR	mammalian target of rapamycin
mW	milliwatt
N	normal
NaCl	sodium chloride
NEAA	non-essential amino acids
NEO	neomycin resistance gene
NeoR	neomycin resistance
NF-L	neurofilament light chain
ng	nanogram
NGF	nerve growth factor
NGS	normal goat serum
NH_4Cl	ammonium chloride
NLS	nuclear localization signal
nm	nanometer
nm	nanomolar
No.	number
NT-3	neurotrophin-3
P	phosphate
P	postnatal day
pA	polyadenylation signal
PARP	periaxoplasmic ribosomal plaque
PBS	phosphate buffered saline

PC	pheochromocytoma
PCR	polymerase chain reaction
PDL	Poly-D-lysine
pDNA	plasmid DNA
PenStrep	Penicilin Streptomycin
pErk	phosphorylated extracellular signal-regulated kinase
PFA	paraformaldehyde
pH	potential hydrogen
PLL	Poly-L-lysine
PNS	peripheral nervous system
Pol	RNA polymerase
qPCR	quantitative PCR
rAAV	recombinant adeno-associated virus
RAG	regeneration-associated gene
RBP	RNA-binding protein
RFP	red fluorescent protein
RNA	ribonucleic acid
RNP	ribonucleoprotein particle
ROSA26 SA	short arm of homologous sequence of *ROSA26*
ROSA26	*Gt(ROSA)26Sor*
RPL10a	ribosomal protein L10a
RPL22	ribosomal protein L22
RPL26	ribosomal protein L26
RPL4	ribosomal protein L4
rpm	revolutions per minute
RPS6	ribosomal protein S6
rRNA	ribosomal RNA
RT	room temperature
RV	ribosome-containing vesicle
SAP	shrimp alkaline phosphatase
SC	Schwann cell
SCa	slow component a
SCb	slow component b
SCI	spinal cord injury
SDS	sodium dodecyl sulfate
SDS-PAGE	SDS-Polyacrylamide gel electrophoresis
Sema3A	semaphorin 3A
siRNA	small-interfering RNA
SLI	Schmidt-Lanterman incisure
SMLM	single molecule localization microscopy
snoRNP	small nucleolar ribonucleoparticle
SPF	specifically pathogen free
SSIM	saturated structured-illumination microscopy
STAT3	signal transducer and activator of transcription
STED	stimulated emission depletion
STOP	transcriptional stop cassette
STORM	stochastic optical reconstruction microscopy
SV40 pA	simian virus 40 polyadenylation signal
T	thoracic level

tdTomato	tandem dimer protein Tomato
TEMED	tetramethylethylenediamine
TF	transcription factor
Tg	transgene
TNT	tunneling nanotube
TRAP	translating ribosome affinity purification
U	units
UTR	untranslated region
UV	ultraviolet
V	volt
WB	Western blot
Wld^s	Wallerian degeneration slow
WPRE2	woodchuck hepatitis virus posttranscriptional regulatory element 2
WT	wild type
YFP	yellow fluorescent protein
ZBP1	zipcode binding protein 1

1. Introduction

Neurons, the main components of the nervous system, are highly polarized cells. They possess widely branched dendrites with many spines to contact axons of other neurons and to receive electrical or chemical signals for the transmission to the neuronal cell body. In the soma, this information is processed and output signals are sent as action potentials along the axon to synaptic sites of downstream targets. Neurons can connect to each other to form neural networks that represent the basis of the central (CNS) and peripheral nervous system (PNS).

1.1 Ribosome biogenesis

In order to fulfill all their tasks and, in the first place, to exist at all, the cell transcribes all necessary information from its deoxyribonucleic acid (DNA) to messenger ribonucleic acid (mRNA). The latter functions as matrix for the translation of proteins that is mediated by ribosomes.

In eukaryotic cells, the 80S ribosome, which has a size of 25-30 nm in diameter, represents a ribonucleoprotein complex built up of ribosomal RNAs (rRNAs) and ribosomal proteins. It consists of two subunits: the large 60S subunit, which comprises the 25S/28S, 5.8S, and 5S rRNAs as well as 46 ribosomal proteins, and the small 40S subunit containing 18S rRNA and 33 ribosomal proteins (Fromont-Racine et al., 2003; Kressler et al., 2010).

The ribosome biogenesis involves a complex interplay of more than 200 transiently associated ribosome assembly factors and the coordinated activity of all three RNA polymerases (Pol I-III). Poll II is responsible for the general transcription of mRNAs in the cell, hence, it also generates the mRNAs for the ribosomal proteins that are subsequently translated in the cytoplasm. Ribosomal proteins are transported into the nucleus, where the ribosome biogenesis begins in a specialized compartment, the so-called nucleolus. There, both other RNA polymerases produce rRNAs: the 18S, 5.8S, and 25S/28S rRNA species are synthesized by Pol I as a single polycistronic transcript, the 35S pre-rRNA, whereas Pol III transcribes the 5S rRNA. Co-transcriptionally, various rRNA residues become modified by many small nucleolar ribonucleoparticles (snoRNPs). Additionally, ribosomal proteins and non-ribosomal factors interact with the rRNAs to form the 90S pre-ribosomal particle. Subsequent cleavage of the rRNA results in the emergence of pre-40S and pre-60S particles, which move from the nucleolar to the nucleoplasmic compartment. Thereby, rearrangements of the RNA and the gradual removal of biogenesis factors occur within the premature subunits. Finally, the ribosomal subunits are exported through the nuclear pore complex into the cytoplasm where their maturation is completed yielding two subunits competent for the translation of mRNA (Figure 1) (reviewed by Tschochner and Hurt, 2003,

Thomson et al., 2013). In the cytoplasm, the ribosomal subunits join together on an mRNA molecule to initiate its translation. Dependent on the produced protein, ribosomes either remain free in the cytoplasm to translate cytosolic proteins, or become associated with the endoplasmic reticulum (forming the rough endoplasmic reticulum [rough ER]) for the production of transmembrane or water-soluble proteins (Alberts et al., 2002).

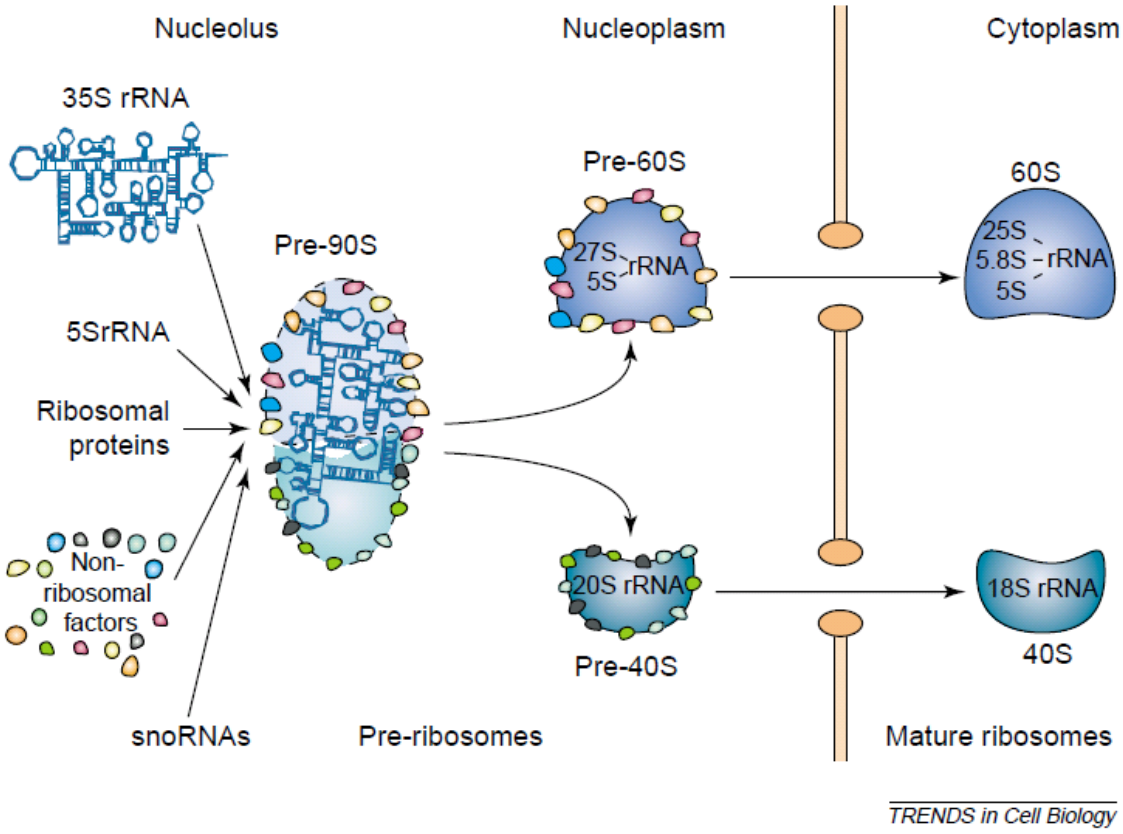

Figure 1: Biogenesis of ribosomal subunits
Schematic representation of the main steps of the ribosome biogenesis. In the nucleolus, the 90S pre-ribosomal particle, consisting of 35S pre-rRNA, 5S rRNA, ribosomal proteins, non-ribosomal factors, and snoRNAs, is formed. Upon cleavage of the 35S pre-rRNA, pre-60S and pre-40S particles arise from the 90S precursor. For maturation, they move to the nucleoplasm and are exported into the cytoplasm via the nuclear pore complex. Thereby, rearrangements of the rRNA and the gradual removal of biogenesis factors occur, finally giving rise to mature 60S and 40S ribosomal subunits. Adapted from Tschochner and Hurt (2003).

1.2 Local protein synthesis in neuronal compartments

Traditionally, it was believed that the cell body of the neuron is responsible for the supply of ribosomes to distal cellular sites, even the distal presynaptic terminals, together with all the proteins needed for proper function and plasticity. There are two ways to transport proteins anterogradely to the axonal compartment; both of them are mediated by kinesins traveling on microtubules (MTs) that run along the entire length of the axon. Transport of membranous organelles, mitochondria, and vesicular cargoes is relatively fast at speeds ranging from 50-400 millimeters per day. On the contrary, the slow axonal transport covers the supply of all other proteins, such as cytoskeletal and most cytosolic proteins. Neurofilaments, MTs and microtubule-associated proteins move at rates of 0.1-1 millimeters per day in the slow component a (SCa) of the slow anterograde transport. The second and faster class, the slow component b (SCb), carries mainly actin, microfilaments, clathrin complexes, and metabolic enzymes at 2-8 millimeters per day (Lasek et al., 1984; Morfini et al., 2012). However, since certain axons, like those in the spinal cord and peripheral nerves, are very long – in humans up to 1 meter, the transport of cytoskeletal proteins from the soma to the tip of the axon would easily exceed their half-lives of 1-2 weeks (Forgue and Dahl, 1978; Alvarez et al., 2000). Thus, the axonal transport cannot be the only mechanism to maintain the steady state of the axonal proteins. Indeed, findings from the last decades led to the conviction that axons synthesize their proteins locally (Koenig and Giuditta, 1999; Alvarez et al., 2000; Giuditta et al., 2002; 2008). Even though this issue has been discussed controversially for decades, it is nowadays generally accepted that protein translation takes place in axons (reviewed in Vogelaar et al., 2009). In addition, this view was strongly supported by the conclusive evidence that proteins can be synthesized locally in dendrites, away from the soma region.

1.2.1 Local protein synthesis in dendrites

Early electron microscopic (EM) studies have demonstrated the presence of ribosomal particles in motoneuron dendrites in the monkey spinal cord (Bodian, 1965) and in the dendritic arbor of the rat dentate gyrus (Steward and Levy, 1982). Strikingly, polyribosomes were predominantly found in the dendritic shaft at the base of dendritic spines (Steward and Levy, 1982; Ostroff et al., 2002), where they were often associated with membranous cisterns in so-called synapse-associated polyribosome complexes (Steward and Reeves, 1988; Steward et al., 1996). In studies using radiolabeled amino acids it was shown that *de novo* protein synthesis occurred in dendrites of CA1 pyramidal cells in hippocampal slices within minutes after electrical stimulation (Feig and Lipton, 1993). In rat hippocampal slices, application of brain-derived neurotrophic factor (BDNF) or neurotrophin-3 (NT-3) led to strengthening of synaptic transmission that was strongly reduced after pretreatment with protein synthesis inhibitors and also after separating the dendrites from the cell bodies via

microlesion (Kang and Schuman, 1996). Further studies also emphasized the important role of local translation in synaptic plasticity (reviewed by Steward and Schuman, 2001), e.g., for long-term depression induced by metabotropic glutamate receptors (Huber et al., 2000), and for tetanically elicited late long-term potentiation (Bradshaw et al., 2003). Finally, the BDNF-induced protein translation in isolated dendrites was proven in cultured hippocampal neurons by means of a fluorescently labeled reporter mRNA (Aakalu et al., 2001).

To date, it is known that the dendritic transcriptome comprises more than 2500 mRNAs, encoding known synaptic proteins, such as signaling molecules, receptors and scaffolds molecules, proteins involved in membrane trafficking, and also members of the protein synthesis and degradation machinery (Poon et al., 2006; Zhong et al., 2006; Cajigas et al., 2012). Interestingly, dendritic stimulation even seems to recruit certain mRNAs to synaptic sites for translation (Steward et al., 1998). Some of the identified transcripts were analyzed in detail by high-resolution ISH revealing that mRNA molecules are very diverse in their abundance and distribution pattern along the dendrite. Notably, some transcripts seem to group in local domains, but not necessarily localized to individual synapses (Cajigas et al., 2012).

Overall, the dendritic compartment is equipped with an enormous repertoire of regulative possibilities to react to localized signals. As the mRNA population in the dendrite is quite diverse, local pools of available transcripts exist. By choosing only some mRNAs to be translated locally, microdomains with a highly specific protein composition can be created within the dendrite, even at the level of single spines. However, the exact procedure and coordination of these molecular processes is still not fully understood.

1.2.2 Local protein translation in axons

1.2.2.1 Historical overview

In parallel to the discovery of local protein synthesis in dendrites, research also focused on ribosomes and RNA potentially existing in axons. The first studies describing axonal RNA was performed on Mauthner neurons (Edstrom et al., 1962) and axons from adult cats (Koenig, 1965). A decade later, RNA and ribosomes were found in the squid giant axon (Koenig, 1979; Giuditta et al., 1980; Martin et al., 1989; Giuditta et al., 1991; Bleher and Martin, 2001) and evidence for actively translating polysomes was provided in the same invertebrate system. Early EM studies had already described occasional clusters of ribosomes in axons and growth cones of developing and mature PNS neurons in vertebrates (Tennyson, 1970; Zelena, 1970; Yamada et al., 1971; Bunge, 1973). Metabolic labeling experiments expanded these findings by proving *de novo* protein synthesis also for vertebrate axons (Koenig and Adams, 1982; Koenig, 1991; Eng et al., 1999). Ultrastructural electron spectroscopic imaging (ESI) analyses and immuno-EM showed localized axonal

ribosomes in discrete domains that were intermittently distributed along the periphery of mammalian myelinated axons (Koenig and Martin, 1996; Koenig et al., 2000; Kun et al., 2007). These so-called periaxoplasmic ribosomal plaques (PARPs) were enriched in F-actin and RNA, and contained molecular motor proteins, such as KIF-3 A and myosin Va. Therefore, PARPs most likely represent focal centers of local protein synthesis within the axon (Sotelo-Silveira et al., 2004; 2006). Among the first transcripts of the approximately 200 heterogeneous mRNA species that have been initially identified in the axonal compartment of the squid giant axon (Capano et al., 1987), many encode cytoskeletal and motor proteins, such as β-actin and β-tubulin, neurofilament, and kinesin (Giuditta et al., 1991; Kaplan et al., 1992; Gioio et al., 1994). These findings additionally confirmed the previously discussed theoretical hypothesis that proteins, especially those that are necessary for the maintenance of the cytoskeleton, cannot exclusively be produced in the cell body and transported to far distant compartments. Instead, neuronal cells presumably take advantage of protein synthesis directly at the location of requirement to overcome their needs in a fast and specific manner.

1.2.2.2 Cell type- and age-related differences

Follow-up studies and more recently performed transcriptome analyses on CNS (Taylor et al., 2009; Zivraj et al., 2010) and PNS neurons (Andreassi et al., 2010; Gumy et al., 2011) at different developmental stages greatly expanded the spectrum of identified axonal mRNAs. Many transcripts seemed to be part of a common repertoire of mRNAs found in axons of various neurons. These included mRNAs encoding cytoskeletal, cytoskeleton-associated, regeneration-associated, and mitochondrial proteins as well as proteins involved in protein synthesis (Vogelaar et al., 2009; Gumy et al., 2010). For example, *β-actin* mRNA is present in axons of embryonic cortical neurons, of sympathetic neurons, and in regenerating dorsal root ganglia (DRG) axons (Olink-Coux and Hollenbeck, 1996; Bassell et al., 1998; Zheng et al., 2001). On the other hand, there are cell type-specific differences in the axonal transcriptome. For instance, the transcript encoding the cAMP-responsive element (CRE)-binding protein (CREB) was detected in PNS (Cox et al., 2008; Andreassi et al., 2010; Gumy et al., 2011) but not in CNS axons (Crino et al., 1998; Taylor et al., 2009; Zivraj et al., 2010).

Beside cell type-related differences, the axonal pool of mRNA seems to be affected by age-related processes. Previous studies reported that axonal transcripts are only detectable in early embryonic cortical and hippocampal neurons (Bassell et al., 1994; Kleiman et al., 1994). These findings were recently challenged by Taylor et al. (2009) who performed microarrays on *in vitro* matured cortical neurons. Age-related differences in axonal transcripts were studied in detail in the PNS. When comparing embryonic and adult sensory neurons, roughly half of their axonal transcriptome overlapped (~1400 transcripts out of 2627 in embryonic and 2924 in adult axons). The amount of axonal localization of some of these

mRNAs decreased with ageing (Gumy et al., 2011), whereas other mRNAs, such as *β-actin*, remained relatively constant in DRG axons during development (Vogelaar et al., 2009). Taken together, the availability of axonal transcripts is highly dynamic in diverse axon types and developmental stages and hence, influences the types of proteins that are translated axonally.

Beside mRNAs, the presence of the translational machinery is essential for axonal protein synthesis. Accordingly, cell type- and age-related differences were also reported for axonal ribosomes. For PNS neurons, early EM studies showed that ribosomes are present in embryonic sensory axons *in vivo* (Tennyson, 1970). In mature peripheral axons, ribosomal proteins were detected by immunohistochemistry (IHC). They were found predominantly near the plasma membrane where they were unevenly distributed in PARPs that also contained RNA (Koenig and Martin, 1996; Koenig et al., 2000; Li et al., 2005; Kun et al., 2007). In order to obtain additional insight, Verma et al. (2005) compared the levels of ribosomal P protein and phosphorylated translation initiation factor phospho-eIF-4E in cultured sensory and retinal axons of different developmental stages. Both components of the translational process were found to decrease with age in DRG axons. In central axons, only very low levels were detected at the embryonic stage and almost none in adulthood (Verma et al., 2005). The latter findings are in line with EM studies showing that various embryonic CNS neurons contain ribosomes in their axons and growth cones *in vitro* (Bunge, 1973; Bassell et al., 1998; Tcherkezian et al., 2010). However, in adult rat CNS neurons *in vivo*, polyribosomes were observed only at the axon initial segment but not in the axon shaft (Steward and Ribak, 1986). Therefore, it has been assumed that axonal protein synthesis in central axons occurs during development only. Recently, this hypothesis has been challenged by Walker et al. (2012), who detected ribosomal protein L10a (RPL10a) tagged with enhanced green fluorescent protein (eGFP) at nodes of Ranvier in corticospinal tract (CST) axons of adult transgenic mice *in vivo*. In addition, regenerating spinal cord axons were reported to contain components of the translational machinery when provided the permissive environment of a peripheral nerve graft (Kalinski et al., 2015).

Overall, local protein synthesis in axons seems to be a highly dynamic process that depends on the availability of translational machinery and cofactors, and on the presence of mRNAs defining the kind of translated proteins. Further, many studies point to differences particularly between PNS and CNS axons that are assumed to be related to the functional implications of local protein translation.

1.2.2.3 The functional role of local protein synthesis in axons

Local protein synthesis fulfills a broad repertoire of diverse functions within the axonal compartment as outlined in the following sections.

1.2.2.3.1 Axon maintenance and growth

Recent studies suggest an important role for local protein translation in axon maintenance. In cultured primary sympathetic neurons, the inhibition of protein synthesis resulted in axon retraction and was associated with a decrease in the membrane potential of axonal mitochondria. The authors hypothesized that many mitochondrial proteins might have a short lifetime and need to be replaced by locally synthesized proteins (Hillefors et al., 2007). Indeed, many mRNAs encoding mitochondrial proteins or proteins important for mitochondrial function were detected in various axons (e.g., Gioio et al., 2001; Aschrafi et al., 2010; Gumy et al., 2011; Yoon et al., 2012). Since mitochondria are the main source of adenosine triphosphate (ATP) in axons, their functionality is essential for the axonal viability (Knott et al., 2008).

During embryonic development axons grow out and find their specific target. Many studies investigated a possible role of axonal translation in different growth processes. Basal growth of various types of axons was shown to occur independently of local protein synthesis since cultured axons continued to grow in the presence of protein synthesis inhibitors (Eng et al., 1999; Leung et al., 2006; Hengst et al., 2009). However, if axon elongation was increased by extracellular stimuli, e.g., by nerve growth factor (NGF) or netrin-1, local translation of proteins, e.g., the polarity complex protein Par3 (Hengst et al., 2009), was required. Beside axon elongation, NGF also initiates collateral branching of sensory axons, again mediated by axonal translation (Spillane et al., 2012).

Local protein synthesis is also required for axon guidance. Growth cone turning in response to chemotrophic guidance molecules, like netrin-1 (Leung et al., 2006), BDNF (Yao et al., 2006), NT-3 (Zhang et al., 1999), Slit2 (Piper et al., 2006), semaphorin 3A (Sema3A) (Campbell and Holt, 2001; Wu et al., 2005), and Engrailed-1 and -2 (Brunet et al., 2005; Wizenmann et al., 2009) is independent from the cell body and is mediated by local protein synthesis. Depending on the mRNAs that are translated within growth cones, the direction of navigation is defined. Attractive turning toward a netrin-1 or BDNF gradient is mediated by asymmetric translation of β-actin on the near side of the growth cone (Leung et al., 2006; Yao et al., 2006). On the other hand, growth cone repulsion or collapse was found to occur in response to Slit2 or Sema3A due to local translation of actin regulatory proteins such as cofilin (Piper et al., 2006) or RhoA (Wu et al., 2005).

1.2.2.3.2 Retrograde signaling and axon regeneration

Interestingly, even transcription factors (TFs) can be produced in the axon. Cox et al. (2008) reported the NGF-stimulated translation of CREB in the axon and its retrograde transport to the nucleus in cultured peripheral sensory neurons, where it initiated transcription-dependent mechanisms for neuronal survival (Cox et al., 2008).

Similar mechanisms have been identified for retrograde signaling in lesioned peripheral nerves. After sciatic nerve injury, axonal translation of *importin β1* and *vimentin* transcripts are increased, which are retrogradely transported together with phosphorylated extracellular signal-regulated kinases, pErk1 and pErk2. Importin α/β heterodimers form high-affinity nuclear localization signal (NLS) binding complexes, which are then responsible for the translocation of pErks to the nucleus where they transcriptionally regulate neuronal regeneration (Hanz et al., 2003; Perlson et al., 2005). Another cargo of the importin-dynein signaling complex is the TF signal transducer and activator of transcription 3 (STAT3). Upon injury of the sciatic nerve, axonal STAT3 is locally translated and activated by phosphorylation. After retrograde transport, STAT3 acts in the cell body to promote the survival of the neuron (Ben-Yaakov et al., 2012). Similar findings have been reported for cultured embryonic hippocampal neurons (Ohara et al., 2011). Many other TFs and signaling networks are probably involved in the initiation and regulation of the injury response as suggested by computational analyses of injured sciatic nerves (Michaelevski et al., 2010; Ben-Yaakov et al., 2012) and by the identification of multiple TF transcripts in several axonal mRNA libraries (Taylor et al., 2009; Zivraj et al., 2010). The cell body response to injury includes a change in the neuronal transcriptional profile induced by the activation of regeneration-associated genes (RAGs), which at least partially depends on local protein synthesis (Ben-Yaakov et al., 2012; Ma and Willis, 2015).

Beside injury signaling, the formation of a new growth cone represents another central step during regeneration processes and was also reported to require local protein synthesis. In adult DRG explants *in vitro*, axotomy led to an increased translation of *β-actin* transcripts in the axonal compartment. This local synthesis of β-actin was shown to be important for successful regeneration since the knockdown of its axonal mRNA levels via small-interfering RNAs (siRNAs) reduced the ability of axons to form new growth cones (Vogelaar et al., 2009).

Taken together, local protein synthesis is an important component of axon regeneration as it is involved in three important steps (summarized in Figure 2): the formation of a new growth cone, retrograde signaling, and axon guidance (Vogelaar and Fawcett, 2008). Differences in the ability to locally synthesize proteins may therefor account for the different regeneration capacities of CNS and PNS axons (Verma et al., 2005).

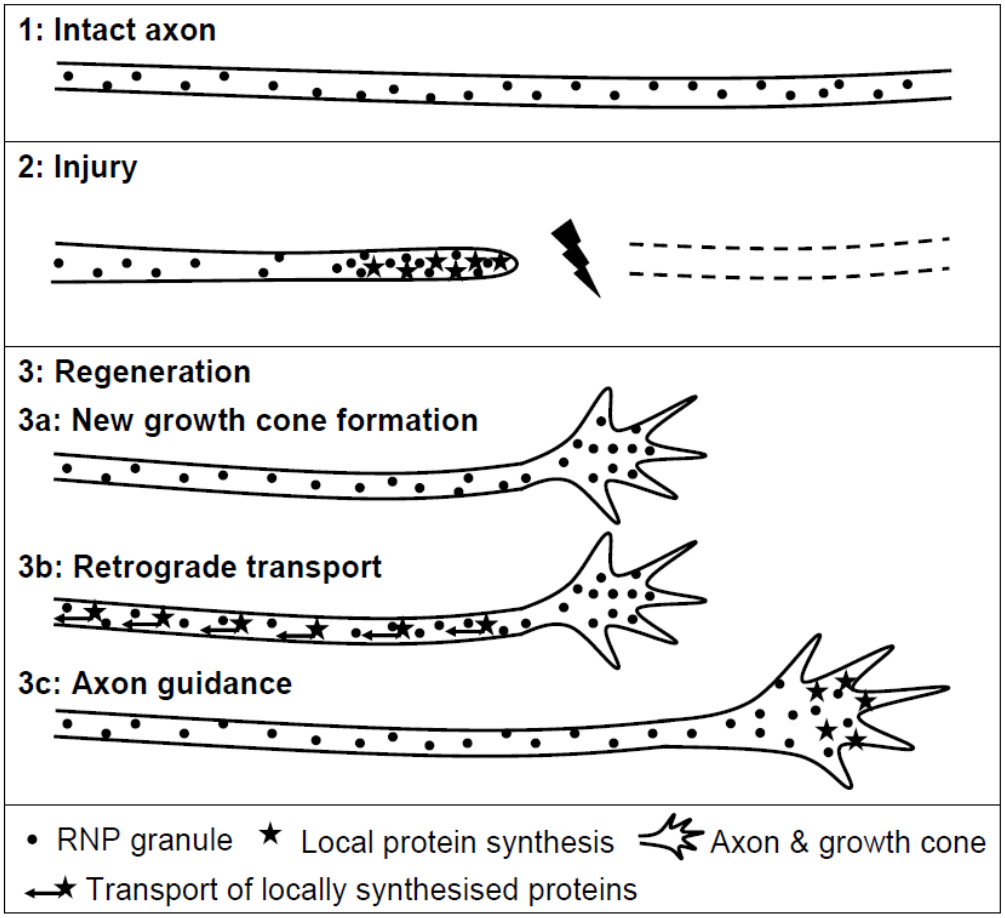

Figure 2: Schematic outline of local translation events involved in PNS axon regeneration after injury
(**1**) In an intact axon, ribonucleoprotein (RNP) granules are assumed to be present all over the axoplasm. (**2**) After injury, the distal stump degenerates. In parallel, the proximal stump reseals and retracts from the lesion site. Local protein synthesis increases to initiate the formation of a new growth cone (**3a**) and to produce proteins and transcription factors, such as importin-β or STAT3, for the retrograde injury signaling to the cell body (**3b**). During the re-growth of the axon, local protein synthesis is probably involved in guidance processes to help the axon reach its target (**3c**). Adapted from Vogelaar and Fawcett (2008).

1.3 Transport mechanisms to enable local protein synthesis

1.3.1 Cytoskeletal organization and polarized transport in neuronal compartments

As mentioned before, neurons are highly polarized cells with various subcellular parts (soma, dendrites, and axon) and distal sites (growth cone, pre-synaptic site). In order to supply cargoes to these neuronal compartments, molecular transport mechanisms exist that exploit the polarized organization of the cytoskeleton for delivery to specific targets. Long-range transport is based on MTs and is driven by motor proteins of the kinesin and dynein family. Here, kinesin moves to the plus-end of MTs, whereas dynein travels in a minus-end oriented way. For the covering of short distances and the local delivery to growth cones and synapses, cargoes are transported via myosin motors that are running on actin filaments.

Since MTs within the axonal compartment are uniformly oriented with their plus-end pointing to the distal site, anterograde transport is mediated by kinesins. In contrast, mature dendrites have MTs of mixed polarity with many minus ends pointing outward (Baas et al., 1988; Burton, 1988) (Figure 3). Consequently, dynein is responsible for the transport of cargoes to dendrites (Kapitein et al., 2010). Beside their orientation, MTs in the axonal and dendritic compartment differ in their microtubule-associated proteins. For instance, tau and microtubule-associated protein 2 (MAP2) are also distributed in a polarized manner with MAP2 being exclusively found in dendrites, whereas tau is present in both process types but predominantly localizes to the distal axon (Dehmelt and Halpain, 2005).

Regarding actin filaments, similar differences in orientation and distribution occur at specific subcellular sites (e.g., axonal growth cone, developing dendrite), however, less details are known so far. Shorter and branched actin filaments are assumed in the shaft of axons and dendrites, as well as in the head of dendritic spines, while the spine neck contains predominantly long actin filaments (Kapitein and Hoogenraad, 2011) (Figure 3). At the axon initial segment, the specialized organization of the actin network is proposed to function as a molecular filter to direct cytoplasmic transport (Song et al., 2009).

All in all, based on the preexisting polarized cytoskeletal structure, neurons achieve sorting of cargos to dendrites or the axon by an active transport depending on the choice of specific motor protein subsets (Kapitein and Hoogenraad, 2011). Possibly, these sorting mechanisms account for the predominantly dendritic localization of RNA in CNS neurons versus the axonal RNA localization in the PNS.

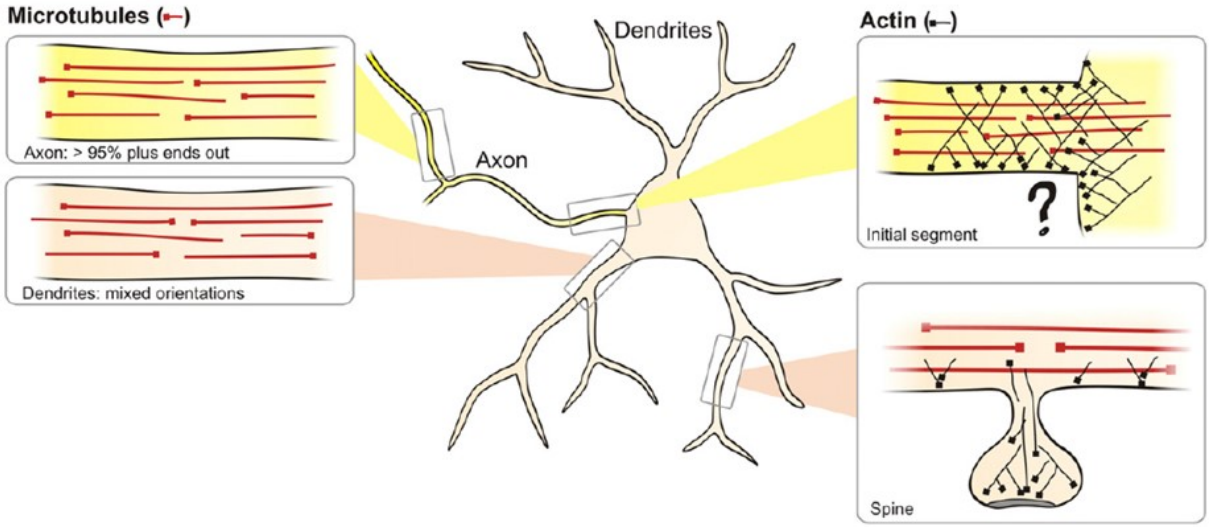

Figure 3: Cytoskeletal organization in neuronal compartments.
Schematic representation of a neuron with close-ups of subcellular compartments to illustrate their specific cytoskeletal organization. In axons, microtubules (red) have a uniform orientation with their plus-ends (marked with boxes) pointing to outwards. At the axon initial segment, actin (black) is assumed to exist as short, branched filaments orientated perpendicularly to the plasma membrane. In contrast, dendrites contain microtubules with mixed orientation. In the spine, long actin filaments are present in the spine neck and shorter, branched ones are found in the spine head. Modified from Kapitein and Hoogenraad (2011).

1.3.2 Intracellular transport of components for local protein translation

Among other cargoes, mRNAs are anticipated to use the cytoskeletal molecular motors, such as kinesins and myosins, for their transport to specific subcellular domains (Holt and Bullock, 2009; Bullock, 2011; Jung et al., 2012). For the transport along cytoskeletal tracks, mRNAs are associated with RNA-binding proteins (RBPs) in so-called transport ribonucleoprotein particles (RNPs) that interact with molecular motors (Krichevsky and Kosik, 2001; Hirokawa, 2006; Donnelly et al., 2010; Xing and Bassell, 2013). Many studies showed that various motor proteins mediate the transport of RNPs since bidirectional movements, most likely based on kinesins, were observed (Zhang et al., 2001; Kanai et al., 2004; Davidovic et al., 2007; Dictenberg et al., 2008; Hirokawa et al., 2010). In addition, RNP complexes were also found to interact with myosin Va and to travel along actin tracts (Muslimov et al., 2002; Ohashi et al., 2002; Nalavadi et al., 2012).

Sorting and targeting of RNPs is determined by specific sequences within the mRNA that are most often located in the 3' untranslated region (UTR) and recognized by RBPs (Yoo et al., 2010). For instance, a 54 nucleotide sequence, termed zipcode, was identified in the 3'UTR of *β-actin* mRNA and has been shown to drive its subcellular localization to dendrites and axons *in vitro* and *in vivo* (Kislauskis et al., 1994; Bassell et al., 1998; Tiruchinapalli et al., 2003; Willis et al., 2011). In contrast, *γ-actin* mRNA encoding another actin isoform, is restricted to the cell body (Bassell et al., 1998). The selective axonal transport of the *β-actin* mRNA is mediated by the RBP zipcode binding protein 1 (ZBP1) (Zhang et al., 2001), which simultaneously controls the translation (Huttelmaier et al., 2005). This interaction seems to

be important for axon regeneration *in vitro* and *in vivo* since mice with reduced ZBP1 levels show decreased axonal outgrowth (Donnelly et al., 2011).

Axonal localization elements were also found in the 3'UTR of other transcripts, such as *tau*, *EphA2*, *RhoA*, *myo-inositol monophosphatase-1*, and *growth associated protein-43 (GAP-43)* mRNA (Aronov et al., 2001; Brittis et al., 2002; Wu et al., 2005; Andreassi et al., 2010; Yoo et al., 2013). In addition, many interacting RBPs have been identified now, including HuD, heterogeneous nuclear ribonucleoprotein R (hnRNP R), fragile x mental retardation protein (FMRP), and cytoplasmic polyadenylation element-binding protein-1 (CPEB1) (Aronov et al., 2002; Rossoll et al., 2003; Antar et al., 2006; Kundel et al., 2009), and even more (~400) are annotated in the mouse genome (Cook et al., 2011). Hence, enormous possibilities exist for the composition of RNPs enabling the neuron to complex regulations for the precise subcellular targeting of the transcripts.

Analyses of dendritic RNPs and of RNA granules isolated from whole brain homogenates revealed the presence of ribosomes within these complexes (Knowles et al., 1996; Krichevsky and Kosik, 2001; Kanai et al., 2004; Elvira et al., 2006; Calliari et al., 2014) and led to the assumption that the protein translation machinery is also targeted to subcellular domains by microtubule-based transport.

Kun et al. (2007) found ribosomes in PARPs at the cortical axoplasm of myelinated sciatic nerve fibers. Additionally, ribosomal clusters were also observed in the axonal core domain suggesting that they represent a population of ribosomes in transit. However, this hypothesis is only based on static experiments consisting of confocal and EM analyses. Live imaging studies to show the movement of RNPs in the axonal compartment have not yet been undertaken and further insights into the axonal transport of ribosomes are missing. Furthermore, the underlying mechanisms for sorting and targeting of ribosomes to axons are still unclear.

1.3.3 Glia-to-axon transfer

Recently, Court and colleagues (2008; 2011) challenged the general assumption that ribosomes are transported from the soma to the axon by proposing Schwann cells (SCs) as alternative source of axonal ribosomes. With a lentiviral approach, they specifically labeled ribosomes of SCs that were detected after sciatic nerve crush in injured and regenerating axons, which contained augmented ribosomal levels. Using confocal and electron microscopy, glial cytoplasmic protrusions that were filled with polyribosomes were observed to invaginate into the axons. These invaginations were present both in internodes and in paranodes. Ribosomal signals were found within the axoplasm directly below the contact site. Based on this close proximity and the finding that axonal polyribosomes were located in multimembrane vesicles, the authors hypothesized that Schwann cell protrusions detached

from the glial cytoplasm to release so called ribosome-containing vesicles (RVs) into the axoplasm.

In cases of neuropathies, such as amyotrophic lateral sclerosis (ALS) or Charcot-Marie-Tooth (CMT), axons had increased amounts of ribosomes and RVs were observed in the axoplasm. Since axonal transport systems were slowed or disrupted in disease-affected axons, a glia-to-axon transfer of ribosomes was assumed (Verheijen et al., 2011; 2014).

Furthermore, it is very likely that not only the translational machinery, but also RNA is transferred from glial cells to the axon. Evidence for an intercellular RNA transfer was provided by Sotelo-Silveira et al. (2000), who detected the mRNA coding for the axon-specific neurofilament light chain (NF-L) in SCs adjacent to injured sciatic nerve fibers. The authors hypothesized that SCs transcriptionally upregulate certain mRNAs for the transfer to injured axons in order to support axonal protein synthesis. Follow-up studies further supported the existence of a glia-to-axon RNA transfer after injury and revealed that this transport is mediated by myosin Va (Sotelo et al., 2013).

Taken together, it can be speculated that ribosomes and RNAs could reach the axonal compartment via two different routes: They are either anterogradely transported in RNPs from the cell body to the axon or, most probably in cases of injury, they are transferred from neighboring glial cells (Figure 4).

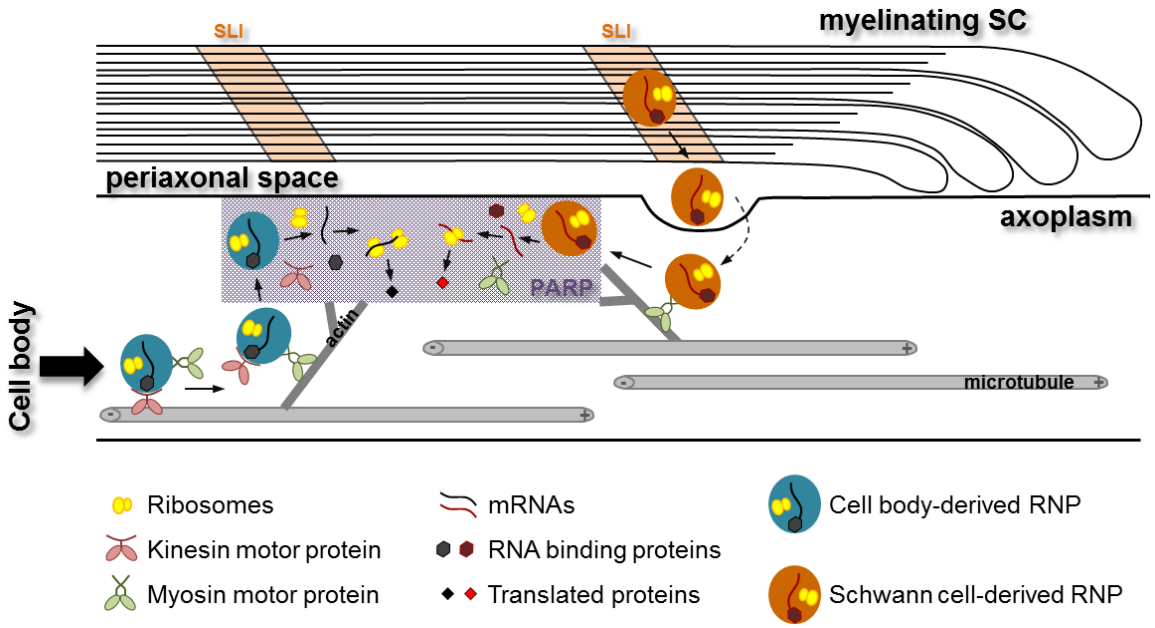

Figure 4: Model showing two possible routes for the axonal delivery of ribosomes and mRNAs
Ribonucleoprotein particles (RNPs) contain mRNAs, RBPs and probably also ribosomes. They are assumed to interact with molecular motors, such as kinesins and myosins, for the long-range anterograde transport along microtubules from the cell body or the local short-range transport on actin fibers, respectively. Periaxoplasmic ribosomal plaques (PARPs) are likely to represent the destination sites within the axonal compartment where constituents of RNPs probably disassemble to effect local protein synthesis. Beside the axonal transport, there is evidence for glia-to-axon transfer of mRNAs and ribosomes. Schwann cell (SC)-derived particles probably cross the myelin sheath along Schmidt-Lanterman incisures (SLIs).

1.4 Aim of the present study

Studies by Court and coworkers led to the hypothesis that glial cells represent an additional source of axonal ribosomes, beside the soma of the neuron, and that this route of transfer accounts for increased amounts of translational machinery found in injured axons (Court et al., 2008; 2011). However, based on their methods, the authors could not exclude the neuronal cell body as source of axonal ribosomes. Additionally, they made use of mutant mice (Wallerian degeneration slow [*Wld*^{S}] mice) and virally transduced, exogenous Schwann cells repopulating a peripheral nerve graft. Therefore, their experimental setup represented a more or less artificial situation. Further, they provided only static results based on confocal and electron microscopy.

To date, it has not been shown whether endogenous Schwann cells transfer ribosomes in non-mutant mice under physiological circumstances. The aim of the present study was to show that axonally localized ribosomes originate from the neuronal cell body *in vivo* in uninjured as well as injured nerves. To address this, tools were developed to visualize specifically neuronal ribosomes. With the help of a viral approach and a transgenic mouse, a cell type-specific fluorescent labeling of ribosomes was intended. Subsequently, the localization of tagged-ribosomes in central and peripheral axons of various cell culture models as well as in the uninjured and crushed sciatic nerve was analyzed in order to prove that axonally localized ribosomes originate from the neuronal cell body.

2. Materials and Methods

2.1 Materials

2.1.1 Chemicals and reagents

Name	Company	Number
10x RotiBlock	Roth	A151.2
2-Propanol	Roth	6752.3
4′,6-Diamidino-2-phenylindole dihydrochloride (DAPI)	Molecular probes	D3571
Acetic acid	Roth	3738.5
Agar	Roth	5210.2
Agarose Basic	Applichem	A8963
Agarose low melt	Roth	6351.2
Albumin bovine fraction V (bovine serum albumin, BSA)	Serva Electrophoresis GmbH	11930.03
Amersham ECL Western Blotting Detection Reagents	GE Healthcare	RPN2106
Ammonium chloride (NH_4Cl)	Applichem	A0988
Ammonium peroxydisulphate (APS)	Roth	9592.3
Ampicillin	Roth	K029.1
Boric acid	Roth	6943.1
Bromophenol blue	Roth	A512.1
Calcium chloride ($CaCl_2$)	Roth	CN93.1
Carprofen (Rimadyl®)	Pfizer	P693088G
Colcemid (10 µg/ml)	Gibco	15212-012
dCTP, [α-32P] 3000Ci/mmol 10mCi/ml EasyTide Lead, 250 µCi	PerkinElmer	NEG513H250UC
Dextrose	Sigma	D9434
DirectPCR®-Tail	peqlab	31-102-T
Dithiothreitol (DTT)	Roth	6908.2
dNTPs (10 mM)	Fermentas	R1121
Ethanol	Roth	9065.3
Ethidium bromide	Roth	HP47.1
Ethylenediamine tetraacetic acid (EDTA)	Roth	8040.2
Ficoll® 400	Roth	CN90
FluorSave™ Reagent	Calbiochem	345789
Genetecin (G418, 50 mg/ml)	Gibco	10131-019
Glycerol	Roth	3783.1
HEPES sodium salt	Sigma	H7006
Hydrochloric acid (HCl)	Roth	T134.1
Isofluran (100%), Forene®	abbvie	
Kanamycin sulphate	Roth	T832
Ketamin-hameln (50mg/ml)	Hameln Pharma Plus GmbH	45481/37/10
Lipofectamine 2000	Invitrogen	11668
Magnesium chloride ($MgCl_2$)	Roth	KK36.2
Mannitol	Sigma	M8429-100G
Methanol	Roth	8388.6
Midori Green	Nippon Genetics Europe GmbH	MG04

Na_2HPO_4 * $2H_2O$	Roth	4984.1
NaH_2PO_4 * $2H_2O$	Roth	T879.2
Paraformaldehyde (PFA)	Merck	1.04005
PBS tablets	Gibco	18912-014
Phenol/Chloroform	Roth	A156.2
Ponceau S	Roth	5938.2
Potassium chloride (KCl)	Roth	6781.1
RNase AWAY	Molecular BioProducts	7002
Rompun	Bayer	
Rotiphorese® Gel 30	Roth	3029.2
Saccharose, D(+)	Roth	4621.1
SOC medium	New England Biolabs	
Sodium chloride (NaCl)	Roth	3957.1
Sodium chloride (NaCl) solution (0.9%)	Braun	5/346177/0310
Sodium deoxycholate	Sigma	D5670
sodium dodecyl sulfate (SDS)	Roth	2326.2
Sodium fluoride (NaF)	Sigma	201154
Sodium hydroxide (NaOH) pellets	Merck	6482
Sodium hydroxide (NaOH) solution	Roth	T135.1
Sodium hydroxide solution (2N)	Roth	T135.1
SuperSignal® West Femto Maximum Sensitivity Substrate	Thermo Scientific	34095
Tetramethylethylenediamine (TEMED)	Roth	2367
Tissue-Tek® O.C.T™ Compound	Sakura	4583
Tissue-Tek® O.C.T™ Compound	Gibco	18912-014
Trichlormethane/Chloroform	Roth	3313.1
Triethylene glycol diamine tetraacetic acid (EGTA)	Roth	3054
Tris	Roth	4855.2
tri-sodium citrate dehydrate	Merck	1.06448
Triton-X 100	Roth	3051.3
Tryptone / Peptone	Roth	8952.3
Tween-20	Roth	9127.1
Xylene cyanole	Roth	A513.1
Yeast extract	Roth	2363.3
β-mercaptoethanol	Sigma	M7522

2.1.2 Media and cell culture supplements

Product	**Company**	**Number**
2i medium (GS2-M^{TM})	StemCells	SF-PS-02-100
B27® Supplement	Gibco	17504-044
Chicken serum	Thermo Scientific	16110082
Collagenase	Sigma	C5138
Dimethyl sulfoxide (DMSO)	Sigma	276855, D2650
Dulbecco's Modified Eagle Medium (DMEM)	Gibco	41966-029
DMEM, high glucose, +glutamine, -sodium pyruvate	Gibco	41965-039
Dulbecco's Phosphate Buffered Saline (DPBS)	Sigma	D8537
Fetal bovine serum (FBS)	Gibco	10270-106, 10500-064
Gelatine solution (2%)	Sigma	G1393

Glucose solution (50%)	Fresenius Kabi	Glucosterile 50%
Glutamax (100x)	Gibco	35050-038
Hank's Balanced Salt Solution (HBSS)	Gibco	14170-088
HEPES (1M)	Gibco	15630-122
Hibernate A – $CaCl_2$	Brain Bits LLC	-
Hibernate A (HA)	Brain Bits LLC	-
Horse serum (HS)	Gibco	16050-122
KNOCKOUT DMEM	Gibco	10829-018
Laminin	Sigma	L2020
Leukemia inhibitory factor (LIF)	medium supernatant from HEK cells stable transfected with a Lif expression vector; kindly provided by AG Waisman, Institute of Molecular Medicine, University medical center, Mainz, Germany	
L-Glutamine (200 mM)	Stemcell technologies	#07100
	Gibco	25030-024
Minimum Essential Medium (MEM)	Gibco	21575-022
Mytomycin C (MMC, 2 mg)	Sigma	M0503
Neurobasal® Medium	Gibco	21103-049
NGF-β human	Sigma	N1408
Non-essential amino acids (NEAA, 10 mM, 100x)	Gibco	11140-050
Normal goat serum (NGS)	Vector	S-1000
OptiPrep® Density Gradient Medium	Sigma	D1556
PBS (1x without Ca^{2+} or Mg^{2+})	Gibco	10270-106
Penicilin Streptomycin (PenStrep)	Gibco	15140-122
Poly-D-lysine (PDL) hydrobromide	Sigma	P1149
Poly-L-lysine (PLL)	Sigma	P1274
Sodium Pyruvate (100 mM, 100x)	Gibco	11360-039
Trypsin-EDTA solution (10x)	Gibco	15400-054
	Sigma	T4174
	PAA	L11-003

2.1.3 Buffers and solutions

Cell culture

HEK293 culture

Growth medium	10% FBS, 0.1 mM (1x) NEAA, 1 mM (1x) Sodium pyruvate, 1x PenStrep in DMEM
Freeze solution	40% FBS, 10% DMSO in DMEM
Starvation medium	5% FCS in DMEM
Trypsin solution	1x EDTA/Trypsin in PBS
2x HEBS	50 mM HEPES, 280 mM NaCl, 1.5 mM Na_2HPO_4 * $2H_2O$, adjust pH to 7.05; filter sterilize and store in aliquots of 14 ml at -20°C
2.5 M $CaCl_2$	2.5 M $CaCl_2$; filter sterilize and store in aliquots of 1.65 ml at -20°C
5 M NaCl	5 M NaCl; autoclave
1 M Tris	1 M Tris, adjust pH to 8.0; autoclave

Resuspension solution	150 mM NaCl, 20 mM Tris
10% sodium deoxycholate	10% Sodium deoxycholate; filter sterilize
Wash solution 1	100 mM NaCl, 20 mM Tris
Wash solution 2	200 mM NaCl, 20 mM Tris
Wash solution 3	300 mM NaCl, 20 mM Tris
Elution solution 1	400 mM NaCl, 20 mM Tris
Elution solution 2	450 mM NaCl, 20 mM Tris
Elution solution 3	500 mM NaCl, 20 mM Tris
EF and ES cell culture	
EF medium	10% FBS, 0.1 mM (1x) NEAA, 1 mM (1x) Sodium pyruvate, 1x PenStrep, 2 mM L-glutamine in DMEM
Inactivation medium for EF	0.01 mg/ml Mitomycin C, 0.05% DMSO in EF medium
Trypsin solution for EF	1x Trypsin EDTA in PBS
ES medium	14.75% FBS, 0.1 mM (1x) NEAA, 1x PenStrep, 2 mM L-glutamine, 1 mM β-Mercaptoethanol, 1 vial LIF in KNOCKOUT DMEM
2x freezing solution	40% FBS, 20% DMSO in ES medium
Geneticin ES medium	14.75% FBS, 0.1 mM (1x) NEAA, 1x PenStrep, 2 mM L-glutamine, 1 mM β-Mercaptoethanol, 1 vial LIF, 200 µg/ml Geneticin in KNOCKOUT DMEM
Trypsin solution for ES	1x Trypsin EDTA, 1% Chicken serum in PBS
PBS/PS	1x PenStrep in PBS
DRG culture	
DRG medium	2% B27, 2% horse serum, 0.5% PenStrep, 1x Glutamax in Neurobasal
HABG	2% B27, 50 mM L-glutamine in Hibernate A
Trituration solution	1% BSA, 0.025 mg/ml DNAse in HBSS
Hippocampal neurons	
PLL coating solution	0.2 mg/ml Poly-L-lysine in 0.1 M Boracic acid, pH 8.5
plating medium	0.6% glucose solution, 10% horse serum, 1x PenStrep in MEM
Neurobasal medium	2% B27, 0.5 mM L-glutamine, 1x PenStrep in Neurobasal
Cortex explant culture	
dissecting medium	10 mM Tris, 1x MEM; filter sterilized, add 0.18 g/ml 1 M dextrose directly before use

SDS-PAGE and Western blotting

Lysis buffer, pH 7.5	50 mM HEPES, 150 mM NaCl, 1 mM EDTA, 1 mM EGTA, 10% Glycerol, 1% Triton-X 100, 25 mM NaF, 10 µM $ZnCl_2$
5x Laemmli Buffer	250 mM Tris-HCl (pH 6.8), 10% SDS, 30% Glycerol, 5%β-mercaptoethanol, 0.02% Bromophenol blue
10% APS	10% Ammonium persulfate; aliquot and store at -20°C
10x TBS	0.5 M Tris, 1.5 M NaCl, adjust pH to 7.4
1x TBST	0.05% Tween-20 in 1x TBS
10x Running Buffer	250 mM Tris, 1.92 M Glycine, 1% SDS, adjust pH to around 8.3.
Blotting Buffer	15% Methanol, 0.1% SDS, 25 mM Tris, 192 mM Glycine; precool to 4°C before use.
Stripping Buffer	6 M Guanidine hydrochloride, 0.2% Nonidet P-40, 20 mM Tris (pH 7.5); add 0.1 M (70 µl/10 ml) β-mercaptoethanol freshly before use
Ponceau Solution	0.1% Ponceau, 5% Acetic acid; store at RT protected from light

Immunocytochemistry and histological analysis

anesthetic solution	10 mg/ml Ketamin, 0,05% Rompun in 0.9% NaCl solution
4% PFA	Heat 40 g Paraformaldehyde in 1 L 1x PB to 60°C, adjust pH to 7.35, filtrate and aliquot. Store at -20°C.
1x PBS	dilute 2 tablets of PBS in 1 L dH_2O
1x PB	Mix 810 ml of solution A (71.2 g Na_2HPO_4*$2H_2O$ in 2 L dH_2O) with 190 ml of solution B (31.2 g NaH_2PO_4*$2H_2O$ in 1 L dH_2O) and 1 L dH_2O, adjust pH to 7.35-7.4
PBSTx	0.2% Triton-X 100 in 1x PBS
50 mMNH_4Cl	50 mM NH_4Cl in 1x PBS

DNA analysis and cloning

LB medium	10 g Tryptone/Peptone, 5 g NaCl, 5 g Yeast extract in 1 L dH_2O, autoclave. Prior to use freshly add antibiotics (final concentration 50 µg/ml). Store at 4°C.
LB agar plates	Add 15 g/l Agar to LB medium and autoclave. Let the solution cool down to about 60°C, add antibiotics (final concentration 50 µg/ml) and fill into 10 cm plates. Store plates at 4°C.
50x TAE	50 mM Tris, 100 mM Acetic acid, 0.05 M EDTA
10x ABI buffer	0.5 M KCl, 0.1 M Tris-HCl pH 8.0, 50 mM $MgCl_2$

Southern blot

TEN	50 mM Tris-HCl pH 8.0, 100 mM EDTA, 100 mM NaCl

TENS	50 mM Tris-HCl pH 8.0, 100 mM EDTA, 100 mM NaCl, 1.0% SDS
ES Lysis Buffer	10 mM Tris-HCl pH 7.5, 20 mM NaCl, 10 mM EDTA pH 8.0, 0.5% Sarcosyl
50x TAE	50 mM Tris, 100 mM Acetic acid, 0.05 M EDTA
10x Ficoll DNA Loading Buffer	0.025% Bromophenol blue, 0.025% Xylene cyanol, 25% ficoll. Incubate at 65°C with occasionally shaking to dissolve components.
Depurination of gel	0.025 M HCl
Denaturation of gel	0.5 M NaOH, 1.5 M NaCl
Neutralization of gel	1.5 M NaCl, 1 M Tris-HCl pH 7.2, adjust pH to 7.2
20x SSC	3 M NaCl, 300 mM Sodium citrate
Denaturation of membrane	0.4 M NaOH
Neutralization of membrane	0.2 M Tris-HCl pH 7.5, 1x SSC
Hyb-Buffer	0.342 M Na_2HPO_4, 0.158 M NaH_2PO_4 pH 7.2, 7.0% SDS, 10 mM EDTA
Wash solution 1	2x SSC, 0.1% SDS
Wash solution 2	0.2x SSC, 0.1% SDS
Wash solution 3	0.1x SSC, 0.1% SDS

2.1.4 Cells and cell lines

HEK293 cell line

Human embryonic kidney (HEK) 293 cells were used to generate recombinant adeno-associated virus.

Murine embryonic stem cells

Agouti JM8A3 C57BL/6N mouse embryonic stem (ES) cells were kindly provided by AG Waisman, Institute for Molecular Medicine, University medical center, Mainz, Germany. ES cells were originally provided by Dr. R. Kühn, Helmholtz Center Munich, Germany (Pettitt et al., 2009).

Murine embryonic feeder cells

Murine embryonic feeder (EF) cells were generated and kindly provided by AG Waisman, Institute for Molecular Medicine, University medical center, Mainz, Germany.

Competent cells from *Escherichia coli*

NEB 10-beta Competent *E.coli* cells (C3019H) were purchased from New England BioLabs and used for amplification of plasmid DNA.

2.1.5 Animals

All animal experiments were performed in accordance with the German animal welfare law. Laboratory animals were bred in the animal housing facility of the Translational Animal Research Center, Mainz, under specifically pathogen free (SPF) conditions in individually ventilated cages. Mice were maintained in 12h/12h day-night cycle with proper access to food and water. The following mouse strains were used in the present study:

Wildtype

Female B6 albino mice (B6N-*Tyr*^{c}/BrdCrCrl) and female CD1 mice used for backcross to establish the RiboTracker mouse line were purchased from Charles River Laboratories (US). C57BL/6J mice from JANVIER LABS (France) were used as wild type control.

YFP-H

YFP-H mice (B6.Cg-TgN(Thy1-YFP-H)2Jrs) were obtained from the Jackson Laboratory and maintained as inbred strain. Expression of the yellow fluorescent protein (YFP) in the cerebral cortex is restricted to pyramidal neurons in layer V (Feng et al., 2000) leading to a strong labeling of the corticospinal tract axons (Carter et al., 2008). Genotyping was performed with primer pair 16072 / 15731 to detect the transgene and primer pair oIMR7338 / oIMR7339 for an internal positive control.

NEX-Cre

NEX-Cre mice express Cre recombinase in a nervous system-restricted manner including different brain areas (e.g., neocortex and hippocampus), the dorsal horn of the spinal cord and some DRG neurons (Goebbels et al., 2006). NEX is a member of the NeuroD-subfamily of neuronal basic helix-loop-helix (bHLH) transcription factors. NEX-Cre mice were kindly provided AG Zipp, Department of Neurology, University Medical Center, Mainz, Germany. Genotyping was performed with primers for the Cre expression cassette (Cre gPCR fw / Cre qPCR rv).

CamKIIα-Cre

CamKIIα-Cre mice (B6.FVB-*Tg(CamKIIalpha iCre*) express Cre recombinase under the promoter of murine calcium/calmodulin kinase II alpha (CamKIIα). Strong expression levels were seen in hippocampus, cortex, and amygdala, and lower levels were detected in striatum, thalamus, and hypothalamus (Casanova et al., 2001). The genetic background is C57BL/6J. Genotyping was performed with the primer pair iCre for neu / iCre rev neu.

Advillin-Cre

Frozen embryos of Advillin-Cre (B6;D2-Tg(Avil-cre)1Phep/Cnrm) mice were purchased from the Emma mouse repository, revitalized and transferred into CD-1 foster mother. The resulting animals were backcrossed with C57BL/6J mice. By brother-sister breeding, the Advillin-Cre mouse line was maintained as inbred strain. This mouse line contains a NLS-

Cre-pA cassette in exon 2 of the *Advillin* locus leading to a sensory neuron specific expression of Cre recombinase (Zurborg et al., 2011). Genotyping was performed with primers for the Cre expression cassette (Cre gPCR fw / Cre qPCR rv).

CNP-Cre

CNP-Cre mice were kindly provided by Eva-Maria Krämer-Albers, Institute of Molecular Cell Biology, Biology, University Mainz, Germany, and originally provided by Klaus-Armin Nave, Department of Neurogenetics, Max Planck Institute of Experimental Medicine, Göttingen, Germany (Lappe-Siefke et al., 2003). CNP-Cre mice were maintained as heterozygotes and genotyped with primers CNCEcre fw1, CNCEcre rev1, EcoIN2 and puro3. This mouse line expresses Cre recombinase under the control of 2′,3′-cyclic nucleotide 3′-phosphodiesterase (CNP) regulatory sequences leading mainly to an expression in oligodendrocytes and Schwann cells (Lappe-Siefke et al., 2003; Kaga et al., 2006).

2.1.6 Enzymes

Name	Concentration	Buffer	Company	Number
Restriction enzymes				
AgeI	10 U/µl	10x Tango	Fermentas	ER1461
AsiSI	10 U/µl	CutSmart®	New England BioLabs	R0630
BamHI	10 U/µl	10x Tango	Fermentas	ER0051
BcuI	10 U/µl	10x G	Fermentas	ER1251
EcoRI	10 U/µl	10x EcoRI	Fermentas	ER0271
EcoRI	100 U/µl	10x EcoRI	New England BioLabs	R0101M
EcoRV / Eco32I	10 U/µl	10x G	Fermentas	ER0304
FD-BamHI	-	10x FD	Fermentas	FD0054
FD-EcoRI	-	10x FD	Fermentas	FD0274
FD-NheI	-	10x FD	Fermentas	FD0973
FD-PvuII	-	10x FD	Fermentas	FD0634
FD-SmaI	-	10x FD	Fermentas	FD0663
FD-SpeI / FD-BcuI	-	10x FD	Fermentas	FD1253
NheI	10 U/µl	10x Tango	Fermentas	ER0971
SalI	10 U/µl	10x Tango	Fermentas	ÊR0641
SgsI	10 U/µl	10x Tango	Fermentas	ER1891
SmaI	10 U/µl	10x Tango	Fermentas	ER0661
XbaI	10 U/µl	10x Tango	Fermentas	ER0681
Polymerases				
FideliTaq DNA Polymerase	5 U/µl	10x Buffer	usb	
Go Taq® DNA Polymerase	5 U/µl	10x GoTaq reaction buffer	Promega	M3175
iTaq DNA polymerase (iQ™ SYBR® Green Supermix)			Bio-Rad	170-8884

Other enzymes / modifying enzymes				
Benzonase endonuclease	300 U/µl		Sigma	E1014
cOmplete, EDTA-free protease inhibitor cocktail	diluted as 25x		Roche	04 693 132 001
DNase I	10 U/µl		Roche	04 716 728 001
DNase I	diluted to 1%		Roche	11 284 932 001
Esgro complete accutase	1x		Millipore	SF006
Pepstatin	diluted to 1 mg/ml		Sigma	P5318
peqGOLD Proteinase K	20 mg/ml		peqlab	04-1076
Proteinase K	20 mg/ml		Roche	03 115 836 001
RNase A	90 U/mg		Roth	7156.1
Shrimp Alkaline Phosphatase (SAP)	1 U/µl	-	Fermentas	EF0511
T4 ligase	-	5x Buffer	Fermentas	

2.1.7 Antibodies

Primary antibody	Species	Company	Number	Application and dilution
Anti-Actin	mouse	MP Biomedicals	#691001	WB: 1:10,000
Anti-CGRP	rabbit	Sigma	C8198	IHC: 1:8,000
Anti-GFP	rabbit	Santa Cruz	sc-8334	WB: 1:1,500
Anti-GFP	rabbit	Abcam	ab290	ICC: 1:500
Anti-IB4	biotin	Sigma	L2140	IHC: 1:200
Anti-MAP2	mouse	Sigma	M4403	ICC: 1:750 IHC: 1:750
Anti-MBP	rat	Abcam	ab7349	IHC: 1:150
Anti-NF200	mouse	Sigma	N0142	IHC: 1:800
Anti-RFP	rabbit	Rockland	600-401-379	ICC: 1:500 IHC: 1:500
Anti-ribosomal P antigen	human	ImmunoVision	HPO-0100	ICC: 1:500
Anti-RPL26	rabbit	Abcam	ab59567	ICC: 1:500 IHC: 1:200 WB: 1:1,000
Anti-RPL4	mouse	Santa Cruz	sc-100838	WB: 1:100
Anti-Tuj1	mouse	Covance	MMS-435P	ICC: 1:500 IHC: 1:500

Secondary antibody	Species	Company	Number	Application and dilution
Anti-Human IgG H&L (DyLight® 550)	goat	Abcam	ab96908	ICC: 1:1,000
Anti-Mouse IgG (H+L), Alexa Fluor® 488 conjugate	goat	Invitrogen	A11001	ICC, IHC: 1:1,000
Anti-Mouse IgG (H+L), Alexa Fluor® 647 conjugate	goat	Invitrogen	A21235	ICC, IHC: 1:1,000
Anti-Rabbit IgG (H+L), Alexa Fluor® 488 conjugate	goat	Invitrogen	A-11008	ICC, IHC: 1:1,000

Anti-Rabbit IgG (H+L), Alexa Fluor® 568 conjugate	goat	Invitrogen	A-11011	ICC, IHC: 1:1,000
Anti-Rabbit IgG (H+L), Alexa Fluor® 647 conjugate	goat	Invitrogen	A-21245	ICC, IHC: 1:1,000
Anti-Rat IgG (H+L), Alexa Fluor® 633 conjugate	goat	Invitrogen	A-21094	IHC: 1:1,000
Perox-AffiniPure Dnk Anti-Rabbit IgG (H+L)	donkey	Jackson ImmunoResearch	711-035-152	WB: 1:10,000
Peroxidase-AffiniPure Goat Anti-Mouse IgG (H+L)	goat	Jackson ImmunoResearch	115-035-003	WB: 1:10,000
Streptavidin, Alexa Fluor® 647 conjugate	-	Molecular probes	S21374	IHC: 1:1,000

2.1.8 Plasmids

Name	Company or reference
R26_CAGs_IRES_EGFP	kindly provided by AG Waisman, Institute of Molecular Medicine, University medical center, Mainz, Germany; originally generated by AG Wunderlich, Institute for Genetics, Cologne, Germany (Belgardt et al., 2008)
pCMV-tdTomato clontech	Clontech Laboratories Inc., Mountain View, USA
pEGFP-N2 L4 temp	kindly provided by Y. Gouwenberg, Department of Molecular and Cellular Neurobiology, Amsterdam, Netherlands(Court et al., 2008)
pFdelta6	kindly provided by AG Lutz, Institute of Physiological Chemistry, University Mainz, Germany
pRV1	
pH21	
#106_pAM-CBA-pL-WPRE-bGHpA	
#329_pAMSyn-MCS-WPRE2-Spa	
pCRII-Rosa3' probe	kindly provided by AG Waisman, Institute of Molecular Medicine, University medical center, Mainz, Germany; originally provided by Dr. R. Kühn, Helmholtz Center Munich, Germany (Meyer et al., 2010)
pCRII-Rosa5' probe	

2.1.9 Kits

Name	Company	Number	Application
In-Fusion® HD Cloning Kit	Clontech		Cloning
Ladderman™ Labeling Kit	Takara	#6046	Radioactive labeling of testing probes for Southern Blot
Maxiprep endofree Plasmid Purification	Qiagen		Isolation of plasmid DNA
PCR Purification Kit	Qiagen		Purification of DNA fragments
peqGold Plasmid Miniprep Kit I	Peqlab	12-6942	Isolation of plasmid DNA
Pierce™ BCA protein assay kit	Thermo Scientific	23225	Protein quantitation
PureLink® HiPure Plasmid Maxiprep Kit	Invitrogen	K2100-07	Isolation of plasmid DNA

QIAquick Gel Extraction Kit	Qiagen		Gel extraction of DNA fragments
Rapid DNA Ligation Kit	Fermentas		Ligation of DNA fragments

2.1.10 Oligonucleotides

For qPCR:

Name	Sequence in 5' → 3' direction	Annealing temperature [°C]	Concentration [mM]
WPRE for	GGC TGT TGG GCA CTG ACA AT	64	100
WPRE rev	CCG AAG GGA CGT AGC AGA AG	64	100

For sequencing of plasmids:

Name	Sequence in 5' → 3' direction	Sequenced plasmid
L4 3.1	TGC AGC AGA CTT TTT TTC TTC TG	pAM-EGFP-L4
L4 5.1	CCA TGG CCT GTG CCC GTC CCC	pAM-EGFP-L4
L4GFP_Seq_3.1	AGG CTT CTT CAG CTT CTT GG	pAM-EGFP-L4, pAM-CAG-EGFP-L4
L4GFP_Seq_3.2	AAT GAA AGC CAT ACG GGA AG	pAM-EGFP-L4, pAM-EGFP, pAM-CAG-EGFP-L4, pAM-CAG-EGFP
L4GFP_Seq_5.1	GTC GTG TCG TGC CTG AGA G	pAM-EGFP-L4, pAM-EGFP
L4GFP_Seq_5.2	AGC CAA ATC GGA GAA GAT TG	pAM-EGFP-L4, pCMV-L4-tdTomato, pAM-CAG-EGFP-L4
p106 forward	ACA GCT CCT GGG CAA CGT G	pAM-CAG-EGFP-L4, pAM-CAG-EGFP
R26_Seq_3.1	AGG GGA TCG GCA ATA AAA AG	R26_CAGs_IRES_EGFP, R26_CAGs_L4-tdTomato
R26_Seq_3.3	CGC CCA TCT TCT AGC GAA T	R26_CAGs_L4-tdTomato
R26_Seq_5.1	CCC CTC GTG ATC TGC AAC	R26_CAGs_IRES_EGFP, R26_CAGs_L4-tdTomato
R26_Seq_5.2	GCC ATA CCA CAT TTG TAG AGG TT	R26_CAGs_IRES_EGFP, R26_CAGs_L4-tdTomato
tdTomato_Seq_3.1	GGG AGG TGT GGG AGG TTT T	pCMV-tdTomato clontech, pCMV-L4-tdTomato
tdTomato_Seq_5.1	CGT CAA TGG GAG TTT GTT TTG	pCMV-tdTomato clontech, pCMV-L4-tdTomato

For PCR amplification during cloning:

(restriction sites are underlined)

Name	Sequence in 5' → 3' direction (restriction site)	Annealing temperature [°C]	Product size [bp]
L4+Tomato_IF_5.1	CGT CAG ATC CGC TAG CCC CGC CAC CAT GGC TTG T	60	1311
L4+Tomato_IF_3.1	GTC CGG TAG CGC TAG CCG ACA TGC AGC AGA CTT T		
L4+Tomato_5.1	TAT AGG CGC GCC GCT GGT TTA GTG AAC CGT CAG (SgsI)	61	2838
L4+Tomato_3.1	AAA ACC CGG GCA AAT GTG GTA TGG CTG ATT ATG (SmaI)		

L4GFP_2a	GCT GACTAG TTG AAC CGT CAG ATC CGC TAG (SpeI)	50	2120
L4GFP_2b	AAA AGA TAT CCA AAT GTG GTA TGG CTG ATT ATG A (EcoRV)		

For Southern blot testing probe:

Name	Sequence in 5' → 3' direction	Annealing temperature [°C]	Product size [bp]
rspNeo4	GGC TAT TCG GCT ATG ACT GGG C	58	624
rspNeo5	GGG TAG CCA ACG CTA TGT CCT G		

For genotyping PCRs:

Name	Sequence in 5' → 3' direction	Annealing temperature [°C]	Product size [bp]
RosaFA	AAA GTC GCT CTG AGT TGT TAT	58	603 (WT) + 241 (Tg)
RosaRA	GGA GCG GGA GAA ATG GAT ATG		
SpliAcB	CAT CAA GGA AAC CCT GGA CTA CTG		
Cre gPCR fw	GAA CGC ACT GAT TTC GAC CA	58	200
Cre gPCR rv	AAC CAG CGT TTT CGT TCT GC		
16072	ACA GAC ACA CAC CCA GGA CA	60	415
15731	CGG TGG TGC AGA TGA ACT T		
oIMR7338	CTA GGC CAC AGA ATT GAA AGA TCT	60	324
oIMR7339	GTA GGT GGA AAT TCT AGC ATC ACT C		
iCre for neu	ATG CTC CTG TCT GTG TGC AG	58	435
iCre rev neu	ATC AGC ATT CTC CCA CCA TC		
CNCEcre fw1	GCC TTC AAA CTG TCC ATC TC	56	496 (WT) + 894 (Tg)
CNCEcre rev1	AAA TCA GGT GGA AGG CA		
EcoIN2	GAT GGG GCT TAC TCT TGC		
puro3	CAT AGC CTG AAG AAC GAG A		

All primers were purchased from Eurofins Genomics.

2.1.11 DNA ladder and protein marker

DNA ladder

Name	Company	Fragment sizes [bp]
GenerRuler 1kb Plus DNA Ladder, ready-to-use	Thermo Scientific, #SM1334	75, 200, 300, 400, 500, 700, 1000, 1500, 2000, 3000, 40000, 5000, 7000, 10000, 20000

Protein marker

Name	Company	Protein sizes [kDa]
PageRuler Prestained Protein Ladder	Thermo Scientific, #26616	10, 15, 25, 35, 40, 55, 70, 100, 130, 170

2.1.12 Consumable and implements

Product	Company
6-, 12-, 24-, 96-well-plates	Greiner bio-one
Amersham Hybond N+ membrane	GE Healthcare
Amicon Ultra-4 Centrifugal Filter Devices	Merck Millipore
Biomax cassette with intensifying screens	Kodax BioMax TranScreen-HE

Carestream MS Biomax film (18x24cm)	Kodak
Cell scraper	Greiner bio-one
CELLSTAR® plates 60x15mm	Greiner bio-one
Coverslips 12mm	neoLab
Dissection tools, diverse	Fine Science Tools
Embedding mold	Polysciences, Inc.
Eppendorf tubes, 0.5 ml, 1.5 ml, 2.0 ml	Greiner bio-one
Falcon tubes, 15 ml, 50 ml	Greiner bio-one
Filter, 0.2 µm	Pall Live Science
Flasks, 175 cm^2	Greiner bio-one
Freezing container	Cryo-SafeTM Cooler, bel-art products
Gloves	Microflex® Xceed
HiTrap Heparin Column	GE Healthcare
illustra MicroSpin G-50 Columns	GE Healtcare Life Science
Menzel-Gläser Microscope slides	VWR
Menzel-Gläser Superfrost® plus microscope slides	Thermo Scientific
Microtube with screw cap	Greiner bio-one
Multiplate™ PCR Plates 96-well, clear + cover	BioRad
Needles, Microlance™3	BD Bioscience
Nitrocellulose membrane, 0.45 µm	Biorad
Nunclon Δ Multidishes 4 well round	Sigma
Parafilm	PM-996
Pasteur pipettes	Roth
PCR reaction tubes, single or 8-strips	Starlab
Pipette tips with or without filter	Starlab
Pipettes, 5 ml, 10 ml, 25 ml, 50 ml	Greiner bio-one
Plates, 10cm, 15 cm	Greiner bio-one
Razor blade	Wilkinson
Super RX, 13x18	Fujifilm
Syringe, 60ml	Braun
Syringes Omnifix®, Venofix®	Braun
TC10 counting slides dual chamber	BioRad

2.1.13 Instruments

Instrument	**Company**
Aspiration system Vacusafe	Integra
Cell incubation shaker Multitron Standard	Infors HT
Centrifuge Biofuge fresco	Thermo Scientific
Centrifuge Fresco21	Thermo Scientific
Centrifuge Multifuge X1R	Thermo Scientific
Clean bench HERAguard	Thermo Scientific
Confocal microscope for SMLM, equipped with LuxX diode laser (Omicron Laserage)	custom-built
Confocal microscope SP5	Leica
Cryostat CM 1900	Leica
Film processor CP1000	Agfa
Fireboy	IBS Integration Bioscience
Freezer Liebherr Comfort or Premium	Liebherr
Fridge Liebherr Comfort	Liebherr
Heating plate SP2	Medax
Incubator Heratherm	Thermo Scientific
Incubator Incusafe	Sanyo
Inverted microscopes CKX31	Olympus

Inverted microscopes IX51	Olympus
Isoflurane Vaporizer	Rothacher &Partner
Light microscope BX51	Olympus
Magnetic stirrer MR Hei-Standard	Heidloph
Microcentrifuge MiniStar silverline	VWR
Microwave	Sharp
Mini-Protean® Tetra System gel chamber	BioRad
PCR cycler peqSTAR 96Universal	peqlab
pH meter	Mettler Toledo
Pipette aid Accu-jet pro	Brandt
Pipettes	Eppendorf Research plus
Power supply Consort EV231	peqlab
Real-time system CFX Connect TM	BioRad
Safety cabinet MSC-Advantage	Thermo Scientific
Scale Acculab	Sartorius group
Scale CPA1003S	Sartorius
Shaker IKA-Vibrax-VXR, Typ VX7	Janke&Kunkel
Shaker Promax 2020	Heidolph
Spectrometer Infinite M200PRO	Tecan
Spectrophotometer NanoDrop 2000c	peqlab
Stereomicroscope S6E	Leica
Stereomicroscope system A60	Leica
Syringe pump PHD 2000 infusion	Harvard apparatus
TC10 automated cell Counter	BioRad
Thermomixer Comfort	Eppendorf
ThermoMixer F1.5	Eppendorf
UV detection system Fusion Fx7	peqlab
Vibratome Microm HM 650V	Thermo Scientific
Vortex-Genie 2	Scientific Industries
Vortex-genie mixer 7-2020	neoLab
Water bath AQUAline AL18	Lauda
Water bath W22	Medingen
Wet blot electrophoretic transfer cell	BioRad

2.1.14 Software

Adobe Photoshop CS5

cellSens Dimension 1.6

CFX Manager, Version 3.1.1517.0823

EMBOSS Pairwise Sequence Alignment (ttp://www.ebi.ac.uk/Tools/psa/emboss_water/nucleotide.html)

EndNote X7

FinchTV Version 1.4.0

FusionCapt Advanced Fx7 software

GraphPad Prism 5

ImageJ (http://imagej.nih.gov/ij/) with the following plugins:

- heat map (http://www.samuelpean.com/heatmap-histogram/)
- Nnd plugin (https://icme.hpc.msstate.edu/mediawiki/index.php/Nearest_Neighbor_Distances_Calculation_with_ImageJ)
- RG2B plugin (http://rsb.info.nih.gov/ij/plugins/rg2bcolocalization.html)

In-Fusion® Primer Design Tool
(http://bioinfo.clontech.com/infusion/convertPcrPrimersInit.do)
MATLAB
Microsoft Excel 2010
Microsoft Word 2010
Nucleic Acid NanoDrop 2000/2000c 1.6.198
Tecan i-control 3.7.3.0

2.2 Methods

2.2.1 Cell culture methods

2.2.1.1 HEK293 cells

2.2.1.1.1 Cultivation of HEK293 cells

Frozen HEK293 cells were thawed in the water bath and the cell suspension was quickly mixed with prewarmed growth medium. Cells were pelleted at 1500 rpm for 2 minutes and plated in 10 ml growth medium for culture at 37°C, 5% CO_2. Every 3-5 days, the adherent HEK293 cells had reached confluence and were passaged. For this, cells were washed with 1x PBS and trypsinized for 1-2 minutes with 2 ml trypsin solution. 10 ml growth medium were added to stop trypsinization and cells were pelleted at 800 rpm for 5 minutes. After resuspension in growth medium, 10-20% of the cell suspension was used for subculture.
For long-term storage, HEK293 cells were trypsinized and pelleted as describe before. The cells were resuspended in 4°C cold freezing solution at a concentration of 2 x 10^6 cells/ml, aliquoted, and frozen at -20°C. For long-term storage, cells were transferred to the liquid nitrogen tank.

2.2.1.1.2 Lipfectamine-mediated transfection

The day before transfection (day 0), HEK293 cells were plated at a concentration of 1.0 x 10^5 cells per well in a 6-well-plate. The next day (day 1), 1-3 µg of pDNA were diluted in 125 µl DMEM and vortexed. In parallel, 5 µl Lipofectamine2000 were mixed with 125 µl DMEM and incubated for 4.5 minutes. Both solutions were combined, mixed, and incubated for 20 minutes at room temperature (RT). 750 µl DMEM + 10% FBS were added and this transfection mix was then used to replace the growth medium of the cells (1 ml/well). Cells were cultivated at 37°C, 5%CO_2. The day after, 1 ml growth medium was added to each well and the culture continued for another 24 h. Microscopic analysis was performed on day 3 with an Olympus IX51 inverted microscope. For protein extraction and Western blot analysis, cells were washed once with 1x PBS, PBS was removed, the 6-well-plate was snap frozen in liquid nitrogen and stored at -80°C.

2.2.1.1.3 Production of recombinant adeno-associated virus

Recombinant adeno-associated viruses (rAAVs) were produced as described by McClure et al. (2011). For the simultaneous production of two virus batches, HEK293 cells from three confluent 175 cm^2 flasks were trypsinized and divided over ten 15 cm^2 plates. At a confluence of around 70%, the growth medium of the cells was replaced by pre-warmed starvation medium 3 h before transfection. For the transfection of five dishes (yielding one virus batch), 12 ml dH_2O were mixed with 1.65 ml 2.5 M $CaCl_2$. The plasmid mix containing

62.5 µg AAV shuttle plasmid, 125 µg pFdelta6, 32.5 µg pRVI, and 32.5 µg pH21 was added and the complete transfection mixture was filtered through a 0.2 µm syringe filter. Whilst vortexing the solution vigorously, 13 ml 2x HEBS buffer were quickly added with a pipette gun and vortexing continued for further 10-20 seconds. The transfection solution was incubated for 2-3 minutes (RT) until a fine, white precipitate became visible, and then added dropwise to the cells (5 ml per plate). 16 h after transfection, the growth medium was renewed. 60-65 h after transfection, cells were trypsinized and harvested as described before while using a volume of 25 ml per 15 cm^2 plate. The cell pellet was resuspended in 50 ml resuspension buffer and divided over two falcon tubes. 1.25 ml freshly prepared 10% sodium deoxycholate (in dH_2O) and 4.25 µl Benzonase endonuclease (300 U/µl) were added to each 25 ml cell suspension to lyse the cells. The falcon tube was mixed thoroughly by inverting. After 1 h incubation at 37°C, falcon tubes were centrifuged at 4000 rpm for 10 minutes to pellet the cell debris. The supernatant containing the virus particles was transferred into fresh falcon tubes and frozen at -20°C. To purify the virus particles from any debris, the frozen supernatants were thawed and centrifuged again at 4000 rpm for 10 minutes at 4°C. In the meantime, a 1 ml HiTrap Heparin Column was fixed on a 60 ml syringe, inserted into a pump, and 12 ml resuspension buffer were pressed with a flow rate of 1 ml/min through the column for equilibration. Next, the prepared supernatant was loaded onto the column at 1 ml/min allowing the virus particles to bind to the heparin surface of the column. The column was washed manually with 3 ml washing solution 1 and 1 ml of washing solution 2 and 3, respectively. To eluate the virus, three elution buffers with increasing salt concentration were applied subsequently (1.5 ml of elution buffer 1, 3 ml of elution buffer 2, 1.5 ml of elution buffer 3) and the eluate was transferred to a small Amicon concentrator. Since the concentrator has a capacity of 4 ml, the following centrifugation step at 3300 rpm for 2 minutes were performed twice to concentrate the total volume of 6 ml eluate to around 250 µl. The virus solution was filtered through a small 0.2 µm filter and aliquoted (20 µl each) for storage at -80°C.

2.2.1.2 Embryonic stem cells

All work with ES cells was performed at the Institute of Molecular Medicine, university medical center of Mainz, Germany.

2.2.1.2.1 Expansion of embryonic feeder cells

A frozen vial of murine EF cells of passage 0 (= EF0) was thawed in the 37°C water bath and the cell suspension was quickly mixed with 6 ml EF medium. Cells were pelleted at 1000 rpm for 3 minutes and resuspended in the final plating volume of 60 ml EF medium to plate 20 ml in three 20 cm^2 dishes (passage 1 = EF1). Cells were cultivated at 37°C, 10% CO_2 and EF medium was renewed the next day.

Three to four days after plating, cells were confluent and needed to be passaged. Each plate was washed two times with PBS and cells were trypsinized with 5 ml Trypsin solution per plate for 4 minutes at 37°C. 10 ml EF medium was added to stop trypsinization, cells from all three dishes were pooled and pelleted at 1000 rpm for 3 minutes. After resuspension in EF medium (600 ml total), cells were split in a ratio of 1:3 by plating them onto ten 20 cm^2 dishes (EF2) and cultivated at 37°C, 10% CO_2. Medium was exchanged the following day. Having again reached confluence three to five days later, cells were split once more 1:3 to end up with 30 plates of embryonic feeder cells of passage 3 (EF3).

2.2.1.2.2 Preparation of MMC-treated EF cells

Confluent EF3 cells were treated with the cytostatic agent Mitomycin C to inhibit cell division. For this, EF medium was replaced by 10 ml inactivation medium containing 0.01 mg/ml MMC and cells were incubated for 2-4 h. Cells were washed with PBS, trypsinized and pelleted as described before, and finally pooled in EF medium. The resulting MMC-treated cells were either plated onto 10 cm^2 dishes at a concentration of 3.5 x 10^6 cells per plate to form a feeder layer for ES cells, or they were frozen at a concentration of 4 x 10^6 cells per vial for later use.

For long-term storage, a defined amount of MMC-treated cells was pelleted, resuspended in cool EF medium on ice and mixed with 2x freezing solution to a final concentration of 4 x 10^6 cells/ml. Cell suspension was aliquoted into cryo vials (1 ml) and were placed in a precooled (-20°C) freezing container at -80°C. Over 24 h later, the vials were transferred to liquid nitrogen for long-term storage.

2.2.1.2.3 Expansion of ES cells

The thawing and splitting of ES cells was performed as described for EF cells with the following differences: ES cells were pipetted with fire-polished Pasteur pipettes, ES medium was used and ES cells grew on dishes coated with MMC-treated feeder cells (3.5 x 10^6 EF cells per plate, plated the day before). Growth medium was renewed every day and two hours before splitting.

2.2.1.2.4 Electroporation and selection of ES cells

First, ES cells were trypsinized, pelleted and resuspended in PBS to a final concentration of 13 x 10^6 cells/ml. 800 µl of cell suspension (1 x 10^7 cells) was mixed with 20-30 µg linearized DNA (dissolved in PBS) and incubated on ice for 10 minutes. The mixture was transferred into a pre-cooled cuvette and pulsed at 240 V, 500 µFD. After incubation on ice for 10-15 minutes, cells were mixed with 50 ml ES medium and plated onto five 10 cm^2 feeder dishes at a concentration of 2 x 10^6 cells per plate. In parallel, control plates with non-electroporated cells consisting of 10%, 25%, and 50% of cell numbers of treated cells were prepared to compare the survival rate after electroporation and during selection. 24-48 h

after electroporation, ES cells were cultivated for 8-12 days in Genetecin ES medium to select Neo-resistant colonies. The plate with Neo-resistant colonies was washed twice with PBS and filled with 8 ml PBS/PS. Single colonies were picked under a microscope and transferred to a round-bottomed 96-well plate with 50 µl trypsin solution for ES per well for trypsinization. Trypsin reaction was stopped by adding 100 µl ES medium and cells were plated into a flat-bottomed 96-well plate coated with feeder cells (2-2.5 x 10^6 feeder cells per 96-well plate). Growth medium was renewed every day (100-250 µl per well). About 5 days after picking, most colonies had reached confluence, hence, each 96-well plate was split into three new 96-well plates, two of which were coated with MMC-feeders (for blastocyst injections) and one was coated with 0.1% gelatin in PBS (for Southern blot). The ES cells were cultivated for three more days, then, the two plates with feeder cells were trypsinized, mixed with 2x freezing medium, frozen for 30 minutes at -20°C and finally transferred to -80°C for long-term storage until used for blastocyst injections. At the same time, ES cells grown on gelatin-coated plates were split 1:4 or 1:3 into new gelatin-coated plates to increase the copy number of each clone. As soon as the colonies started to overgrow, the plates were washed once with PBS and frozen on -20°C for later analysis by Southern blot.

2.2.1.2.5 Expansion of ES cells for blastocyst injection

The 96-well plate containing the positive colony chosen for blastocyst injection was thawed and the ES cell clone was expanded at different concentrations on 10 cm feeder plates. During the first splitting, feeders were separated by several steps of 20 minutes plating on untreated 10 cm plates. The floating ES cells were finally plated in 2i medium into a gelatin-coated 6-well plate. On the day of injection, ES cells were trypsinized with accutase, washed once in EF medium and ultimately resuspended in EF medium containing 20 mM HEPES in a 15 ml falcon tube at 1-2 x 10^6 cells/ml. Cells were kept on ice and directly delivered to Dr. Leonid Eshkind (Transgenic Facility Mainz) for blastocyst microinjections.

2.2.1.3 Culture of primary dorsal root ganglia

2.2.1.3.1 Isolation of dorsal root ganglia

Mice were decapitated and the spinal cord was extracted or moved aside so that the DRGs became accessible. Using micro forceps, all DRGs of one animal were extracted and collected in a plate filled with HBSS. Surrounding connective tissue and nerve fibers were removed from each DRG by cutting with micro scissors. Trimmed DRGs were then either plated as explant on coverslips or used for dissociated cultures.

2.2.1.3.2 DRG explant culture (neonatal or adult)

One to two trimmed DRGs of neonatal (P2-5) or adult mice were placed onto each coverslip in a 4-well plate coated with PDL (0.5 mg/ml in dH_2O) and Laminin (1 µg/ml in Neurobasal). Explants were cultivated in 190 µl DRG medium supplemented with 10 ng/ml NGF. Medium was renewed every day and axon outgrowth was controlled under an inverse microscope. After 4-6 days *in vitro* (DIV), DRG explants were fixed for 10 minutes with 4% PFA, washed twice with PBS and stored in PBS at 4°C until immunocytochemistry (ICC) was performed.

2.2.1.3.3 Adult dissociated DRGs

To obtain a dissociated culture, the previously described protocol for adult CNS neurons (Brewer and Torricelli, 2007) was adapted for adult DRGs.

All trimmed DRGs from one mouse were collected in a 6 cm plate in HBSS. To digest the DRGs, HBSS was replaced by 2 ml of 0.1% collagenase diluted in Hibernate A minus calcium and the plate was incubated for 40 minutes at 37°C, 5% CO_2. In the meantime, a density gradient consisting of four layers with different densities of OptiPrep 1.32 diluted in HABG was prepared in a 15 ml falcon tube (Table 1).

Table 1: Composition of density gradient for enrichment of neurons.
Each layer was prepared separately in an Eppendorf tube and subsequently pipetted one on top of the other in a 15 ml falcon tube.

Layer	OptiPrep 1.32 [µl]	HABG [µl]	Total [ml]
1 (bottom)	173	827	1.000
2	124	876	1.000
3	99	901	1.000
4 (top)	74	926	1.000

After the digestion, DRGs were transferred with a pipette on top of 5 ml HA in a 15 ml falcon tube to remove the collagenase. As soon as the DRGs have sunken to the bottom, the medium was replaced with 2 ml fresh HA and cells were triturated by pipetting up and down 20 times. The cell suspension stood for 1 minute, then, the supernatant was transferred to a new 15 ml falcon tube. Trituration was repeated once more with 2 ml HA and the final supernatant of 4 ml was applied on top of the prepared density gradient. By centrifugation at 800 x g for 15 minutes, neurons were enriched in layer 2 and 3 and simultaneously separated from cell debris and glia cells. Layer 2 and 3 were transferred into a new tube, mixed with 5 ml HA to dilute the gradient material and cells were pelleted at 400 x g for 2 minutes. This washing step was repeated once more and neurons were finally resuspended in 100 µl trituration solution. The cell suspension was diluted with DRG medium supplemented with 10 ng/ml NGF to the final plating volume and cells were plated onto PDL- and laminin-coated (see above) coverslips. For viral transduction of dissociated DRG neurons, 1×10^8 genomic copies of rAAVs were added into the medium. Medium was renewed every other day and at 4-6 DIV, cells were fixed as described above, and stored in PBS at 4°C for ICC.

2.2.1.4 Culture of primary hippocampal neurons and cortex explants

2.2.1.4.1 Isolation and cultivation of dissociated hippocampal neurons

Primary embryonic hippocampal neurons were prepared as described inBrandt et al. (2007).Briefly, adult pregnant mice werekilled by cervical dislocation and embryos (E17-18) were isolated and transferred into an ice-cold plate filled with HBSS. The brain of each embryo was extracted, cerebral membranes were removed and the hippocampi were dissected and collected in a falcon tube with HBSS. Hippocampi were washed once with HBSS and incubated in 9 ml HBSS mixed with 100 µl Trypsin-EDTA solution and 10 µl 0.1% DNase I for 30 minutes at 37°C (water bath). Hippocampi were transferred into 1 ml plating medium and triturated by pipetting up and down (20-30 times) with a fire-polished glass pipette. Cells were counted and plated onto coverslips that have been incubated with PLL coating solution the day before and washed twice with PBS before plating. For ICC,1.5 $x10^5$ cells per coverslip were plated in a 24-well plate. 4 h after plating, cells were carefully washed with PBS and maintained in Neurobasal medium at 37°C, 5% CO_2. Medium was renewed every other day. For viral transduction at day 3, 1 x 10^8 to 1 x 10^{10} genomic copies of rAAVs were added into the medium of each well and culture continued. After 8-10 days *in vitro*, cells were fixed with 4% PFA for 10 minutes, washed twice with PBS and stored in PBS at 4°C for ICC.

2.2.1.4.2 Culture of cortex explants

Previously described protocols (Liu et al., 2005; Niquille et al., 2009) were adapted and modified to obtain explants of motor cortex layer V.

Neonatal mice (P0-P5) were decapitated and the brains were isolated and transferred into a tissue-embedding mold filled with warm 3% low melting point agarose diluted in dissecting medium. Each brain was cut in coronal sections and 4-5 slices of 250 µm thickness comprising the motor cortex were collected in dissection medium on ice. Layer Vof the motor cortex was cut out, divided in half, and every explant was placed separately onto a PDL-/laminin-coated coverslip (see above) in a 4-well plate. Explants were cultivated in 190 µl DRG medium at 37°C, 5% CO_2 and medium was renewed every other day. At DIV 4-6, cortex explants were fixed as described above, and stored in PBS at 4°C for ICC.

2.2.1.5 Immunocytochemistry (ICC)

Coverslips were washed twice with PBS and permeabilized for 10 minutes with 0.3% Triton-X in PBS. After three washing steps with PBS, antibody solution (1x TBST+ 0.2% Triton-X) with 15% NGS was applied for 1 h to block unspecific binding site before cells were incubated with the first antibody diluted in antibody solution with 5% NGS overnight at 4°C. The next day, cells were washed three times with 1x TBST, secondary antibody diluted in antibody solution with 1% BSA was added for 1-2 h, then cells were washed again with

1x TBST, stained with DAPI (1:10.000 in 1x TBST) for 10 minutes, washed and mounted with FluorSave™ Reagent upside-down onto glass slides. Having dried overnight at RT, slides were stored at 4°C for microscopic analysis.

2.2.2 Cytogenetic analysis

2.2.2.1 Chromosome preparation of ES cell clones

ES cell clones were cultivated on 10 cm gelatin-coated dishes and used for chromosome preparation while growing in an exponential stage. 0.2 µg/µl colcemid was added to the culture medium for 1 h to arrest cells in metaphase. Cells were trypsinized as described before and pelleted in a 15 ml falcon tube. Supernatant was removed except for about 0.5 ml and cells were resuspended by flicking the tube. 10 ml hypotonic solution (75 mM KCl) was added dropwise while gently flicking the tube, followed by incubation for 10 minutes at RT. Cells were pelleted at 1100 rpm for 10 minutes and resuspended in 0.5 ml supernatant. 2-3 ml fixative (methanol and acetic acid mixed 3:1) was added dropwise while gently flicking the tube. The tube was filled up with fixative (15 ml in total) and placed at -20°C for 30 minutes. Cells were pelleted at 1500 rpm for 10 minutes and the fixation step was repeated once or twice to finally obtain the cells resuspended in 15 ml fixative. The samples were stored at -20°C until sent for analysis. For transportation, cells were pelleted again, resuspended in 1 ml fixative and transferred into a microtube with screw cap.

2.2.2.2 Mouse “quick test” and chromosome counting

The cytogenetic analysis of ES cell clones was performed by ChromBios GmbH (Rabuling, Germany; now located in Nussdorf, Germany). A “quick test” analysis based on fluorescence *in situ* hybridization (FISH) tested for the ploidy of chromosomes 8, 11, X, and Y. Additionally, samples were stained with DAPI and chromosomes were counted microscopically. A more detailed description of the standard protocol used by ChromBios GmbH is available online on their homepage (www.chrombios.com).

2.2.3 Cloning procedure

Figure 5 outlines the general steps of a cloning procedure. Detailed protocols for each step are described in the corresponding method sections below.

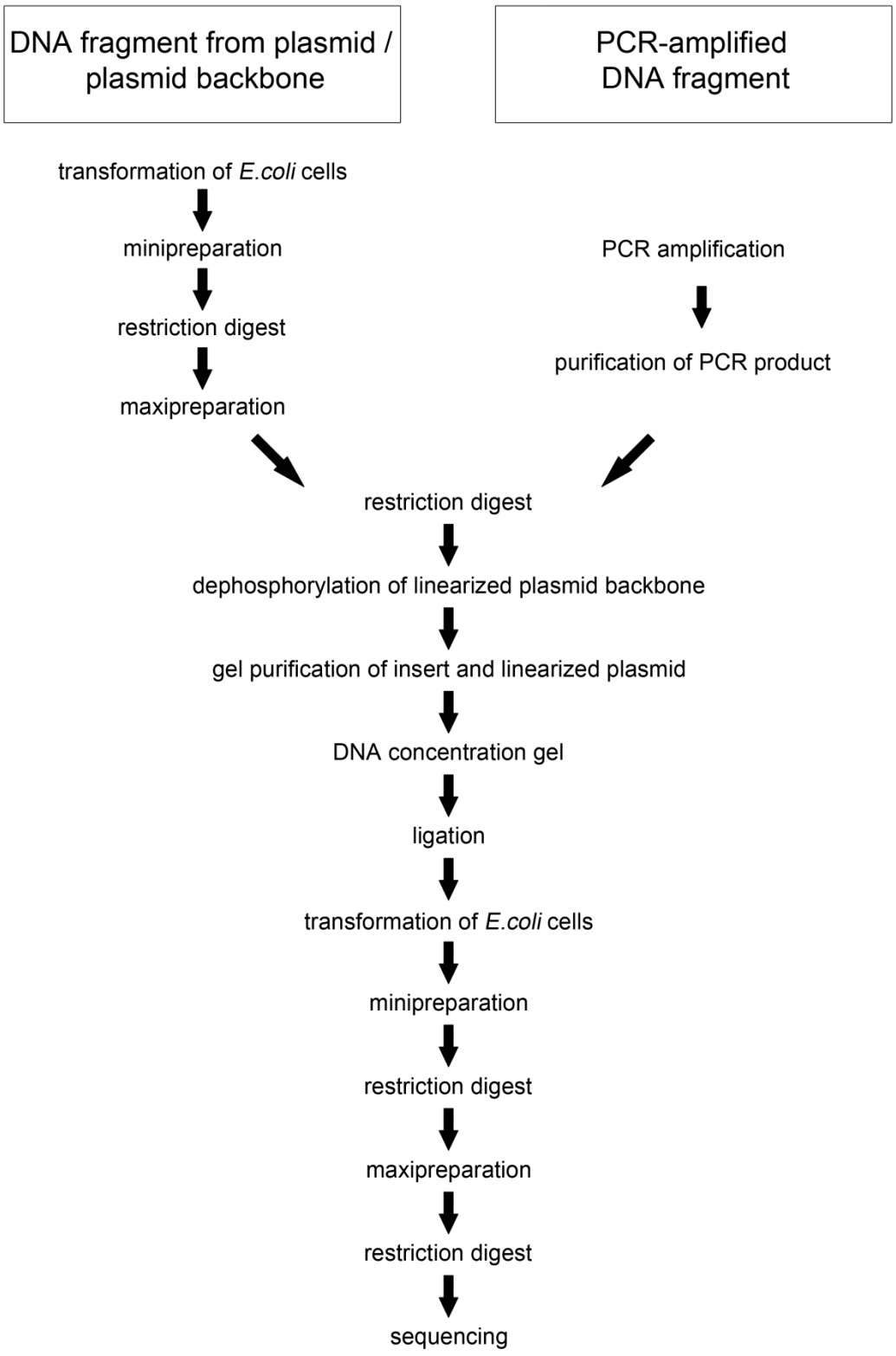

Figure 5: Flow chart of a general cloning procedure.

2.2.4 Microbiology methods

2.2.4.1 Transformation of competent *E.coli* cells

One vial of *E.coli* cells was thawed on ice for 10 minutes, 5 µl of 1 pg-100 ng of plasmid DNA diluted in water were added and the tube was flicked 4-5 times to mix. After incubation on ice for 30 minutes, cells were heat shocked for 30 seconds at 42°C and again placed on ice for 5 minutes. 500 µl of SOC medium was pipetted into the mixture before the cells were incubated for 1 h at 37°C while shaking at 1200 rpm. For selection of successfully transformed cells, different volumes (20 µl, 50 µl, 100 µl, and the remaining volume) of the mixture were spread on pre-warmed LB agar plates containing the required antibiotics (kanamycin or ampicillin, 50 µg/ml). These selection plates were incubated overnight at 37°C. The amount of grown colonies was evaluated the following day and DNA was isolated from single colonies for further analysis as described below.

2.2.4.2 Isolation of plasmid DNA from *E.coli* cells

2.2.4.2.1 Minipreparation

1.5 ml of LB medium with 50 µg/ml antibiotics in a 2 ml tube (with a whole in the cap) were inoculated with *E.coli* carrying the desired plasmid and grown at 37°C, 1200 rpm overnight. In parallel, the same colonies were scratched out on a control agar plate to obtain a reserve of the colonies for further use. Plates were incubated at 37°C overnight. The following day, cells of the suspension were pelleted and the plasmid DNA (pDNA) was isolated using the peqGold Plasmid Miniprep Kit I according to manufacturer's protocol. pDNA was eluted in water and the final concentration was measured with the NanoDrop spectral photometer. For control analysis, the isolated pDNA was digested with restriction enzymes.

2.2.4.2.2 Maxipreparation

In order to obtain higher amounts of pDNA, maxipreperations were performed similarly to the above-mentioned minipreparation. 200 ml of LB medium supplemented with 50 µg/ml antibiotics in a 500 ml Erlenmeyer flask were inoculated with *E.coli* carrying the desired plasmid and incubated at 37°C, 220 rpm overnight. The following day, the pDNA was extracted with a Maxiprep Kit according to manufacturer's protocol. Mostly, the Maxiprep endofree Plasmid Purification Kit was chosen, only pDNA used for rAAV production was isolated with the PureLink® HiPure Plasmid Maxiprep Kit. pDNA was eluted in water and the final concentration was measured with the NanoDrop spectrophotometer. For control analysis of the isolated pDNA, restriction digest and sequencing was performed.

2.2.4.3 Storing of bacterial samples

For long term storage of one colony of *E.coli* cells carrying the desired plasmid, 850 µl bacteria solution of overnight culture (e.g., from maxipreparation before DNA isolation) were mixed with 150 µl glycerol in an 1.5 ml Eppendorf tube and frozen at -80°C. This glycerol stock was used for direct inoculation of LB medium for maxipreparation.

2.2.5 Molecular biology methods – DNA analyses

2.2.5.1 Standard polymerase chain reaction

The polymerase chain reaction (PCR) is a molecular biology technique to amplify DNA fragments in a high copy number. To specify the DNA sequence of interest, oligonucleotide primers are selected that bind complementary to the 3' end of each single-strand of DNA framing the target region. The PCR is based on thermal cycling that compromises three main steps which are repeated 30-40 times to achieve an exponential amplification of the target DNA (Table 2). During the first phase of the PCR, the double-stranded DNA is separated at 94°C (denaturation) allowing the primers to bind to the single-stranded DNA in the course of the following annealing step. Starting from the primers, the DNA polymerase synthesizes a new DNA strand complementary to the template strand in 5' to 3' direction (elongation) that will again be used as template in the next cycle.

Table 2: standard PCR program

reaction	temperature [°C]	duration [mm:ss]	
initial denaturation	94	02:00	
denaturation	94	00:30	35 cycles
annealing	primer-dependent	00:30	
elongation	68 or 72 (depending on DNA polymerase)	depends on product size (~ 1 kb per minute)	
final elongation	68 or 72	05:00	

Dependent on the application, 20 µl or 50 µl reaction mixture were used with following components:

Table 3: standard PCR reaction mixture

component	volume for 20 µl reaction mixture	volume for 50 µl reaction mixture	final concentration
10x Buffer	2.0 µl	5.0 µl	1x
10 mM dNTPs	0.4 µl	1.0 µl	200 µM
10 µM forward primer	0.4 µl	1.0 µl	0.2 µM
10 µM reverse primer	0.4 µl	1.0 µl	0.2 µM
DNA polymerase	0.2 µl	0.75 µl	0.05-0.075 U/µl
DNA template	variable	variable	< 1 µg
MQ water	to 20 µl	to 50 µl	-

To amplify DNA fragments for cloning, 0.75 µl FideliTaq polymerase were used with additional 1.0 µl 25 mM $MgCl_2$ at an elongation temperature of 68°C.

For genotyping, 1 µl lysate was mixed with 25 µl reaction mixture containing 1x GoTaq reaction buffer with 0.38 µM of each primer, 0.1 mM dNTPs (10 mM each), and 0.125 µl GoTag polymerase.

2.2.5.2 Quantitative polymerase chain reaction

For a standard quantitative PCR (qPCR), the iQ™ SYBR® Green mix (Bio-Rad) was used which included most necessary components like dNTPs, polymerase, $MgCl_2$ and SYBR® Green, for the polymerase chain reaction. Forward and reverse primer were added to the master mix at a final concentration of 100 nm or 200 nm (depending on the primer pair). In a 96-well plate, 15 µl master mix and 5 µl template DNA were mixed per well. To correct for pipetting inaccuracy, each sample was prepared in triplicates. The qPCR reaction was performed with a standard program (Table 4) and final analysis was done with the CFX Manager software and Excel 2010. To enable a quantitative statement of the analyzed DNA sample, a known standard with a defined number of DNA copies for standard curve for normalization ran in parallel on the same plate.

Table 4: standard qPCR program

reaction	temperature [°C]	duration [mm:ss]	analysis	
initial denaturation	95	03:00		
denaturation	95	00:10		40 cycles
annealing & elongation	primer-dependent	00:45	plate read	
denaturation	95	01:00		
cooling	55	01:00		
Melt curve	55-95 (0.5 increment after each step)	00:10	plate read	80 cycles

2.2.5.3 Agarose gel electrophoresis

To separate DNA fragments by their sizes, agarose gel electrophoresis was performed. The simultaneous run of a DNA marker allowed the estimation of the size and molecular weight of the DNA fragments. Visualization of the DNA fragments was achieved by adding an intercalating agent (ethidium bromide or Midori Green) that works as a fluorescent tag and was visualized by ultraviolet (UV) light.

A 1% agarose gel (diluted in 1x TAE and mixed with ethidium bromide or Midori Green; for Southern blot: 0.8% agarose gel) was prepared in a cast and placed into a running chamber filled with 1x TAE buffer. DNA samples were mixed with 6x loading buffer and loaded onto the gel. A DNA ladder was added in an extra slot. The electrophoresis was performed at 110 V for 45-60 minutes (restriction analysis of pDNA) or overnight at 30 V (for Southern blot). Afterwards, the gel was photographed with an UV transilluminator.

2.2.5.4 Purification of DNA fragments

In between of two different applications and especially before a ligation step during the cloning procedure, DNA fragments were purified. A column-based method was chosen for PCR-amplified DNA fragments. After restriction digests, another purification technique was necessary as the mixture contained not only the DNA fragment of interest but also additional DNA segments e.g., the plasmid backbone or unwanted restriction fragments. Therefore, the complete restriction mixture was loaded onto a 1% agarose gel. Electrophoresis was performed in order to detect the DNA fragment of interest by its specific size and to purify it from the gel.

2.2.5.4.1 Column-based purification

PCR-amplified DNA was purified with the PCR Purification Kit according to manufacturer's protocol. DNA was eluted in 50 µl MQ water.

2.2.5.4.2 Gel purification

For gel purification of DNA fragments after restriction digest and agarose gel electrophoresis, the QIAquick Gel Extraction Kit was used as described in the manufacturer's protocol. DNA was eluted in 50 µl MQ water.

2.2.5.5 Concentration measurement of nucleic acids

2.2.5.5.1 Spectrophotometer

The concentration of pDNA was quantified using the NanoDrop spectrophotometer according to manufacturer's instructions.

2.2.5.5.2 DNA concentration gel

To determine the concentration of a specific DNA fragment (e.g., after gel extraction), defined volumes of the sample (1 µl and 5 µl) and the DNA Ladder (2.5 µl and 5 µl; 0.1 µg/µl) were separated in a 1% agarose gel. The concentration of the DNA fragment was estimated by visual comparison of its intensity with the known reference of the two marker lanes.

2.2.5.6 Restriction digest of DNA

Restriction endonucleases cut DNA at a specific nucleotide position. They were used to create DNA fragments for cloning or as Sothern blot probes, to perform restriction analyses of pDNA, or to digest genomic DNA for Sothern blot analysis. The restriction enzyme that was used for each application respectively is mentioned in the result part or marked in the corresponding vector maps (restriction sites used for control analyses are written in smaller letters). According to the particular application, different reaction mixtures and incubation times were used:

Table 5: Application-dependent composition of reaction mixtures and incubation times for restriction digest of diverse DNA samples

application	composition of reaction mixture					incubation time
	DNA	**enzyme**	**buffer**	**additional components**	**total volume**	
Control digest of pDNA	200-300 ng	0.5 µl	2.0 µl	-	20 µl	2 h at 37°C
restriction digest of DNA fragments or pDNA for cloning	1.0 µg	1.0 µl	5.0 µl	-	50 µl	overnight at 37°C
linearization of pDNA for electroporation	18-25 µg	1.5 µl	10.0 µl		100 µl	overnight at 37°C
	If the digest was incomplete the following day, reaction mixture was increased by a volume of 50 µl containing 5.0 µl 10x buffer and 5.0 µl enzyme diluted in water. Incubation was extended for 3-4 h at 37°C. If necessary, the volume was increased further until digest was completed.					
restriction digest of genomic DNA isolated from ES cell pellet or mouse tail samples (for Southern blot)	30.0 µl	7.0 µl	25.0 µl	2.0 µl RNase A (10 U/µl)	250 µl	overnight at 37°C
	If the digest was incomplete the following day, reaction mixture was increased by a volume of 50 µl containing 5.0 µl 10x buffer and 2.0 µl enzyme diluted in water. Incubation was extended for 3-4 h at 37°C.					
restriction digest of genomic DNA precipitated in a 96-well plate (for Southern blot)	DNA precipitate in well	0.5 µl	4.0 µl	0.4 µl RNase A (10 U/µl), 0.1 µl 1 M Spermidin, 0.1 µl 1 M DTT	40 µl	overnight at 37°C
	If the digest was incomplete the following, reaction mixture was increased by a volume of 10 µl containing 1.0 µl 10x buffer and 0.6 µl enzyme diluted in water. Incubation was extended for 3-4 h at 37°C					

Enzymes were used in combination with the buffers recommended by the manufacturer for single or double digest. If fast digest (FD) enzymes were used, the incubation time was reduced to 7 minutes.

Digested DNA fragments were subsequently loaded onto an agarose gel for analysis or purification.

2.2.5.7 In Fusion cloning

Additionally to the standard cloning procedure based on restriction, purification and ligation steps, the In-Fusion® HD Cloning Kit was used, which enables a direct cloning of PCR fragments into a linearized vector. The DNA sequence was amplified by PCR (see 2.2.5.1) with particular primers (designed with the In-Fusion® Primer Design Tool) in order to add 15 bp extensions at each end of the insert. During the In-Fusion cloning reaction, the insert was fused into the open vector based on the homologous 15 bp extensions. For this step, 20 µl reaction mixture containing 4 µl 5x Enzyme Premix, 100 ng purified insert and 100 ng purified, linearized vector were incubated for 15 minutes at 50°C. Afterwards, 5 µl were used

to transform competent *E.coli* cells (see 2.2.4.1) and resulting clones were screened by restriction digest for the correct cloning product.

2.2.5.8 Dephosphorylation

To minimize the possibility of recirculation of linearized pDNA, the 5' phosphates, which are necessary for the formation of a phosphodiester bond between adjacent nucleotides, were removed from both ends of the linear vector directly after the restriction digest. For this, 1 µl SAP was pipetted into the restriction mixture of the vector and incubated for 30 minutes at 37°C followed by an inactivation step of 15 minutes at 65°C.

2.2.5.9 Ligation

To ligate the restricted and purified insert and the linearized (and dephosphorylated) vector, the Rapid DNA Ligation Kit was used. In 20 µl reaction mixture containing 1 µl T4 ligase and 4 µl 5x Buffer, 25 ng vector was mixed with the insert fragment in a ratio of 1 : 3. The required amount of insert was calculated with the following equation:

$$mass_{insert} = \frac{3 \times mass_{vector} \times length_{insert}}{length_{vector}}.$$

The ligation mix was incubated for 5 minutes at 22°C and 5 µl were subsequently used to transform competent *E.coli* cells (see 2.2.4.1).

2.2.5.10 Sequencing

For sequencing of plasmid DNA, samples were sent to StarSEQ® GmbH (Mainz, Germany) after having prepared the sequencing mix with selected primers (see0) according to the company's instructions. Result files were opened and visualized with FitchTV and the sequencing reads were analyzed with the online tool EMBOSS Pairwise Sequence Alignment.

2.2.5.11 Isolation of genomic DNA

2.2.5.11.1 Genomic DNA for genotyping-PCR

Mouse tail biopsies were lysed in 200 µl DirectPCR®-Tail buffer with 3 µl peqGOLD proteinase K (20 mg/ml) overnight at 55°C while shaking at 950 rpm. The next day, lysates were incubated at 85°C for 45 minutes for heat inactivation of proteinase K. 1 µl of lysate was directly used for a 25 µl genotyping PCR reaction (see 2.2.5.1).

2.2.5.11.2 Genomic DNA for Southern blot

ES cell pellet

Pellets of ES cells from one 10 cm² dish were resuspended in 5.5 ml TEN buffer, 550 µl 10% SDS, 500 µl Proteinase K (10 mg/ml) and water were added to a final volume of 7 ml, and cells were lysed overnight at 56°C. If the lysis was not complete, the reaction volume

was increased with 4 ml TENS buffer and 500 µl Proteinase K and incubation was proceeded for another day. The DNA was then precipitated by phenol-chloroform extraction (see 2.2.5.13.1), spooled on a glass micropipette, washed two times with 70°% ethanol and dissolved in dH_2O (1-2 h at 56°C). The amount of isolated DNA was estimated in a DNA concentration gel (see 2.2.5.5.2).

ES cells in 96-well plate

To lyse ES cells plated in a 96-well plate, 40 µl ES Lysis Buffer and 3 µl Proteinase K (10 mg/ml) were pipetted into each well and incubated overnight at 56°C. The next day, DNA was precipitated with ethanol (see 2.2.5.13.3) and directly used for subsequent digest in the well.

2.2.5.12 Extraction of viral DNA

To measure the amount of genomic copies within one virus batch, viral DNA was extracted and the copy number was quantified by qPCR (see 2.2.5.2).

2 µl of virus stock was diluted in 10 µl 10x ABI buffer and 86 µl dH_2O. 1 µl DNase (10 U/µl) was added and the mixture war incubated for 30 minutes at 37°C to digest non-viral DNA. DNase was inactivated for 10 minutes at 70°C. To digest the capsid of the virus particles and free the viral DNA, the mixture was incubated with 1 µl Proteinase K (20 mg/ml) for 1 h at 50°C followed by an inactivation step of 20 minutes at 95°C. The extracted DNA was stored at 4°C and used in a 1/50 dilution for analysis by qPCR.

2.2.5.13 DNA precipitation

2.2.5.13.1 Phenol-chloroform extraction

DNA solution was mixed with Phenol/Chloroform in a ratio of 1:1 and centrifuged at 700 x g for 10 minutes to separate proteins that partitioned in the lower, organic phase. The upper, aqueous phase containing the DNA was isolated, mixed with chloroform (ratio of 1:1), and centrifuged. Again, the upper phase was isolated and the last purification step was repeated once more. To precipitate the DNA, 0.8 volumes of isopropanol were added to the isolated aqueous phase and the tube was inverted several times until the DNA became visible as white cloud.

2.2.5.13.2 DNA precipitation with isopropanol

Lysed DNA samples in 1.5 ml Eppendorf tubes were spun down at 13.000 rpm for 10 minutes to pellet cell debris. The supernatant was transferred into new Eppendorf tubes containing 500 µl isopropanol to precipitate the DNA. DNA was pelleted and washed twice with 200 µl 70% ethanol in between of centrifugation steps performed at 13.000 rpm for 10 minutes. The final DNA pellet was dried for 30 minutes up to 1 h at 37°C and dissolved in 100-200 µl dH_2O (1-2 h at 56°C).

2.2.5.13.3 DNA precipitation with ethanol

After lysis of cells plated in a 96-well plate, the plate was shortly spun down and 200 µl 100% ethanol were added to each well to precipitate the DNA while shaking for 2 h at room temperature. Afterwards, the plate was quickly turned around to remove the liquid and the precipitated DNA in each well was washed twice with 200 µl 70% ethanol by the same method. Finally, the DNA was dried for 10-50 minutes at 37°C.

2.2.5.14 Southern blot analysis

2.2.5.14.1 Preparation and digest of DNA samples and agarose gel

First, genomic DNA was isolated from ES cells (see 2.2.5.11.2) and purified by DNA precipitation (see 2.2.5.13.2 or 2.2.5.13.3). After an enzymatic digest with EcoRI (see 2.2.5.6), DNA fragments were loaded with 10x Ficoll loading dye onto a 0.8% agarose gel (see 2.2.5.3) and electrophoretically separated overnight at 30°V. A picture of the gel with apposed ruler was taken for later analysis and the gel was shaken for 10 minutes in depurination solution and afterwards rinsed well with dH_2O. Next, double-stranded DNA was denatured by incubating the gel for 30 minutes in denaturation solution. Finally, the gel was transferred into neutralization solution for 30 minutes.

2.2.5.14.2 Transfer onto membrane (Southern blot)

Next, the DNA fragments were transferred from the agarose gel onto an Amersham Hybond N+ membrane. The blot was built up as shown in Figure 6 after the membrane has been soaked in water and 10x SSC. Air bubbles between single layers of filter papers, membrane and gel were removed carefully and the gel was placed in the inverted way, so that the DNA was blotted onto the overlaying membrane in the direction of the capillary action that persisted overnight.

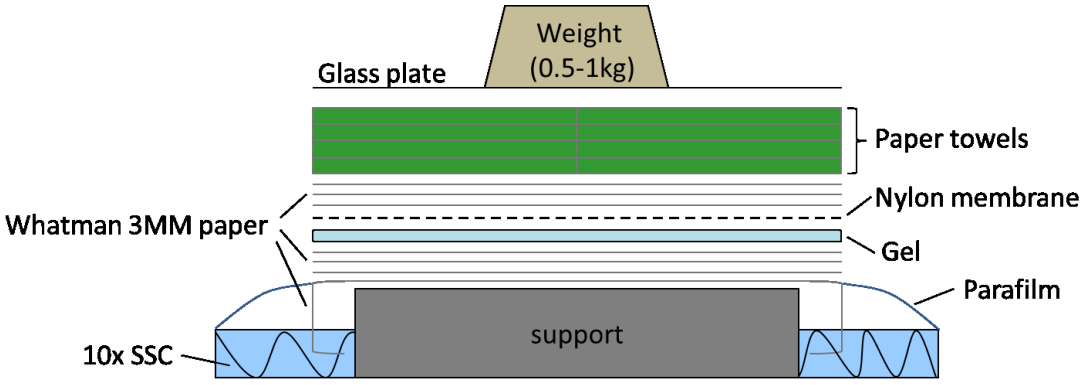

Figure 6: Setup of Southern blot to transfer DNA fragments from an agarose gel onto a nylon membrane by capillary action.

The next day, slots of the gel were marked on the membrane and the membrane was incubated 1 minute in denaturation solution, 1 minute in neutralization solution, and finally dried on a filter paper for 2 h at 80°C.

2.2.5.14.3 Hybridization with radioactive testing probes

The dry membrane was soaked in 2x SSC and pre-hybridized with 40 ml warm Hyb-buffer for 4 h at 65°C under rotation. In the meantime, the testing probes (30 ng of template DNA) were radioactively labeled using the Ladderman™ Labeling Kit according to manufacturer's protocol. The labeling reaction was performed with 3 µl ^{32}P-dCTP (3000 Ci/mmol, 50 µCi) for 1.5-2 h at 55°C and stopped with 100 µl dH_2O. Probes were purified with prepared illustra MicroSpin G-50 Columns by centrifugation at 3.000 rpm for 2 minutes. To denature the labeled testing probes, they were heated for 3 minutes at 95°C and then kept 5 minutes on ice until they were finally mixed with 10 ml warm Hyb-buffer. The prehybridization buffer of the membrane was removed and hybridization with the radioactively-labeled probe was performed overnight at 65°C.

The following day, excess probe was washed away in several washing steps performed at 65°C. Wash solutions 1 to 3 were used successively for 5 minutes up to 30 minutes and the radioactivity of the membrane was measured in between of each washing step. Having reached values around 70-100 counts per second (cps), washing was finished and the membrane was used for autoradiography.

2.2.5.14.4 Autoradiography and analysis

The membrane was sealed in a plastic foil filled with 2x SSC and fixed in a Biomax cassette with intensifying screens. To visualize the hybridization pattern, MS Biomax films were exposed to the beta radiation of ^{32}P for 1-3 days at -80°C and developed with a film processor. The slots of the gel that were marked on the membrane were copied to the film and the distances between slot and signal of the testing probe were measured. The comparison of these measurements with the previously taken picture of the agarose gel with DNA ladder enabled the sizing of the hybridization pattern and the consequent analysis.

2.2.6 Protein biochemistry methods

2.2.6.1 Protein isolation

The frozen plate with HEK293 cells or hippocampal neurons was thawed on ice, 200 µl lysis buffer supplemented with 1x cOmplete, EDTA-free protease inhibitor cocktail and pepstetin (diluted 1:1,000) were added to each well and incubated for 10 minutes on ice while shaking. Cells of each well were harvested separately with a cell scraper and collected in an Eppendorf tube. After incubation for 10 minutes on ice, cell debris was pelleted for 5 minutes at 13,000 x g and the supernatant was transferred into a new Eppendorf tube for further experiments.

2.2.6.2 Quantification of protein concentration

To quantify the amount of isolated protein, the Pierce™ BCA protein assay kit was used according to manufacturer's instructions. Absorbance at 562 nm was measured with a spectrometer and the protein amount of each sample was calculated in comparison to a BSA standard serial dilution that run in parallel.

2.2.6.3 SDS-Polyacrylamide gel electrophoresis (SDS-PAGE)

A discontinuous polyacrylamide gel consisting of a 10% resolving gel with overlaying 5% stacking gel (Table 6) was prepared and transferred into an electrophoresis cell filled with 1x running buffer. 25 µl of each protein sample (if necessary diluted with water in order to obtain equal protein amounts) were mixed with 5 µl 5x Laemmli-Buffer and incubated for 5 minutes at 95°C to destroy the tertiary structure and disulfide bonds of the proteins. Samples and 6 µl protein ladder were loaded onto the gel and a voltage of 80-120 mV was applied for 1.5-2 h.

Table 6: Composition of discontinuous polyacrylamide gel

Component	volumes for 10% resolving gel	volumes for 5% stacking gel
dH_2O	1.7 ml	2.38 ml
30% Polyacrylamide (Rotiphorese® Gel 30)	315.5 µl	2.0 ml
1 M Tris, pH 6.8	425 µl	-
1.5 M Tris, pH 8.8	-	1.5 ml
10% SDS	25 µl	60 µl
TEMED	2.5 µl	2.38 µl
10% APS	25 µl	60 µl
total volume	2.5 ml	6.0 ml

2.2.6.4 Western blot (WB)

In a next step, proteins were transferred from the polyacrylamide gel onto a nitrocellulose membrane by the wet blot procedure. For this, the membrane was placed on top of the gel between two buffer-soaked filter papers in a cassette that was then put into a transfer cell filled with precooled blotting buffer. Transfer was performed for 1.5 h at 100 V. The effectiveness of the blotting was verified by staining the membrane with Ponceau solution for some minutes. After washing with distilled water, the presence of bands on the membrane confirmed the successful transfer of proteins. Next, the membrane was incubated on a shaker for 1.5 h in 1x RotiBlock (10x RotiBlock diluted in MQ water) to block unspecific binding sites, then the first antibody diluted in 1x RotiBlock was applied. The membrane was incubated overnight at 4°C, then washed three times for 5 minutes with 1x TBST and exposed to the secondary antibody diluted in 1x TBST for 2 h at RT.

For detection, the membrane was washed again three times, Amersham ECL Western Blotting Detection Reagent was applied and the signal of the chemiluminescent reaction was either detected with the Fusion Fx7 imaging system or exposed to Super RX films that were

developed with a film processor. If the signal was too weak, the membrane was washed again twice and the detection procedure was repeated with the more sensitive SuperSignal® West femto reagent.

2.2.7 Surgical procedures

2.2.7.1 Sciatic nerve crush

A crush lesion of the sciatic nerve was performed in adult mice as described by Vogelaar et al. (2004). Briefly, mice were anesthetized (inhalation anesthesia via a mask with 2% isoflurane added to oxygen stream, 3 L/min) and the skin over the left thigh was cut open. The sciatic nerve was carefully exposed and crushed for 30 sec with fine forceps. The wound was closed with a clip and animals were returned to their cage for 24 h.

2.2.7.2 Spinal cord injury (SCI)

The previously described protocol for dorsal spinal cord hemisections (Vogelaar et al., 2015) was adopted for adult mice. In short, mice were anesthetized by isoflurane inhalation (see above) and their skin was opened dorsally from T6 to T11. Laminectomy was performed for T8 and T9. The dura mater was opened and the spinal cord was cut with spring scissors at a depth of 1 millimeters. Muscles over injury site were sutured and the wound was closed with a clip. Before surgery, animals obtained subcutaneous injection of Rimadyl® (4 mg/kg in 100 µl) per 10 g weight for pain relief that lasted minimum for 24 h. Post-operative care included manual bladder emptying until normal function returned and daily control for abnormal behavior and weight control. In cases of increased weight loss, mice obtained saline injections.

2.2.7.3 Injections of rAAVs

The protocol for intrathecal (i.t.) delivery of rAAVs by direct lumbar puncture was adapted from Vulchanova et al. (2010) and Lu and Schmidtko (2013). In short, adult mice received 200 µl of 12.5% mannitol solution (in PBS) via intravenous (i.v.) injection into the tail vein. 20 minutes later, 5 µl of virus solution (5 x 10^8 genomic copies of rAAV-eGFP in PBS) were injected intrathecally by direct lumbar puncture between spinal segments L4 and L5 of awake mice. Animals were monitored regularly for 28 days.

2.2.8 Histological methods

2.2.8.1 Perfusion of mice

For histological analyses, the tissue was preserved by fixation via the blood flow, the so-called perfusion method. First, the mouse was anesthetized by intraperitoneal injection of 1 ml anesthetic solution. As soon as the tail and toe reflexes were not present anymore, the

mouse was fixed on a cork tile, the skin over the thorax was removed and the rib cage was opened laterally on both sides to enable free access to the heart. A cannula was inserted into the left ventricle of the heart, a small cut was made in the right atrium allowing the blood to be washed out while 15-20 ml 1x PBS were slowly injected. Directly after, the perfusion with 15-20 ml 4% PFA was performed. Finally, the tissue of interest (brain, spinal cord, sciatic nerve or dorsal root ganglia) was dissected from the fixed animal and kept overnight in 4% PFA at 4°C for post-fixation.

2.2.8.2 Preparation of tissue sections: Cryosectioning

After post-fixation, the tissue was washed overnight with 1x PBS at 4°C and then transferred into a 15% and subsequently a 30% sucrose solution (diluted in PBS) for cryo preservation (1 day respectively at 4°C). The sample was placed in a mold filled with cryo protective embedding medium (Tissue-Tek® O.C.T™ Compound), snap frozen in dry ice and stored at -80°C until cutting. The sectioning was performed at a cryostat. 10 µm slices were mounted on glass slides, dried for 30 minutes on a heating plate and stored at -20°C.

2.2.8.3 Immunohistochemistry (IHC)

Slides with cryo sections were dried on a hotplate for 1 h, incubated with 0.2% PBSTx for 10 minutes and washed three times with 1x PBS for 5 minutes each. To damask antigens, 50 mM NH_4Cl was applied for 10 minutes, slides were washed again three times with 1x PBS, and transferred horizontally into a humidified dark chamber. Blocking solution (5% NGS + 1% BSA in 0.2% PBSTx) was applied and slides were covered with Parafilm to prevent draining. After 1 h, blocking solution was replaced with the first antibody diluted in blocking solution and slides were incubated overnight at 4°C. Slides were washed three times 5 minutes with 1x PBS and incubated with secondary antibody and DAPI (1:10.000 diluted in blocking solution) for 2 h at RT in the dark. Slides were washed again and a cover glass was mounted with FluorSave™ Reagent. Having dried overnight at RT, slides were stored at 4°C.

2.2.9 Microscopic analysis

2.2.9.1 Wide-field fluorescence microscopy

Transfected HEK293 cells were imaged by epifluorescence using an inverted microscope. Exposure-matched images were acquired with the cellSense Dimension software and post-processed with ImageJ.

2.2.9.2 Confocal laser scanning microscopy

Confocal microscopy at the Leica SP5 microscope was used to image immunostained cultured cells or tissue sections. Depending on the magnification of interest, the 20x objective, 40x or 63x oil-immersion objective were used. Xyz-stacks with 0.3-1.0 µm interval between planes were acquired for each channel. For orthogonal projections, pictures were taken with a z-step size of 0.08 µm.

Confocal images were post-processed with ImageJ to generate orthogonal projections and maximum projections of z-stacks. Brightness and contrast were adjusted equally for all images of one condition and sample. To extract the colocalization signals of the ribosomal signals (RPL26 or RFP) with the axonal marker (Tuj1), the RG2B plug-in for ImageJ was used based on the procedure described by Kalinski et al. (2015). For the red and green channel, RG2B colocalization was calculated with a minimum ratio of 0.5 and the colocalized pixels were set to the max of both channels. The extracted colocalization signals were displayed as heat map in a separate channel.

2.2.9.3 Single-molecule localization microscopy

Single molecule localization microscopy (SMLM) was performed at the Institute of Molecular Biology (Mainz, Germany) with a custom-built microscope setup equipped with a 63x oil-immersion objective. Data were analyzed as previously described (Szczurek et al., 2014). Briefly, the Alexa Fluor 647 dye was excited with a 647 nm laser running at a laser power of 90 mW and emission was collected with a 655 nm longpass filter. 10,000 frames with an integration time of 35 ms were recorded for each experiment. Images were post-processed with MATLAB using fastSPDM software (Grull et al., 2011) to detect and localize the signals. Single molecule localizations were blurred with localization precision and plotted in joint localization map (a superresolution image). For analysis of the ribosomal particles, the image was opened in ImageJ, converted to 8-bit grayscale and thresholded, so that single particles became identifiable. Particles that represented unspecific background signals far away from the biological structure (based upon the axon marker) were deleted manually. All thresholded particles were then analyzed automatically with the software resulting in the number of particles with their corresponding X and Y coordinates of each particle's centroid. This coordinates were used by the Nnd plugin (nearest neighbor distances calculation with ImageJ) to calculate the shortest distance of each particle to its closest neighbor. The data from the result table were imported into Excel and plotted as histogram. Data from several experiments were combined in GraphPad Prism to yield the final histogram.

3. Results

3.1 Axonal localization of endogenous ribosomes

3.1.1 Analysis of ribosomes in axons *in vitro*

In order to model the long axon tracts *in vitro*, various explant cultures were used in this project (Figure 7). The advantage of explant culture is that neurons remain embedded in their tissue environment and their axons grow up to 1 millimeter in three days (Vogelaar et al., 2009; and own observations) compared to dissociated cells whose axons extend maximally 200 µm. Sensory neurons of DRGs are pseudounipolar cells that do not develop dendrites, but extend a single axon per neuron that splits into a central and a peripheral branch. Cultures of DRG neurons contain only axonal processes (Zheng et al., 2001) making them a suitable model system to study. As shown in Figure 7, explant cultures of adult DRGs possess long axons (Figure 7A) with prominent growth cones (Figure 7B), hence, they represent an appropriate PNS model.

Most neurons of the CNS are multipolar cells with many dendrites and one axon. Both dendritic and axonal processes would therefore be expected in cultures of central neurons. However, it has been shown by Liu et al. (2005) that the explants of motor cortex layer V extend processes representing CST axons. These central axons grow over equally long distances but in a less straight way as compared to axons of DRG explants (Figure 7C vs. A). Furthermore, CST axons and growth cones are thinner (Figure 7C, D) in relation to their sensory counterparts and appear to form networks close to the explant (Figure 7C). This reflects the *in vivo* morphology of the CST axons. Taken together, these cortical explant cultures are a suitable CNS equivalent to the explant system of peripheral DRG neurons.

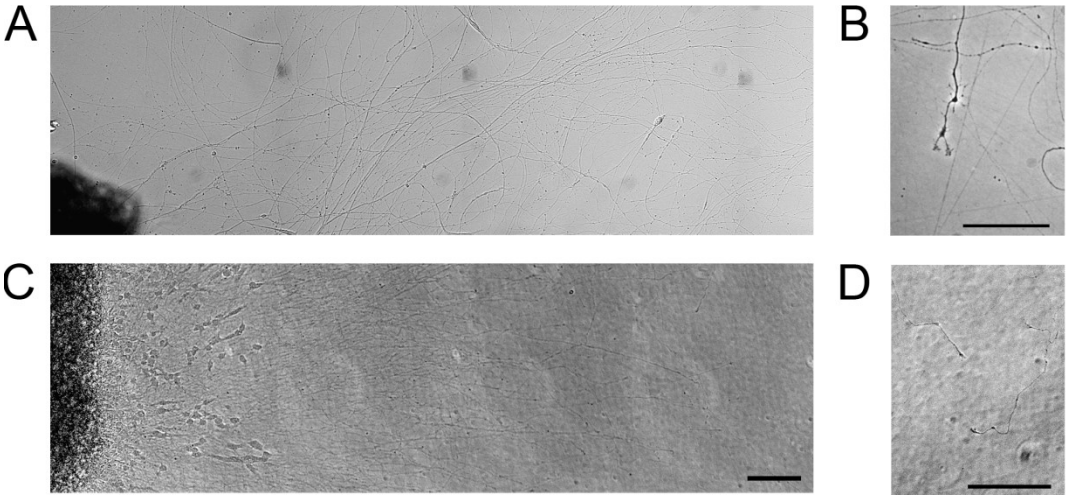

Figure 7: Explant culture models for PNS and CNS axons
(**A-D**) Bright field microscopic images of adult DRG (A, B) and neonatal cortex (C, D) explant cultures at 3DIV. Sensory axons grow over long distances (A) and possess prominent growth cones at their distal ends (B). In comparison, CST axons are thinner (C) and have smaller growth cones (D). Scale bars: 100 µm.

For investigation of the physiological distribution of ribosomes in axons, ICC stainings were performed. To date, the most frequently used antibody to detect ribosomal proteins is the human-anti-ribosomal P antigen (Court et al., 2008; Calliari et al., 2014). This antibody was also utilized for ICC in early experiments of the present study but displayed only diffuse stainings of the complete axons (Figure 8A), which did not correspond to the expected punctate pattern of axonally localized ribosomes. Moreover, a lot of non-specific background puncta (arrows in Figure 8A) were observed that potentially compromise the analysis of axonal ribosomes. Instead of the anti-ribosomal P, an antibody against the ribosomal protein L26 (RPL26) of the large 60S subunit was applied to stain ribosomes for studying their localization in axons of cultured cells and tissues. This anti-RPL26 antibody is highly specific as evaluated by immunoblotting, showing only one major band of the expected molecular weight of 17 kDa (Figure 8D).

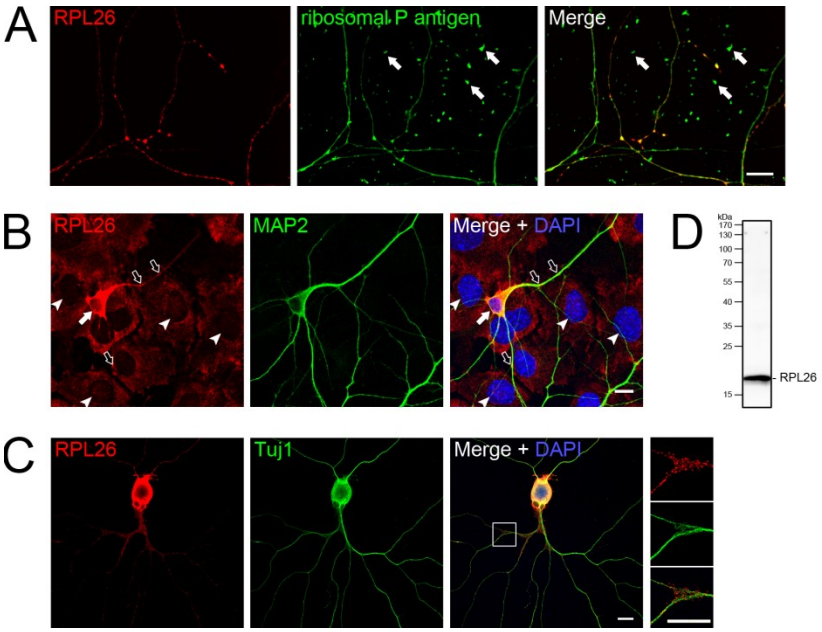

Figure 8: The anti-RPL26 antibody as marker for endogenous ribosomes *in vitro*
(**A-C**) ICC for RPL26 (red), ribosomal P antigen, MAP2 or Tuj1 (green), and DAPI (blue) on neonatal DRG explants (**A**), neonatal dissociated hippocampal neurons (**B**), and adult dissociated DRGs (**C**) in culture. In sensory neurons, RPL26 was primarily located in neuronal cell bodies (**C**) and displayed a granular distribution in the axons(**A**, **C**) with slightly increase levels in branching points (**C**, enlarged inset of boxed area). Immunostaining for ribosomal P antigen was more diffusely distributed, showed non-specific background puncta (arrows in A) and was therefore less specific than RPL26. (**B**) RPL26 was present in the cell body (filled arrow) and dendrites (unfilled arrows) of hippocampal neurons and was also expressed in non-neuronal cells (arrowheads).Scale bars: 10 µm (A); 50 µm (B); 20 µm (C). (**D**) Immunoblot of HEK293 cell homogenate confirmed the specificity of the anti-RPL26 antibody.

In neonatal hippocampal neurons (Figure 8B), RPL26 was enriched in the neuronal cell body (filled arrow) and also localized to dendrites (unfilled arrows) marked by MAP2. This is consistent with previous reports showing the dendritic localization of ribosomes in CNS neurons (Steward and Levy, 1982; Tiedge and Brosius, 1996; Ostroff et al., 2002), and therefore validates the usage of the anti-RPL26 antibody as marker for ribosomes that localize to neurites. Since ribosomal proteins are expressed ubiquitously in all cells, also MAP2-negative non-neuronal cells present in the cell culture showed RPL26

immunoreactivity (arrowheads in Figure 8B). Strong cytoplasmic signals were present in cell bodies of Tuj1-stained adult DRG neurons and focusing on axons with higher magnification revealed a punctate pattern of RPL26 in these neuronal processes (Figure 8C).

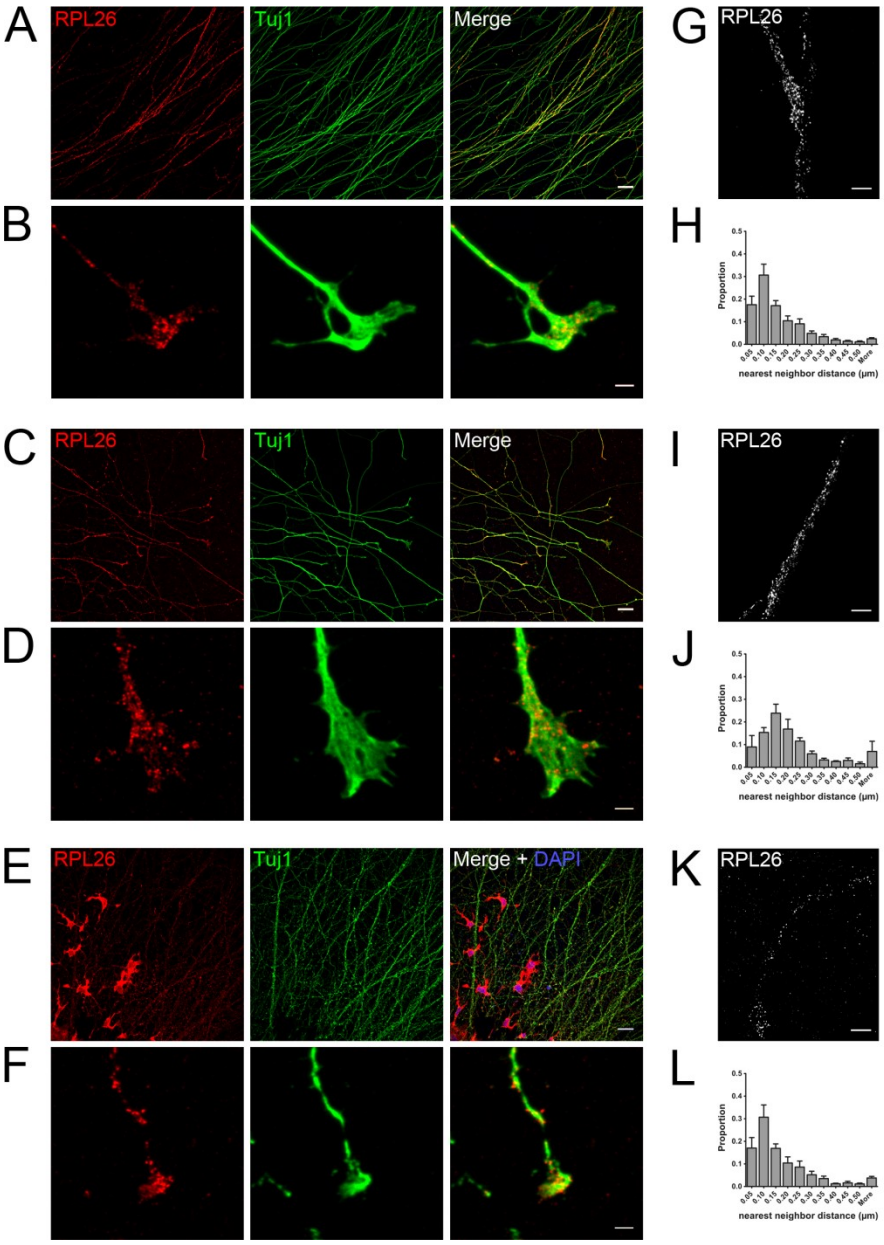

Figure 9: Expression and localization of endogenous ribosomal protein L26 *in vitro*
(**A-F**) ICC for RPL26 (red), Tuj1 (green), and DAPI (blue) on axons from neonatal (**A**, **B**) and adult (**C**, **D**) DRG explants, and neonatal cortex explants (**E**, **F**) in culture. RPL4 displayed a granular distribution in axons (**AC**, **E**) and growth cones (**B**, **D**, **F**).(**G-L**) Using SMLM, distinct clusters of RPL26 were visualized with high resolution in axons of neonatal (**G**) and adult DRG explants(**I**), and neonatal cortex explants (**K**). Nearest neighbor distances were calculated for all RPL26 clusters and displayed in 0.05 µm bins as histogram (**H**: average of 9 neonatal DRG axons; **J**: average of 4 adult DRG axons; **L**: average of 7 neonatal cortical axons). Columns represent mean with standard error of mean. Scale bars: 20 µm (A,C, E); 2 µm (B, D, F, G, I, K).

In explant cultures of neonatal and adult DRGs, ribosomes were detected in β-III-tubulin (Tuj1)-positive axons and growth cones as demonstrated by ICC with the anti-RPL26 antibody (Figure 9A, C). Higher magnification of growth cones revealed a punctate pattern of RPL26 signals (Figure 9B, D). Similar distributions were observed in explant cultures of

neonatal motor cortex layer V neurons where RPL26-positive signals existed in axons and growth cones (Figure 9E, F).

In order to analyze the distribution of ribosomes with a higher optical and structural resolution, SMLM was applied. Figure 9G, I and K show clear granular signals of RPL26 in axons of DRG neurons (neonatal and adult) and of cortex explants. Ribosomal clusters appeared in a relatively equal distribution. In order to describe the pattern of these granular signals and to make it comparable between different samples, images were thresholded to obtain single RPL26 particles. The distance of the nearest neighbor for each particle was calculated with ImageJ. The resulting values were divided into bins of 0.05 µm and their proportions are displayed by means of histograms in Figure 9H, J and L. More than 80% of the particles within the analyzed axon segment were between 100 and 300 nm apart. The distribution of the distances was similar in different developmental stages (neonatal versus adult) of DRG explants (Figure 9H versus J) and comparable between PNS and CNS axons (Figure 9H versus L).

3.1.2 Analysis of ribosomes in axons *in vivo*

Next, the anti-RPL26 antibody was applied for IHC studies with the aim to visualize ribosomes in axons *in vivo*. It has been shown that injured axons contained increased levels of ribosomes (Court et al., 2008). For this reason, sciatic nerve crush or spinal cord injury were performed before peripheral (sciatic nerve) or central branches (dorsal columns, DC) of DRG were assayed for the presence of RPL26 signals. Sciatic nerve tissue was dissected one day after crush in order to analyze in addition to the proximal nerve stump also the distal axons that have not yet been degenerated. For spinal cord injury experiments, spinal tissue was analyzed seven days after SCI. After this time, disconnected axons were already fragmented at the proximal site of the injury.

As expected, the glial cells lining the axons in sciatic nerve and the axon tracts of the spinal cord (Schwann cells and oligodendrocytes, respectively) displayed strong fluorescence for RPL26 (Figure 10 and Figure 11B, C). In order to focus on RPL26 signals in axons only, confocal image stacks were post-processed with the RG2B NIH ImageJ plug-in. This processing approach allowed the extraction of RPL26 signals which overlapped with the axonal marker β-III-tubulin in each plane of the image stack as described in detail by Kalinski et al. (2015). The isolated axon-only signals of single planes were combined in maximum projection images and displayed as intensity spectrum. Only very few ribosomes were detected in Tuj1-stained axons in uninjured sciatic nerve (Figure 10A). One day after sciatic nerve crush, more RPL26-positive signals were observed in axons proximal (Figure 10B) and distal (Figure 10C) to the injury site. This is evident from the increased amount of RG2B-extracted axon-only signals when compared with the uninjured control. Higher magnification of injured sciatic nerve fibers revealed a prominent punctate pattern of axonally localized

RPL26 signals in Remak fibers at both sides of the injury (Figure 10D, E). Remak fibers were distinguished from other axons based on their specific morphology and on the absence of myelin. Orthogonal projections of ribosome puncta of high signal intensities confirmed the intra-axonal localization of these RPL26 signals (arrows in Figure 10D, E). Additionally, high RPL26 immunoreactivity existed in areas around the myelinated axon where Schwann cell cytoplasm and the myelin sheath were located. Even if a myelin marker was missing, it could be speculated that RPL26 was also present in the myelin sheath adjacent to nodes of Ranvier, which were identified by their prominent morphology (arrowhead in Figure 10E).

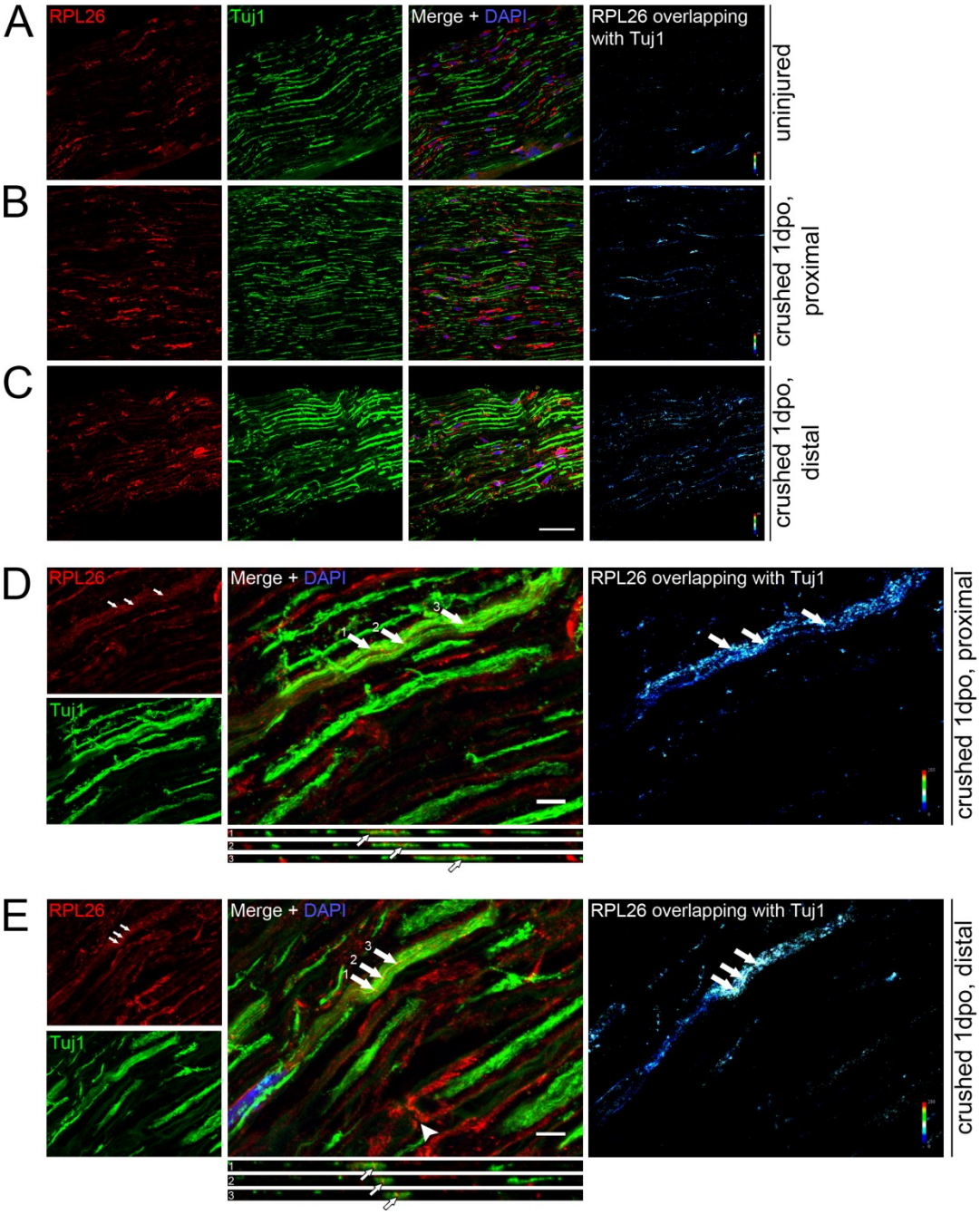

Figure 10: Expression and localization of endogenous ribosomal protein L26 in the PNS *in vivo*
(**A-E**) Longitudinal sections of sciatic nerves were stained for RPL26 (red), Tuj1 (green), and with DAPI (blue). The panels on the right show the overlap between RPL26 and β-III-tubulin as an intensity spectrum (RG2B algorithm), thus displaying axon-only ribosomes. Schwann cells in the sciatic nerve show strong RPL26 signals as expected. (**A**) Uninjured axons contained sparse patches of ribosomes. (**B**, **C**) After sciatic nerve crush (1 dpo),

an increased proportion of axonally localized RPL26 signals was found proximal (**B**) and distal to the injury site (**C**). Orthogonal xz projections constructed from 18 (**D**) and 22 (**E**) optical sections taken at 0.08 µm z-step intervals. RPL26 signals overlapped with β-III-tubulin-positive axons of Remak fibers in the sciatic nerve proximal (**D**) and distal (**E**) to the injury site one day after sciatic nerve crush (arrows). The arrowhead in E is pointing to a node of Ranvier. Abbreviation: dpo, days post operation. Scale bars: 50 µm (C); 5 µm (D-E).

In order to investigate if ribosomes were also present in central axons of the spinal cord, mice from the YFP-H line were used. These mice express YFP in various neuronal subtypes including layer V pyramidal neurons in the cortex, resulting in labeled axons of the CST, but also in DRG neurons, so that parts of the dorsal columns are also marked (Carter et al., 2008). Hence, no additional axonal marker was necessary for the analysis. Depending on the location of their cell bodies and therefore the orientation of the axons (ascending or descending), axon tracts of the spinal cord degenerated at different sites after a SCI. The CST axons, originating in the brain, degenerated distally to the lesion site whereas the DRG axons proximal to the lesion site were cut off from their cell bodies and therefore fragmented. This can clearly be observed in a parasagittal section of the spinal cord from an YFP-H mouse seven days after injury (Figure 11A).

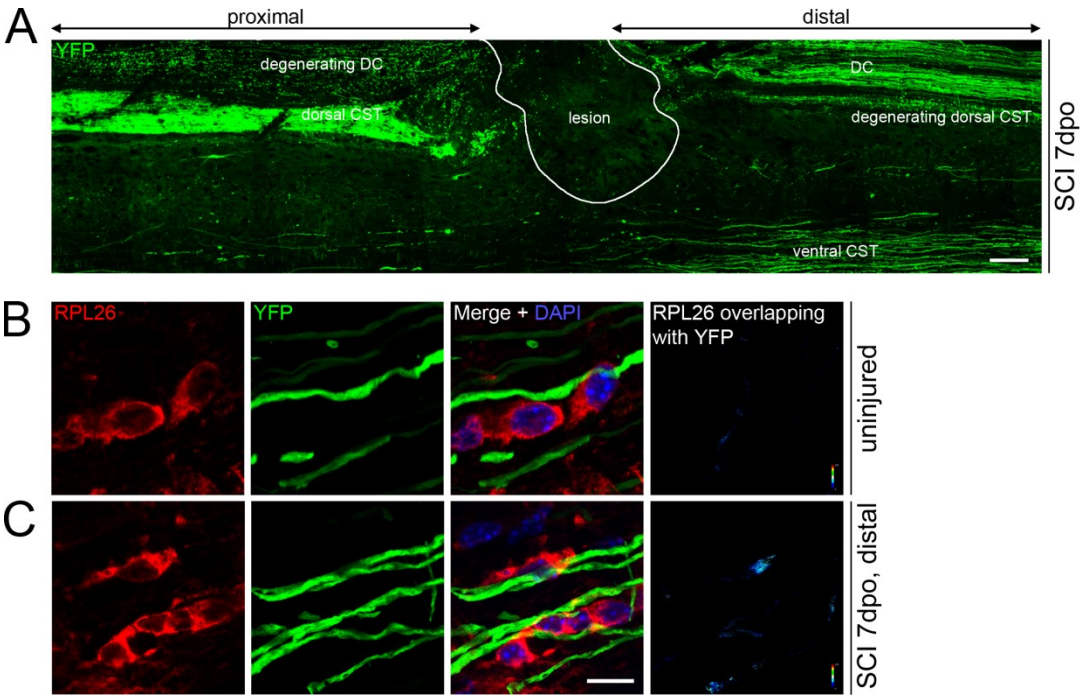

Figure 11: Expression and localization of endogenous ribosomal protein L26 in the CNS *in vivo*
(**A**) Parasagittal section of the spinal cord from a YFP-H mouse showing the effect of a spinal cord injury (SCI) at 7 days post operation (dpo) on spinal axon tracts (green). At the proximal side of the injury, the descending dorsal corticospinal tract (CST) is intact and ascending sensory axons in the dorsal columns (DC) are degenerating. Distally to the injury, axons of the dorsal CST are degenerated and fibers of the DC are intact. The ventral CST is not affected by the injury. (**B**, **C**) IHC for RPL26 (red) and DAPI (blue) on longitudinal spinal cord sections of an uninjured (**B**) and 7dpo SCI YFP-H mouse (**C**). The subtracted RG2B panels on the right show the axonal RPL26 signal as an intensity spectrum. After SCI, more colocalization between RPL26 and YFP (green) positive DC fibers was found distal to the injury site (**C**) when compared with the uninjured control (**B**). Scale bars: 200 µm (A); 10 µm (C).

When focusing on the dorsal columns, which comprise the ascending fibers of the DRGs, IHC with the anti-RPL26 antibody showed no signals in the YFP-labeled axons of an uninjured animal (Figure 11B). After spinal cord injury, faint axon-only signals of RPL26 could be extracted in DC fibers distal to the lesion (Figure 11C). However, no punctate pattern, as

observed in the sciatic nerve (Figure 10D, E), was visible. In the multichannel overlay image, the close vicinity of the glial cells to the axons is visible leading to the assumption that RPL26-immunoreactive cell protrusions might have caused the overlap signal.

In summary, RPL26-positive ribosomes were detected in axons of peripheral and central neurons *in vitro*, and in sciatic nerve fibers *in vivo* that displayed increased amounts of ribosomes after injury.
Since neurons and glial cells all contain the same ribosomal proteins, a neuron-specific labeling of ribosomes was needed to investigate whether ribosomes are transported from the cell body to the axon. Two different strategies were pursued for this aim: A neuron-specific virus was produced that encoded an eGFP-tagged ribosomal protein and a transgenic mouse line was generated that expressed tdTomato-labeled ribosomes in neuronal cell populations after Cre-mediated recombination.

3.2 Viral expression of eGFP-tagged ribosomes

In order to label ribosomes with the enhanced green fluorescent protein, the ribosomal protein L4 (RPL4) was fused to eGFP (L4-eGFP). RPL4 is part of the 60S ribosomal subunit and its C-terminus is partially exposed to the surface of the complex so that a tag could easily be added. The L4-eGFP construct (from rat) was provided by the group of Jan van Minnen who had already shown that the fusion protein of RPL4 and eGFP was indeed incorporated into ribosomes (Court et al., 2008). This indicates that the fluorescent tag at the C-terminus did not interfere with the localization and function of the ribosomal protein L4. For this reason and due to a high similarity (94%) between the rat and mouse sequence of RPL4, the L4-eGFP construct was used in the present work to be expressed by recombinant adeno-associated virus.
rAAV is an adeno-associated virus (AAV) whose coding region of *Rep* and *Cap* genes is replaced with an exogenous gene expression cassette. Therefore, helper plasmids are needed during the generation of rAAV particles to provide the missing genes together with helper genes from adenovirus, the latter of which are always required by the replication-deficient AAV. AAV is a single-stranded DNA virus that can infect non-dividing cells and integrates its viral DNA into the host genome for long-term expression. Further, the immune response after injection of AAV into animals is very mild. Due to these characteristics, the AAV is a suitable tool for *in vivo* expression of exogenous genes in the nervous system. Based on the capsid proteins that the AAV expresses on its surface, different serotypes can be distinguished that provide diverse cell tropisms. In this study, rAAVs with capsid proteins of serotype 1 and 2 (rAAV 1/2) have been used to specifically target neuronal cells. Both serotypes efficiently transduce DRG neurons (Mason et al., 2010). Serotype 1 has been

shown to be optimal for cortical and corticospinal neurons (Hutson et al., 2011), and previous studies have already revealed that AAVs of serotype 2 specifically infect neurons in the brain (Bartlett et al., 1998).

3.2.1 Cloning and generation of recombinant adeno-associated viruses

The expression cassette encoding the fusion protein L4-eGFP was amplified from pEGFP-L4 temp (Court et al., 2008) by PCR with the oligonucleotides L4GFP_2a and L4GFP_2b (see 2.1.10). Thus, restriction sites for SpeI and EcoRV were introduced at the 5' and 3' end, respectively. Subsequently, the PCR product was inserted into the multiple cloning site of plasmid #329_pAMSyn-MCS-WPRE2-SpA (Figure 12A). This plasmid contains all components needed for the packaging into rAAVs and the subsequent expression of the inserted gene, namely a synapsin promoter, woodchuck hepatitis virus posttranscriptional regulatory element 2 (WPRE2), a polyadenylation signal (pA), and the two flanking AAV2 inverted terminal repeats (ITR). After insertion of the L4-eGFP expression cassette, the resulting plasmid pAM-EGFP-L4 (Figure 12A) was expressed in HEK293 cells for functional verification (Figure 12B). In parallel, HEK293 cells were transfected with the control plasmid pAM-EGFP which was produced by BamHI excision of the L4 expression cassette from pAM-EGFP-L4 (Figure 12A). Microscopic analyses of the fluorescent proteins showed that the fusion protein L4-eGFP encoded by pAM-EGFP-L4 localized primarily to nucleoli (Figure 12B), the site of ribosome biogenesis within the cell, and cytoplasmic regions. This confirmed the correct incorporation of the eGFP-tagged RPL4 into ribosomes. In contrast, transfection with the control plasmid pAM-EGFP resulted in strong eGFP fluorescence in the whole cell with no specific subcellular localization (Figure 12C).

To generate the recombinant adeno-associated virus rAAV-L4-eGFP or rAAV-eGFP, HEK293 cells were transfected with either of the AAV shuttle plasmids (pAM-EGFP-L4 or pAM-EGFP) and with the helper plasmids pFdelta6, pRVI, and pH21. The genomic titer (amount of genomic copies per milliliter) of rAAVs was determined by qPCR with primers WPRE for and WPRE rev (see 2.1.10) and calculated relative to plasmid #329_pAMSyn-MCS-WPRE2-SpA that functioned as standard.

First transduction experiments on DRG explant cultures and dissociated hippocampal neurons showed very weak fluorescence for L4-eGFP or eGFP when using the synapsin-driven rAAV-L4-eGFP and rAAV-eGFP, respectively (data not shown). It was decided to use the stronger, ubiquitously expressed cytomegalovirus early enhancer/chicken-beta actin (CAG) promoter instead of the actual neuronal synapsin promoter. Based on the tropism of rAAV serotype 1/2 for neurons, the neuron-specific expression of the encoded protein was still ensured.

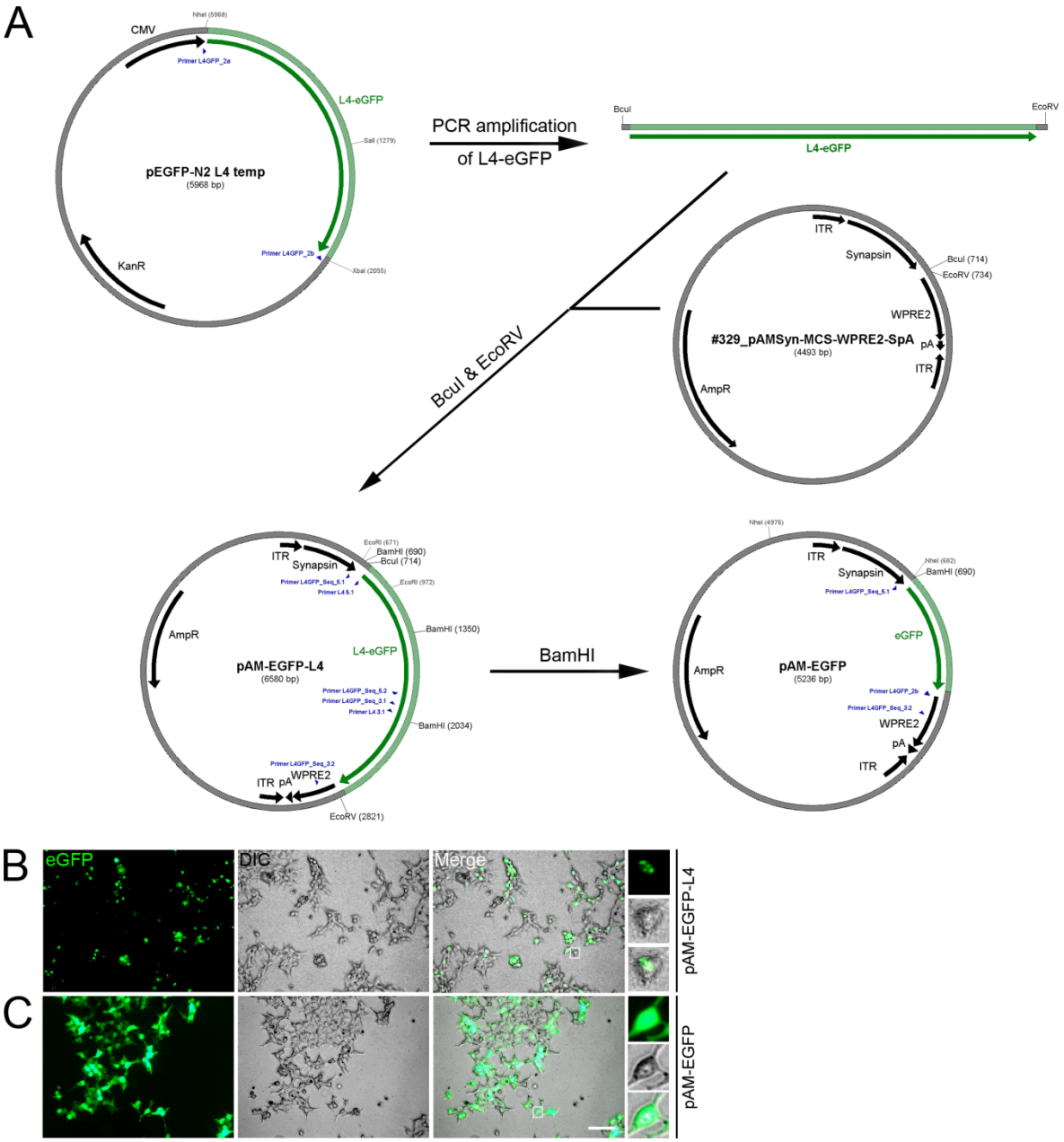

Figure 12: Cloning and expression of AAV shuttle plasmids pAM-EGFP-L4 and pAM-EGFP
(**A**) Schematic outline of the cloning strategy for pAM-EGFP-L4 and pAM-EGFP. Abbreviations: CMV, cytomegalovirus; KanR, kanamycin resistance; ITR, inverted terminal repeats; WPRE2, woodchuck hepatitis virus posttranscriptional regulatory element 2; pA, polyadenylation signal; AmpR, ampicillin resistance. (**B**) The fusion protein L4-eGFP (green) localized predominantly to nucleoli in HEK293 cells that were transiently transfected with pAM-EGFP-L4. (**C**) Transfection with the control plasmid pAM-EGFP resulted in an eGFP fluorescence (green) present throughout the cell (higher magnification of box marked in the merge image). Abbreviation: DIC, differential interference contrast. Scale bar: 50 µm.

Starting with the recently generated plasmid pAM-EGFP-L4, the expression cassette for L4-eGFP was cloned into the SpeI/EcoRV restriction sites of the multiple cloning site of the empty AAV shuttle plasmid #106_pAM-CBA-pL-WPRE-bGHpA to obtain pAM-CAG-EGFP-L4. Following this, BamHI-based excision of the L4 fragment led to the generation of pAM-CAG-EGFP, which was used as a control vector (Figure 13A). The functionality of both plasmids, pAM-CAG-EGFP-L4 and pAM-CAG-EGFP, was again tested by Lipofectamine-mediated transfection of HEK293 cells. As presented in Figure 13C and D, L4-eGFP showed a ribosome-characteristic localization with strong preference for nucleoli and weaker

presence in the cytoplasm of HEK293 cells transfected with pAM-CAG-EGFP-L4 (Figure 13C). Transfection with the control vector pAM-CAG-EGFP led to the diffuse expression of eGFP with no specific subcellular localization (Figure 13D). Additionally, Western blot analysis of HEK293 cells transfected with pAM-CAG-EGFP-L4 confirmed the expression of the correct fusion product. Immunostaining with the anti-RPL4 antibody revealed two bands, the endogenous ribosomal protein L4 (48 kDa) and the eGFP-tagged RPL4 (75 kDa). The latter band was absent in non-transfected HEK293 cells (Figure 13B).

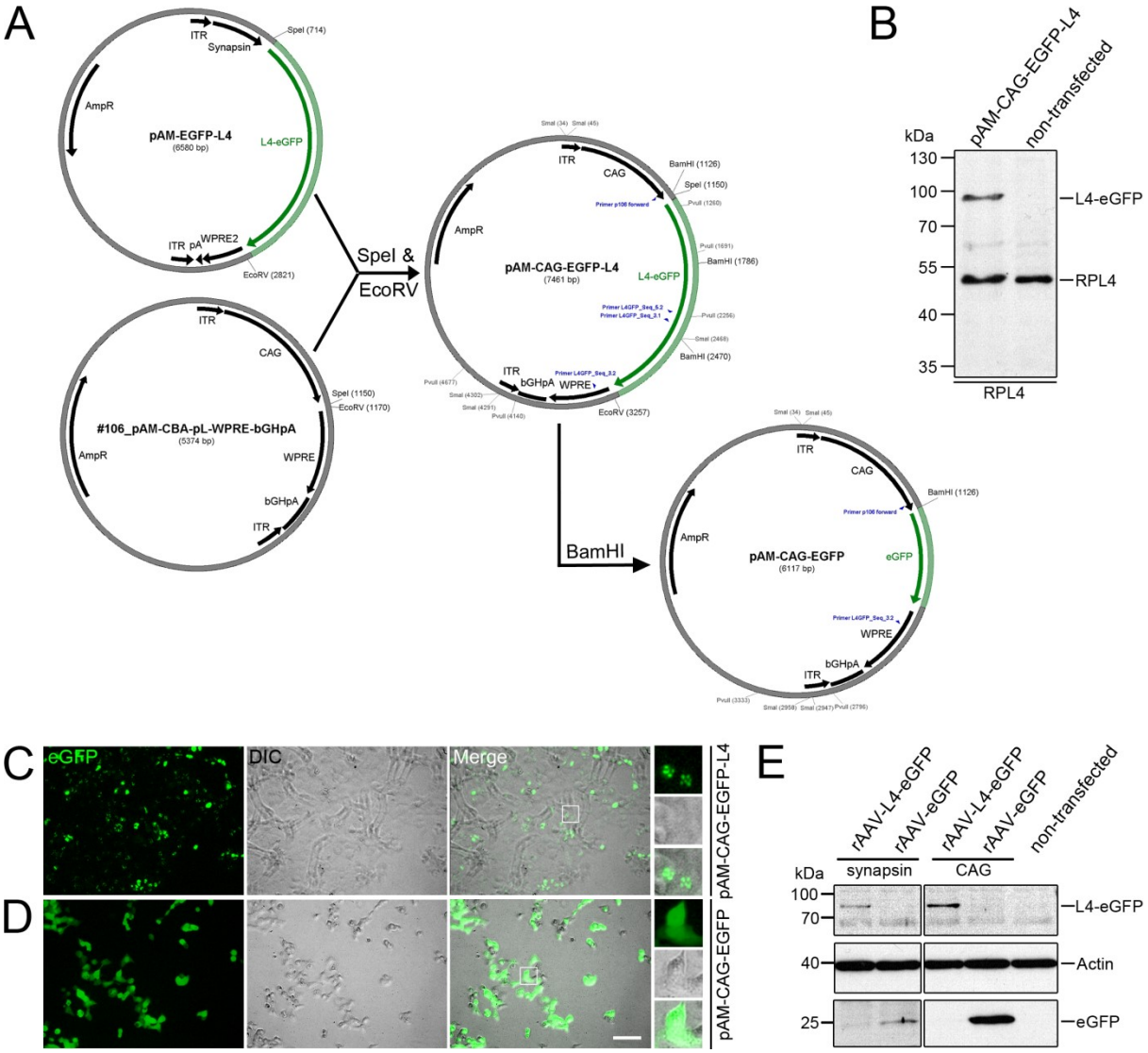

Figure 13: Exchange of the synapsin promoter against CAG promoter in AAV shuttle plasmids led to higher expression rates

(**A**) Outline of the cloning strategy for pAM-CAG-EGFP-L4 and pAM-CAG-EGFP. Abbreviations: ITR, inverted terminal repeats; WPRE2, woodchuck hepatitis virus posttranscriptional regulatory element 2; pA, polyadenylation signal; AmpR, ampicillin resistance; CAG, cytomegalovirus early enhancer/chicken-beta actin; bGHpA, bovine growth hormone polyadenylation signal. (**B**) Immunoblot of HEK293 cells transfected with pAM-CAG-EGFP-L4 or non-transfected control. Immunostaining with anti-RPL4 antibody showed the presence of endogenous ribosomal protein L4 in both samples and of L4-eGFP only in the transfected cells. (**C**) Transfection of HEK293 cells with pAM-CAG-EGFP-L4 resulted in a strong expression of L4-eGFP (green) in nucleoli and the cytoplasm. (**D**) HEK293 cells transfected with the control plasmid pAM-CAG-EGFP showed broad eGFP fluorescence (green) throughout the cell. Higher magnification of box marked in the merge image is shown on the right. Abbreviation: DIC, differential interference contrast. Scale bar: 50 µm. (**E**) Immunoblot of virally transduced embryonic (E18) hippocampal neurons showed higher expression levels of L4-eGFP or eGFP (both stained with anti-GFP) under the control of the CAG promoter as compared to the synapsin promoter. Actin was stained as loading control.

Having verified the newly cloned AAV shuttle plasmids, both were used to produce rAAVs again named rAAV-L4-eGFP and rAAV-eGFP. A first control experiment was carried out to analyze the impact of the promoter exchange on the expression rate. Embryonic hippocampal neurons were transduced with equal amounts (0.5×10^8 genomic copies) of rAAV-L4-eGFP or rAAV-eGFP with synapsin and CAG promoter, respectively. Cells were cultivated for several days, lysed, and proteins were extracted for Western blot analysis with an anti-GFP antibody that recognized both expression products, the fusion protein L4-eGFP (75 kDa) and eGFP (27 kDa). The blot in Figure 13E illustrates a clear increase in protein levels of L4-eGFP and eGFP with the exchange of promoter from synapsin to CAG. Based on this result, only rAAVs generated from plasmids with CAG promoter were used for all following experiments.

3.2.2 eGFP-tagged ribosomes are present in peripheral axons *in vitro*

First, various cultures of dissociated neurons were transduced with rAAV-L4-eGFP or rAAV-eGFP to analyze the expression pattern and localization of the encoded proteins by microscopic analyses. As displayed in Figure 14A and B, hippocampal neurons were successfully transduced. Depending on the virus applied, neurons showed either a strong eGFP fluorescence throughout the cell (Figure 14A) or the ribosome-specific localization of L4-eGFP in nucleoli and cytoplasm of the cell (Figure 14B). Even without the enhancement with the anti-GFP antibody, weak signals of eGFP-tagged ribosomes were visible in neurites (arrows in Figure 14B). These results are in agreement with previous findings showing the presence of endogenous RPL26 in dendrites of hippocampal neurons (Figure 8A).

Dissociated DRG neurons displayed similar subcellular localization of the viruses' products, with eGFP diffusely distributed in the cell bodies (Figure 14C) and L4-eGFP localizing to ribosomes in nucleoli and cytoplasm (Figure 14D). Furthermore, signal enhancement with an anti-GFP staining revealed a punctate pattern of eGFP-tagged ribosomes in axons of these peripheral neurons (Figure 14E) paralleling the observations with the ribosomal RPL26 marker as shown in Figure 8C. Non-neuronal cells, presumably Schwann cells, which were also present in the culture but not labeled by the anti-Tuj1 antibody, showed no green fluorescence (arrowheads in Figure 14D). This observation confirmed the neuron-specific tropism of the recombinant adeno-associated viruses.

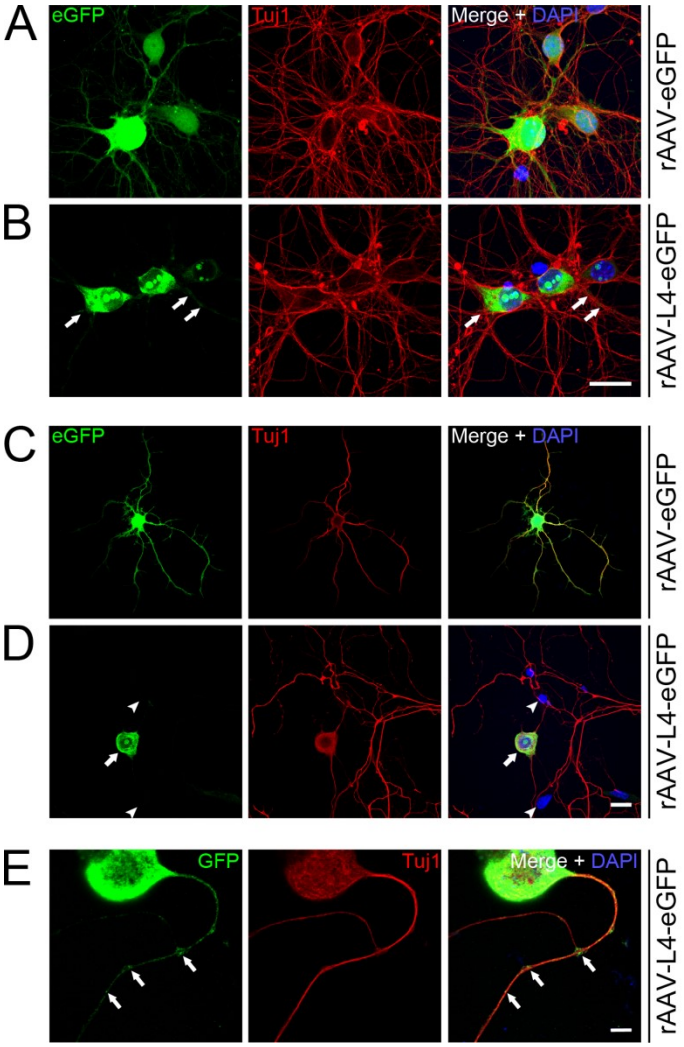

Figure 14: Expression and localization of eGFP-tagged ribosomes *in vitro*
(**A**, **B**) Embryonic (E18) hippocampal neurons were virally transduced with rAAV-eGFP (**A**) or rAAV-eGFP-L4 (**B**) and stained for Tuj1 (red) to visualize their processes. DAPI (blue) was used as nuclear marker. In the control sample, green fluorescent signals of eGFP were present throughout the cell (A). The fusion protein L4-eGFP (green) showed high fluorescent signals in nucleoli and cytoplasm, and occasional, weaker signals in processes (arrows, B). (**C**-**E**) ICC of virally transduced adult dissociated DRGs for Tuj1 (red) and DAPI (blue). (**C**) DRG neurons transduced with rAAV-eGFP express eGFP diffusely in the cell body and processes. In contrast, L4-eGFP (green) encoded by rAAV-L4-eGFP was localized predominantly to the nucleolus and the cell body of DRG neurons (arrow) but was not expressed in non-neuronal cells (arrowheads, **D**). (**E**) Immunostaining with anti-GFP antibody (green) revealed a punctate signal of L4-eGFP in neuronal processes (arrows). Scale bars: 20µm (B, D); 5µm (E).

3.2.3 *In vivo* injections of rAAVs

To show that ribosomes are transported from the neuronal cell body to the axon, the aim of *in vivo* experiments with the generated rAAV-L4-eGFP was to express eGFP-tagged ribosomes in motor and peripheral sensory neurons and to look for their presence in peripheral axons. Pilot experiments were carried out to establish and optimize the virus administration to living mice. rAAV-eGFP was delivered intrathecally by direct lumbar puncture that represented a relatively non-invasive route of administration without the necessity of surgery. Animals were additionally pretreated with mannitol (i.v.) to increase the access of AAV particles to the spinal cord parenchyma and the DRG neurons (Vulchanova et al., 2010). The timeline of the experiment is outlined in Figure 15A.

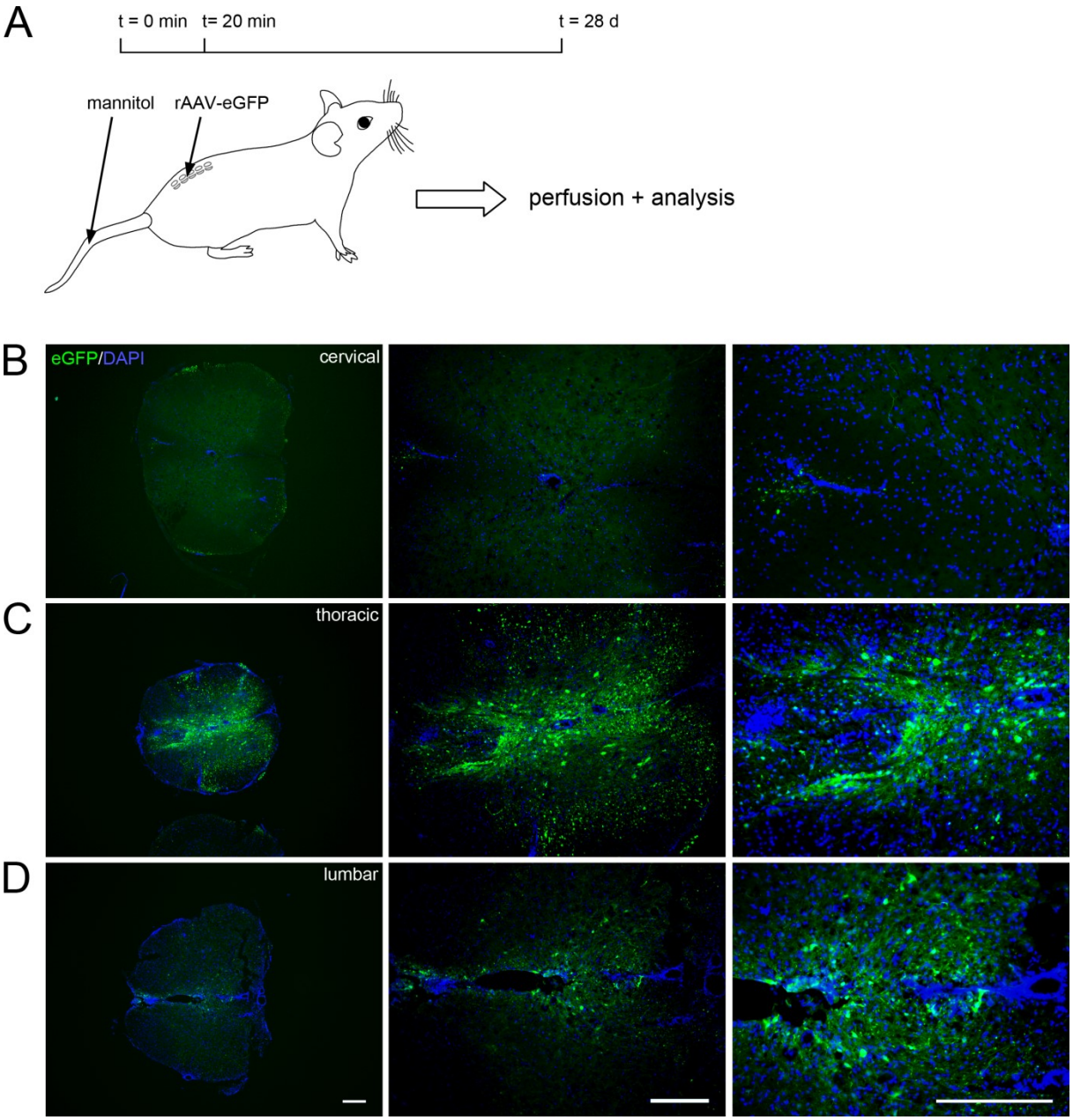

Figure 15: Spread of lumbarly injected rAAV-eGFP in the spinal cord
(**A**) Timeline of lumbar injection: Mannitol was injected into the tail vein of the mouse 20 minutes before the virus (rAAV-eGFP) was injected into the lumbar cerebrospinal fluid. Animals were perfused 28 days later and tissues of interest were analyzed by IHC. (**B-D**) Increasing magnifications of cross sections of cervical (B), thoracic (C), and lumbar (D) spinal cord after lumbar injection of rAAV-eGFP. The highest amount of eGFP signal (green) was found at thoracic level where many cells expressed eGFP. In lumbar spinal cord sections, the green fluorescence was slightly weaker and at cervical level, only some green spots were visible. Cell nuclei were stained with DAPI (blue). Scale bars: 500µm.

Four weeks after injection, strongest expression occurred at thoracic and to a lesser extend at lumbar spinal levels (Figure 15C, D). In both sections, eGFP signals mainly localized to the gray matter with highest incidence in the area surrounding the central channel (lamina X) and Clarke's columns. Higher magnification of the eGFP-positive area suggested that most probably local interneurons and their branches were labeled (observations based on morphology combined with colocalization with DAPI, Figure 15C). In the cervical spinal cord (Figure 15B), eGFP fluorescence was only detected in one region at the dorsal site, where they likely represent cross sections of ascending fiber of interneurons transduced at lower

spinal levels. However, additional analyses with glial and neuron-specific markers are needed to analyze the expression pattern of lumbarly injected rAAV-eGFP in more detail. In addition to spinal cord tissue, lumbar DRGs have also been isolated and analyzed, but these did not display any eGFP signal (data not shown).

3.3 Generation of RiboTracker mouse line

A transgenic mouse line was generated providing a second tool for neuronal expression of fluorescently-labeled ribosomes. RPL4 was fused to the red fluorescent tandem dimer protein Tomato (tdTomato) and inserted into the first intron of the *Gt(ROSA)26Sor* (*ROSA26*) locus for constitutive and ubiquitous expression. An additional stop codon flanked by loxP sites preceded the L4-tdTomato sequence in the transgenic RiboTracker mouse; hence, neuron-restricted expression of the transgene was achieved by crossbreeding with specific Cre expressing mouse lines.

3.3.1 Design and cloning of the targeting vector

First, the fusion construct L4-tdTomato was generated. The sequence of the ribosomal protein L4 was amplified from pAM-EGFP-L4 by PCR with specific In-Fusion compatible oligonucleotides (L4+Tomato_IF_5.1 and L4-Tomato_IF_3.1, see 2.1.10) and cloned into the multiple cloning site of pCMV-tdTomato clontech at the NheI restriction site by In-Fusion reaction (Figure 16A). To verify the correct fusion of RPL4 with tdTomato, HEK293 cells were transiently transfected with the resulting plasmid pCMV-L4-tdTomato or with pCMV-tdTomato clontech as control. As illustrated in Figure 16B, L4-tdTomato showed a ribosome-specific localization within the cell and was predominantly found in the nucleoli and the cytoplasm. This expression pattern matched previous observations with L4-eGFP (Figure 12B and Figure 13C) and led to the conclusion that the fluorescent tag of tdTomato was not interfering with the function and localization of RPL4. Transfection with the control plasmid resulted in a strong expression of tdTomato distributed all over the cytoplasm (Figure 16C). Additionally, HEK293 cells transfected with pCMV-L4-tdTomato were analyzed by Western blot with the anti-RPL4 antibody that detected the endogenous RPL4 at 48 kDa and the fusion construct L4-tdTomato at 102 kDa. The latter was not found to be expressed by non-transfected cells (Figure 16D).

In the next cloning step, during PCR amplification with oligonucleotides L4+Tomato_5.1 and L4+Tomato_3.1 (see 2.1.10), restriction sites for SmaI and SgsI were inserted at the 3’ and 5’ end of the fusion construct L4-tdTomato, respectively. This amplified DNA fragment was then inserted into the SmaI/SgsI linearized *ROSA26* targeting vector R26_CAGs_IRES_EGFP replacing the IRES-EGFP cassette (Figure 16A). The resulting targeting vector R26_CAGs_L4-tdTomato contained two genomic fragments of the *ROSA26*

locus that were homologous to the region between exon 1 and 2 of the wild type allele and necessary for the integration via homologous recombination in embryonic stem cells. Since the *ROSA26* promoter provided only moderate strength, the exogenous CAG promoter was present in the targeting vector to drive a high transgene expression. Upstream of the fusion construct, the stop codon and a selection marker for neomycin resistance (neo) were present, both flanked by loxP sites to get eliminated by Cre-mediated recombination (Figure 17A).

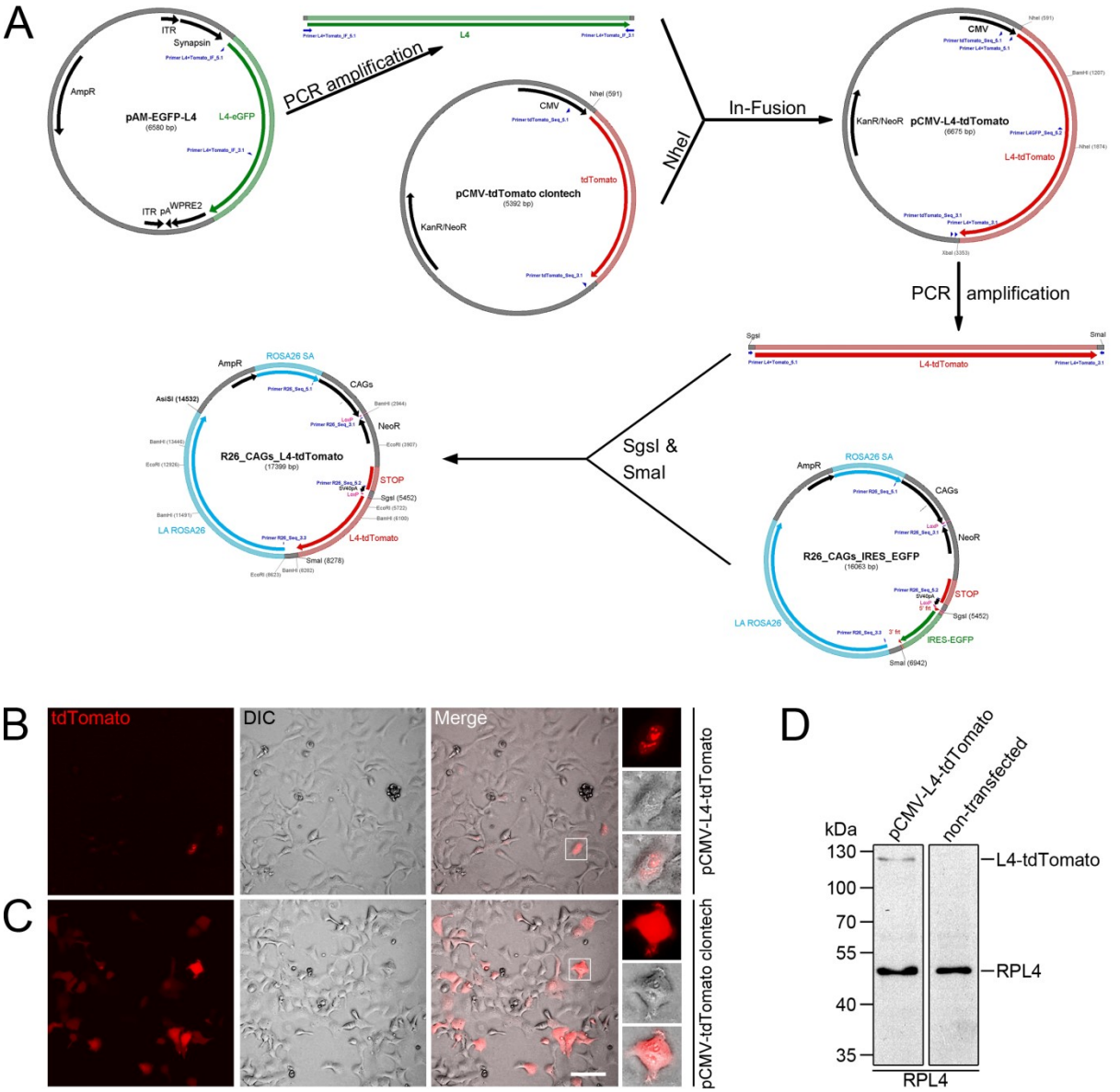

Figure 16: Generation of the targeting vector to express L4-tdTomato from the *ROSA26* locus
(**A**) Outline of the cloning strategy for the targeting vector R26_CAGs_L4-tdTomato. Abbreviations: ITR, inverted terminal repeats; WPRE2, woodchuck hepatitis virus posttranscriptional regulatory element 2; pA, polyadenylation signal; AmpR, ampicillin resistance; CMV, cytomegalovirus; KanR, kanamycin resistance; NeoR, neomycin resistance; ROSA26 SA, short arm of homologous sequence of *ROSA26*; LA ROSA26, long arm of homologous sequence of *ROSA26*. (**B**) The fusion protein L4-tdTomato (red) localized to nucleoli and the cytoplasm in HEK293 cells that were transiently transfected with pCMV-L4-tdTomato. (**C**) Transfection with the control plasmid pCMV-tdTomato clontech led to a strong tdTomato (red) expression diffusely in the cell. Higher magnification of box marked in the merge image is shown on the right. Scale bar: 50 µm. (**D**) Immunoblot analysis of HEK293 cells transfected with pCMV-L4-tdTomato or non-transfected control stained with anti-RPL4 antibody. The endogenous RPL4 protein was expressed in both samples, whereas the fusion construct L4-tdTomato was only present in transfected cells.

3.3.2 Homologous recombination in ES cells

In order to insert the targeting vector into the *Gt(ROSA)26Sor* locus, R26_CAGs_L4-tdTomato was linearized with AsiSI and electroporated into JM8A3 murine ES cells. Transfected ES cell clones (called JM8-L4 clones) were selected by genetecin. To confirm homologous recombination, the genomic DNA of genetecin-resistant clones was screened by Southern blot probed with a radioactively-labeled DNA fragment binding in the 5' region of the first exon in the *ROSA26* locus (Rosa 5' probe in Figure 17A; 460 bp fragment of EcoRI digested pCRII-Rosa5' probe). 42 out of 96 analyzed ES cell clones were positively tested for the targeted allele $R26^{tg}$ as the DNA fragment of 6.8 kb could clearly be distinguished from the wild type fragment ($R26^{WT}$) of 15.6 kb (Figure 17B). Out of these 42 positive clones, six clones (2F, 3C, 4D, 6G, 9D, 10D) were selected and tested by Southern blot with different probes to verify the correct insertion site of homologous recombination. Using once more the Rosa 5' probe (top panel in Figure 17C), the heterozygosity of all six JM8-L4 clones was confirmed by the presence of the EcoRI fragments from the targeted (6.8 kb) and wild type (15.6 kb) allele. In addition, a testing probe binding downstream of the target region at exon 2 in the *ROSA26* locus (Rosa 3' probe in Figure 17A; 680 bp fragment of EcoRI digested pCRII-Rosa3' probe) and an internal transgene probe that was complementary to 624 bp within the *neo* gene (neo probe in Figure 17A; prepared by PCR amplification with primer pair rspNeo4/rspNeo5 (see 2.1.10) from R26_CAGs_L4-tdTomato) were applied. DNA fragments of the wild type (15.6 kb) and the mutant allele (11.6 kb) were detected in all six clones when hybridized with the Rosa 3' probe (middle panel in Figure 17C). In addition, they all showed the 6.8 kb fragment identified by the neo probe that was not present in the wild type control (bottom panel in Figure 17C).

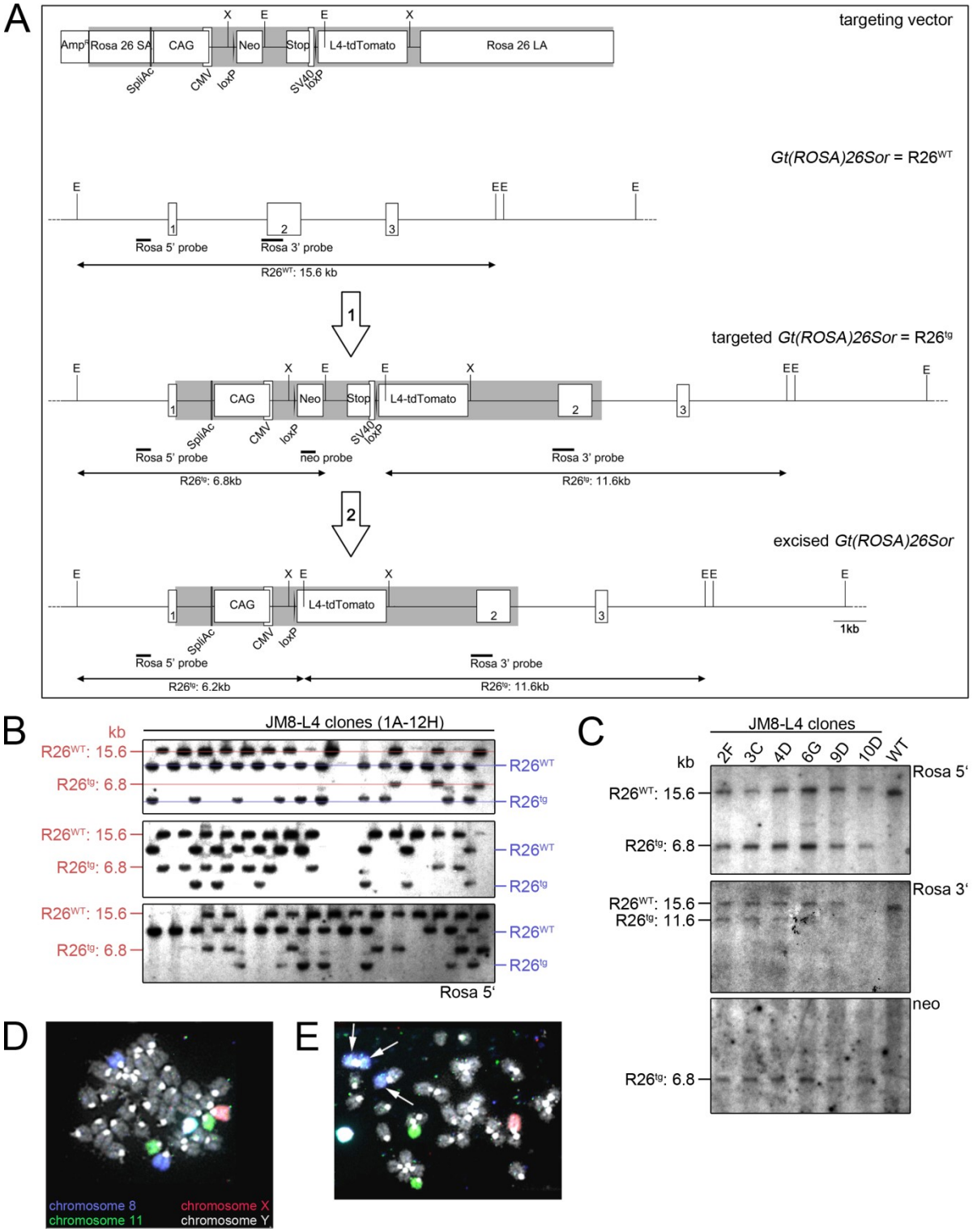

Figure 17: Homologous recombination in ES cells
(**A**) Schematic illustration of the targeting strategy to insert the targeting vector R26_CAGs_L4-tdTomato into the *Gt(ROSA)26Sor* locus by homologous recombination in ES cells (arrow 1). Subsequent Cre-mediated recombination (arrow 2) deleted the loxP-flanked transcriptional STOP cassette. Sizes of DNA fragments and location of restriction sites (E, X) and Southern blot probes (Rosa 5', Rosa 3', and Neo probe) are indicated. Abbreviations: Amp^R, ampicillin resistance; ROSA26 SA, short arm of homologous sequence of *ROSA26*; SpliAC, splice acceptor; CAGs, cytomegalovirus early enhancer/chicken-beta actin promoter; CMV, cytomegalovirus; X, Xba restriction site; NEO, neomycin resistance gene; E, EcoRI restriction site; STOP, transcriptional stop cassette; SV40 pA, simian virus 40 polyadenylation signal; LA ROSA26, long arm of homologous sequence of *ROSA26*. (**B**) Southern blot analysis of EcoRI digested genomic DNA of geneticin-resistant JM8 ES cell clones transfected with R26_CAGs_L4-tdTomato. Samples were loaded in slots at alternating heights so that DNA fragments of wild type ($R26^{WT}$) and targeted ($R26^{tg}$) alleles for each neighboring lane run at slightly different height (red vs. blue). Screening with Rosa 5' probe identified 42 positive out of 96 analyzed clones. (**C**) Confirmation Southern blot of six selected, EcoRI digested JM8-L4 ES cell clones with Rosa 5' (top), Rosa 3'

(middle), and neo probe (bottom) to confirm homologous recombination. Genomic DNA of JM8 ES cell was used as wild type (WT) control. The sizes of the respective EcoRI fragments from the targeted ($R26^{tg}$) and wild type ($R26^{WT}$) alleles are indicated. (**D**, **E**) Single cell examples from the karyotype analysis of JM8-L4 ES clone 9D (**D**) and 4D (**E**) by *in situ* hybridization with fluorescently-labeled probes. All analyzed cells of clone 9D showed a normal ploidy with an X (red) and Y chromosome (white) and no trisomy was detected (**D**). In contrast, one of 30 analyzed cells of clone 4D had a trisomy of chromosome 8 (blue, arrows in **E**).

3.3.3 Generation and genotyping of the transgene mice

Out of the six ES cell clones that were positively tested for homologous recombination, clones 4D and 9D were chosen for cytogenetic analyses (consisting of a mouse "quick test", see Figure 17D and E, and chromosome counting, see Table 7) performed by Chrombios GmbH. For clone 4D, 29 of 30 cells (97%) analyzed by the "quick test" showed a normal ploidy and one cell had a trisomy 8 (arrows in Figure 17E). Chromosome counting revealed that 13 of 15 cells (87%) had a normal chromosome count of 2n = 40 and two cells had more than 40 chromosomes (Table 7). The "quick test" of ES cell clone 9D detected no trisomy (Figure 17D) and all 30 analyzed cells (100%) showed a normal ploidy. 14 of 15 cells (93%) analyzed by chromosome counting had a normal count of 2n and only one cell contained less than 40 chromosomes (Table 7).

Table 7: Summary of chromosome counting for JM8-L4 ES cell clones 4D and 9D.

	Chromosome counts					
Cell line	*38*	*39*	*40 (%)*	*41*	*42*	***total***
JM8 4D	-	-	13 (87)	2	-	15
JM8 9D	-	1	14 (93)	-	-	15

Embryonic stem cells of clones 4D and 9D were used for microinjection into blastocysts that were subsequently implanted into pseudopregnant females to obtain chimeric pups. These experiments as well as the first mating were performed by Dr. Leonid Eshkind at the Transgenic Facility Mainz (University Medical Center Mainz). The JM8A3 stem cells had the dominant allele of the agouti B6 background at one coat color locus unlike the C57Bl6 albino or CD1 donor strains of the blastocysts. Accordingly, the degree of chimerism of the first offspring was estimated by coat color. Male chimeric mice were crossed with B6 albino females with the result that germline transmission (GLT) could directly be detected by color coat (agouti or black) (Figure 18A). From the breeding of male chimera mice of clone 4D with B6 albino females, the efficiency of germline transmission was very low, so that only one black offspring was obtained. Among the offspring based on clone 9D, seven GLT mice (#6369, 6485, 6486, 6491, 6492, 6498, 6500), all with agouti coat color, were generated. Tail samples of these mice were used to isolate DNA and the presence of the transgene was analyzed by PCR. Oligonucleotides RosaFA, RosaRA and SpliAcB (see 2.1.10) produced a transgene-specific fragment of 241 bp that was present in addition to the 603 bp PCR product of the wild type allele in heterozygous GLT animals (Figure 18B). Of the seven GLT mice from clone 9D, males #6369 and #6500 were backcrossed with B6 albino females to

establish the RiboTracker mouse line. The homozygous RiboTracker (RiboTracker^{ho}) mice bred normally and the offspring were all viable and fertile.

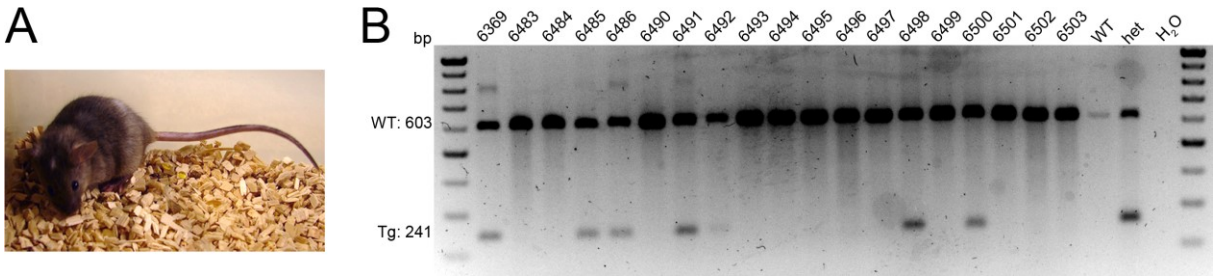

Figure 18: Germline-transmission of RiboTracker mouse
(**A**) Example of a germline transmission (GLT) mouse identified by agouti color coat. (**B**) Genotyping PCR of tail samples from chimeric offspring generated originally from ES cell clone 9D identified seven heterozygous GLT mice that showed the wild type (WT, 603 bp) and transgene PCR product (Tg, 241 bp). Abbreviations: WT, wild type; het, heterozygous; H_2O, water.

3.3.4 tdTomato-tagged RPL4 localizes to ribosome-specific subcellular domains

Expression of the tdTomato-tagged RPL4 in RiboTracker^{ho} mice was suppressed by the stop codon. Therefore, animals were crossbred with various mouse lines that expressed Cre recombinase in defined cell types. Cre-mediated recombination of the loxP sites resulted in the excision of the stop cassette and the subsequent expression of the L4-tdTomato fusion construct in RiboTracker^{ho}-Cre^{+} mice.

To evaluate the correct subcellular localization of tdTomato-tagged RPL4, homozygous RiboTracker animals were crossed with the neuron-specific NEX-Cre mouse line to drive expression of the transgene in hippocampal neurons. The NEX promoter activity starts around E11.5 and is restricted to the nervous system with high expression in the brain including the hippocampus formation (Goebbels et al., 2006).

Signal enhancement with an anti-red fluorescent protein (RFP) antibody that recognized the tdTomato protein showed a strong expression of L4-tdTomato in nucleoli and the cytoplasm of cultured hippocampal neurons (Figure 19A). Red RPL4 particles were detected in dendrites, which were immunoreactive for MAP2. Non-neuronal cells did not express the transgene because the NEX promoter was not active in these cells (arrowheads, Figure 19A). In adult RiboTracker^{ho}-NEX-Cre^{+} mice, a similar subcellular localization of tdTomato-tagged RPL4 was found in CA1 hippocampal neurons *in vivo*. Likewise, RFP signals were also detected in dendrites (arrows, Figure 19B). This ribosome-specific subcellular localization of L4-tdTomatoin hippocampal neurons confirmed its correct incorporation into ribosomes and indicated that the tag did not interfere with the ribosomal protein in neuronal cells.

Homozygous RiboTracker animals were also crossed with mice that expressed the Cre recombinase under the transcriptional regulation of the calcium/calmodulin-dependent protein kinase II alpha (CamKIIα) promoter. In this Cre line, expression of the recombinase

enzyme started after birth (around P3) and occurred in different brain regions including cortex and hippocampus region (Casanova et al., 2001). Immunohistochemical analysis of CA1 pyramidal cells in adult RiboTracker^{ho}-CamKIIα-Cre^{+} mice (Figure 19C) again confirmed the ribosomal localization of tdTomato-tagged RPL4 by showing the same subcellular distribution as previously described for the RiboTracker^{ho}-NEX-Cre^{+} mice (Figure 19B).

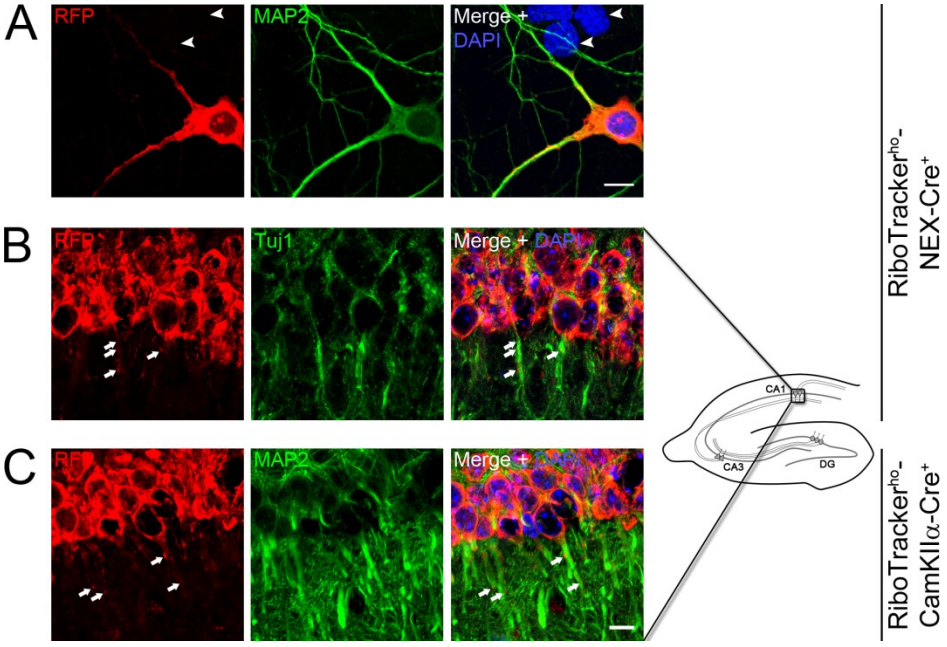

Figure 19: Dendritic localization of L4-tdTomato
(**A**) ICC with anti-RFP antibody (red) showed the localization of L4-tdTomato in nucleoli, cytoplasm, and dendrites of neonatal (P1) dissociated hippocampal neurons of RiboTracker^{ho}-NEX-Cre^{+} mouse. Non-neuronal cells did not express L4-tdTomato (arrowheads). Anti-MAP2 antibody (green) was used as dendritic marker and cell nuclei were stained with DAPI (blue). (**B**, **C**) IHC for RFP (red), MAP2 or Tuj1 (green), and DAPI (blue) of coronal brain sections of adult RiboTracker^{ho}-NEX-Cre^{+} (**B**) and RiboTracker^{ho}-CamKIIα-Cre^{+} mouse (**C**). RFP-stained L4-tdTomato is present in the cell body and dendrites (arrows) of CA1 hippocampal neurons. The schematic view of a hippocampus cross section on the right illustrates the examined region. Abbreviations: CA, cornu ammonis; DG, dentate gyrus. Scale bars: 10 µm.

3.4 tdTomato-tagged ribosomes in RiboTracker^{ho}-CamKIIα-Cre^{+} and RiboTracker^{ho}-Advillin-Cre^{+} mice

Having validated the functionality of the RiboTracker mouse line as a tool to label ribosomes specifically in defined cell types, next, experiments were performed with the aim to prove the axonal localization of cell body-derived ribosomes *in vivo*. To address this question, tdTomato-tagged RPL4 was restricted to neuronal cell populations by crossing RiboTracker^{ho} mice with neuron-specific Cre lines. The aforementioned CamKIIα-Cre line was used to express the transgene in CNS and PNS neurons since the CamKIIα-Cre promoter is also active in some cells of the DRGs (Bruggemann et al., 2000; Carlton, 2002). Additionally, the Advillin-Cre line was chosen because of its specificity for sensory neurons and early onset of promoter activity (trigeminal ganglia at E14.5 to E16.5 and DRG at P1) (Zurborg et al., 2011).

3.4.1 Analysis of neuronally-expressed L4-tdTomato *in vitro*

The initial study of RiboTracker^{ho}-CamKIIα-Cre^{+} and RiboTracker^{ho}-Advillin-Cre^{+} comprised ICC analyses of different culture systems. Cultures of adult dissociated DRG neurons confirmed the neuronal specificity of both lines as L4-tdTomato was exclusively expressed in β-III-tubulin-positive neurons (arrows) while non-neuronal cells were negative (arrowheads, Figure 20A, B). Signals of the tdTomato-labeled RPL4 were strongest in neuronal cytoplasm and nucleoli, and overlapped completely with the anti-RFP staining. In axons, however, the fluorescence of the tdTomato protein was too weak to be measured without enhancement. The use of the anti-RFP antibody enabled the visualization of punctate ribosome clusters in axons (right panels in Figure 20A and B).

In explant cultures of adult DRGs, many neurons expressed L4-tdTomato in RiboTracker^{ho}-CamKIIα-Cre^{+} (Figure 20C) and RiboTracker^{ho}-Advillin-Cre^{+} mice (Figure 20E) but no tagged ribosomes were detected by the anti-RFP antibody in axons of these explants (Figure 20D, F). Similarly, tdTomato-labeled RPL4 was present in the cell bodies of layer V cortex neurons in explant cultures of neonatal RiboTracker^{ho}-CamKIIα-Cre^{+} mice (Figure 20G), but axons did not display any RFP signals (Figure 20H). RiboTracker^{ho}-Advillin-Cre^{+} mice did not express Cre recombinase in central neurons since the Advillin promoter is exclusively active in sensory neurons (Hasegawa et al., 2007). Hence, no signals of L4-tdTomato or RFP were found in neonatal cortex explants of these mice (Figure 20I).

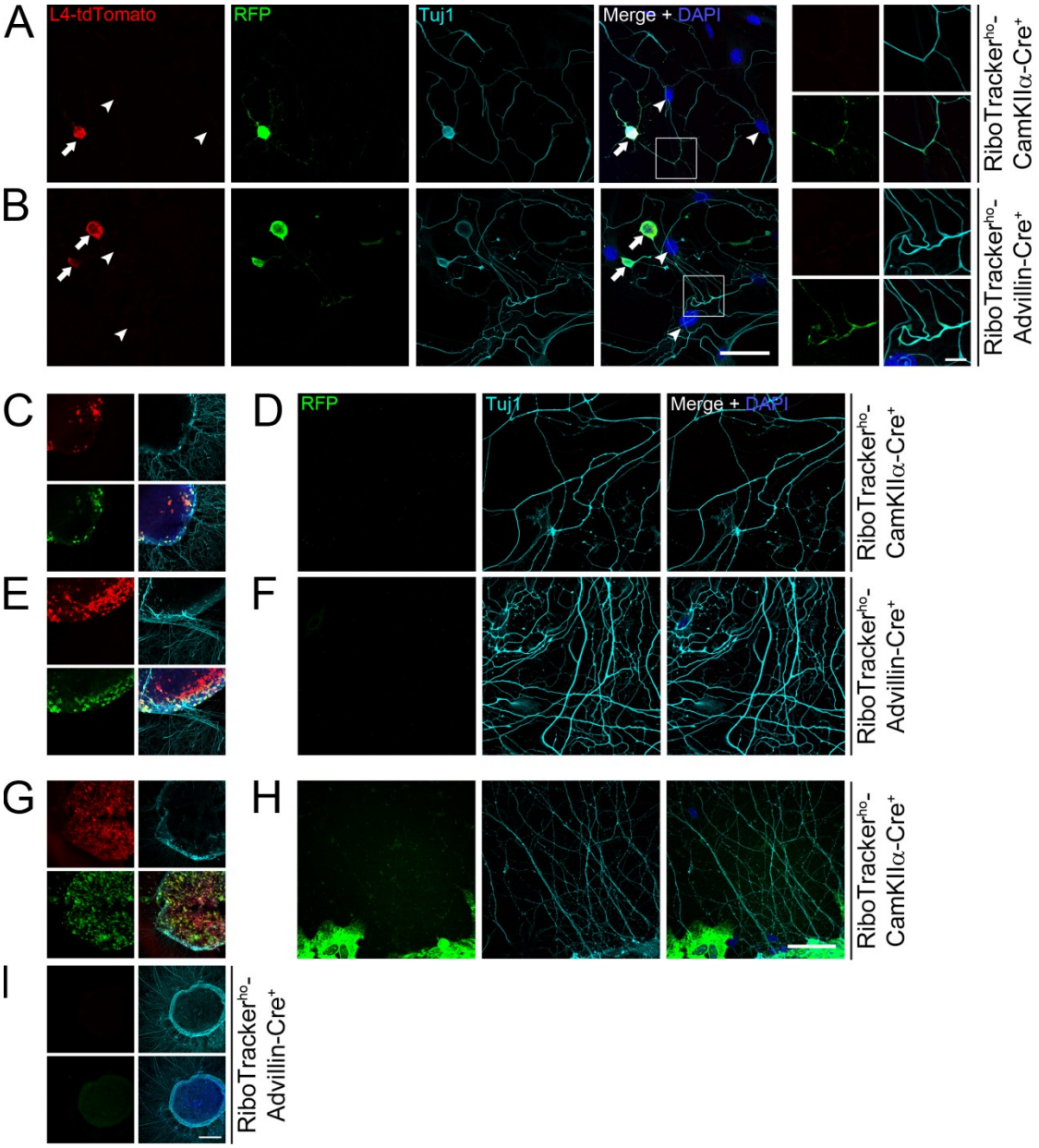

Figure 20: Localization of neuronally-expressed L4-tdTomato in various culture systems *in vitro*
(**A-I**) ICC for RFP (green), Tuj1 (cyan), and DAPI (blue) on cultures of sensory neurons and cortex explants. L4-tdTomato is shown in red. (**A**, **B**) Adult dissociated DRG neurons (arrow) of RiboTracker^{ho}-CamKIIα-Cre^{+} (**A**) and RiboTracker^{ho}-Advillin-Cre^{+} mouse (**B**) expressed L4-tdTomato in nucleoli and the cytoplasm. Signal enhancement with an anti-RFP antibody revealed a punctate pattern in axonal processes as shown in the higher magnification of the boxed area on the right panel. Non-neuronal cells (arrowhead) did not express L4-tdTomato. (**C**-**F**) Adult DRG explants of RiboTracker^{ho}-CamKIIα-Cre^{+} (**C**, **D**) and RiboTracker^{ho}-Advillin-Cre^{+} mouse (**E**, **F**). L4-tdTomato is present in many neurons of the explants (C, E) but absent from axonal processes (D, F). (**G**, **H**) Neurons of neonatal (P7) cortex explants of RiboTracker^{ho}-CamKIIα-Cre^{+} mouse contained L4-tdTomato in their cell bodies (**G**), but not in their neuronal processes (**H**). (**I**) As expected, neurons of neonatal (P0) cortex explants of RiboTracker^{ho}-Advillin-Cre^{+} mouse did not express L4-tdTomato. Scale bars: 50 µm (B, H); 10 µm (boxes enlarged on right panel in B); 200 µm (I).

3.4.2 Analysis of neuronally-expressed L4-tdTomato *in vivo*

To investigate the axonal ribosome transport *in vivo*, IHC analyses of DRGs and sciatic nerves of both neuronal RiboTracker-Cre lines were performed. As shown in Figure 20, a strong expression of L4-tdTomato was found in many neurons of adult DRGs in both neuron-specific RiboTracker^{ho}-Cre^{+} lines. Depending on the expression pattern of the Cre recombinase, only subpopulations of DRG neurons expressed labeled ribosomes. In

RiboTracker^{ho}-CamKIIα-Cre^{+} mice, mostly small-diameter sensory neurons, which comprised peptidergic cells positive for calcitonin gene-related protein (CGRP) and non-peptidergic neurons identified by their binding capacity of isolectin B4 (IB4), expressed L4-tdTomato. Occasionally, few neurons of large diameter, stained with the anti-NF200 antibody as marker for the neurofilament heavy chain, were positive for tdTomato-tagged RPL4 (Figure 21A). RiboTracker^{ho}-Advillin-Cre^{+} mice had a similar expression pattern of L4-tdTomato in subtypes of sensory neurons as RiboTracker mice crossed with the CamKIIα-Cre driver. The majority of neurons with tagged ribosomes had a small diameter and belonged to the non-peptidergic, IB4-positive group of sensory neurons. To a smaller extent, CGRP+ neurons were also found to express L4-tdTomato, but rarely large NF200-stained cells (Figure 21B).

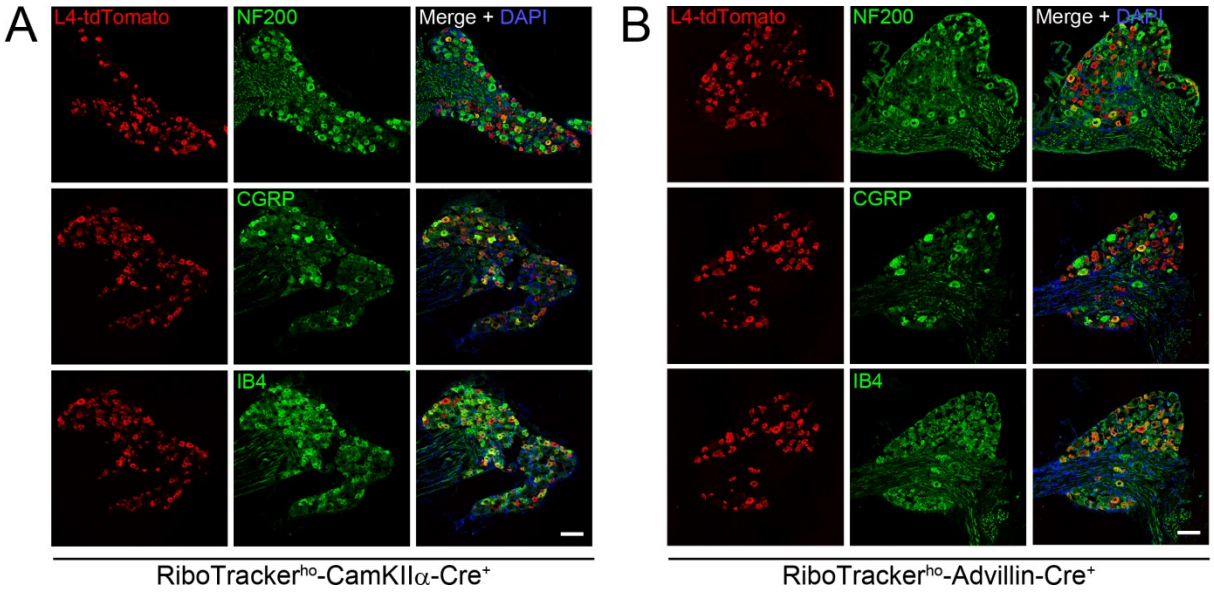

Figure 21: Expression pattern of neuron-specific L4-tdTomato in the PNS *in vivo*
(**A**, **B**) IHC of adult DRG cross sections with different markers (green) for neuronal subpopulations. L4-tdTomato is shown in red color. (**A**) Very few NF200-positive DRG neurons expressed L4-tdTomato in the RiboTracker^{ho}-CamKIIα-Cre^{+} mouse, but many L4-tdTomato-expressing neurons were positive for CGRP or IB4 (green). (**B**) In DRGs of the RiboTracker^{ho}-Advillin-Cre^{+} mouse, only very few or almost no L4-tdTomato expressing neurons were found in NF200- or CGRP-stained subpopulations, but many were positive for IB4 (green). Scale bars: 100 µm.

Focusing on the sciatic nerve, no tdTomato-tagged ribosomal protein L4 (stained with the anti-RFP antibody) was detected in the DRG axons (Figure 22A, B) even though their cell bodies contained the labeled ribosomes in both neuronal RiboTracker^{ho}-Cre^{+} lines (Figure 21). To make sure that the small population of axonal ribosomes in uninjured axons has not been overlooked, sciatic nerves of RiboTracker^{ho}-CamKIIα-Cre^{+} and RiboTracker^{ho}-Advillin-Cre^{+} mice were crushed and axons at both sides of the injury were analyzed the next day (Figure 22C-F). Close attention has been paid to Remak fibers that are built-up of unmyelinated C-type axons from small-diameter sensory neurons and that were demonstrated above to contain ribosomes (Figure 10D, E). However, no RFP signals of L4-tdTomato were found proximally (Figure 22C, D) as well as distally (Figure 22E, F) to the injury, neither in Remak fibers (arrows) nor in myelinated axons. Overall, these findings indicate that neuronally-expressed ribosomes were not transported into axons.

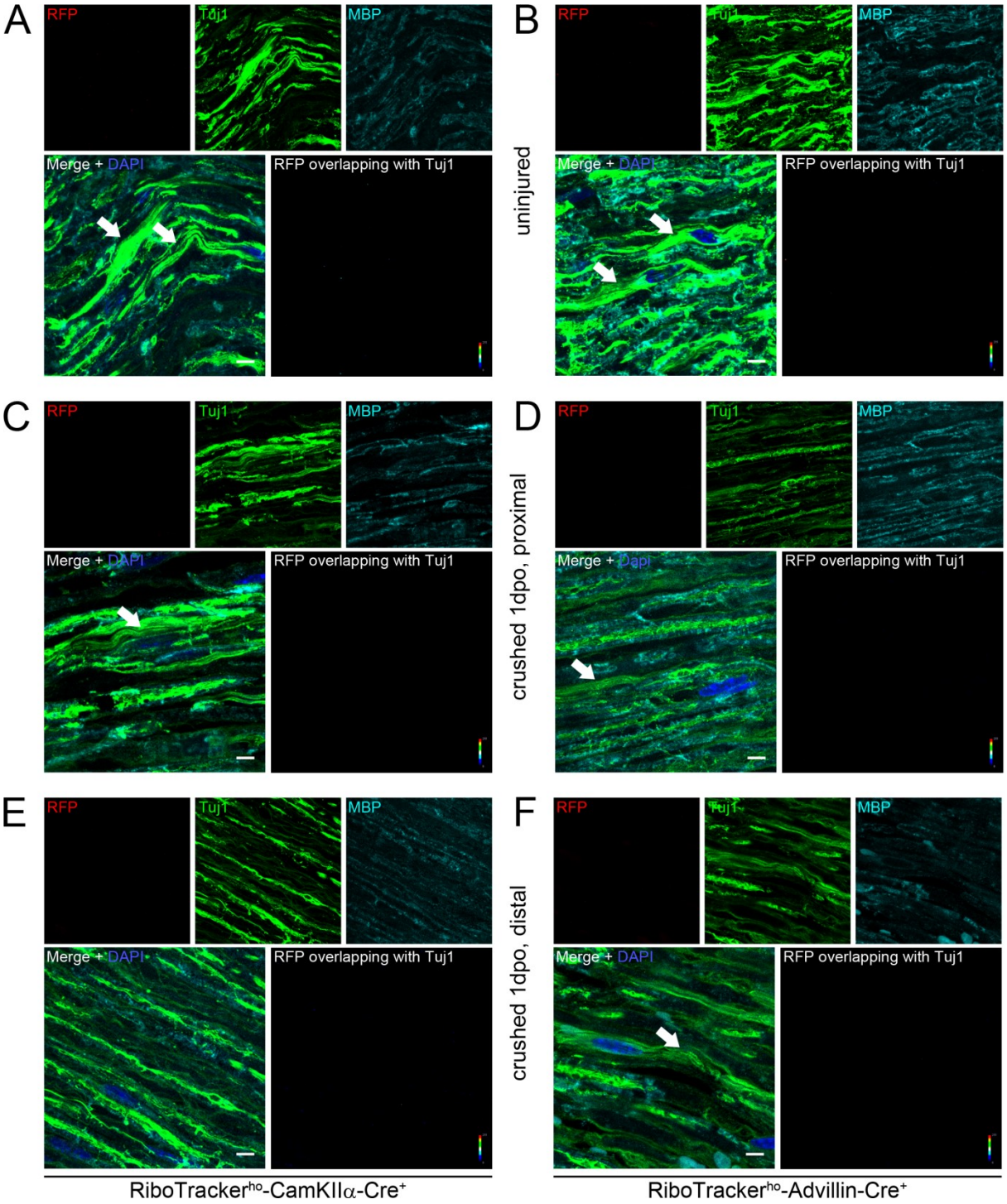

Figure 22: Neuronally-expressed L4-tdTomato is absent in peripheral axons *in vivo*
(**A-F**) Longitudinal sections of sciatic nerves from adult RiboTracker^{ho}-CamKIIα-Cre^{+} (**A**, **C**, **E**) and RiboTracker^{ho}-Advillin-Cre^{+} (**B**, **D**, **F**) mice were stained for RFP (red), the axonal marker β-III-tubulin (Tuj1, green), myelin basic protein (MBP, cyan), and DAPI (cell nuclei, blue). No RFP signal was detectable in sciatic nerves of unlesioned animals (**A**, **B**) or after sciatic nerve crush (1dpo) at sites proximal (**C**, **D**) or distal to the injury (**E**, **F**). Therefore, no colocalization signals of the red (RFP) and green (Tuj1) channels could be extracted. Arrows point to Remak fibers. Scale bars: 5 µm.

3.5 tdTomato-tagged ribosomes in RiboTracker^{ho}-CNP-Cre^{+} mice

The above-described experiments were speaking against the neuronal cell body as the origin of axonal ribosomes. Therefore, the transfer of ribosomes from glial cells to the axon was reconsidered as alternative and investigated next. In order to obtain a glial expression of L4-tdTomato, RiboTracker^{ho} mice were crossed with a Cre-line that expressed the recombinase enzyme under the regulatory control of the *Cnp1* gene (Lappe-Siefke et al., 2003). The encoded 2′,3′-cyclic nucleotide 3’phosphodiesterase (CNP) is a marker protein of myelin-forming glial cells and is almost exclusively expressed in oligodendrocytes and Schwann cells (Vogel and Thompson, 1988; Sprinkle, 1989; Chandross et al., 1999). Accordingly, RiboTracker^{ho}-CNP-Cre^{+} mice are expected to express tdTomato-tagged ribosomes in glial cells in the CNS and PNS.

3.5.1 tdTomato-tagged RPL4 is expressed by glial and neuronal cells *in vitro*

The experiments focused on the origin of ribosomes found in peripheral axons, so the expression pattern of L4-tdTomato in the PNS was first analyzed in dissociated and explant cultures of adult sensory neurons derived from RiboTracker^{ho}-CNP-Cre^{+} mice (Figure 23). In the dissociated culture system, L4-tdTomato was found in nucleoli and the cytoplasm of all non-neuronal cells (arrowheads, top panel in Figure 23A). Surprisingly, some (filled arrows), but not all neurons (unfilled arrow) also expressed tdTomato-tagged ribosomes. Likewise, in addition to the glia, neurons were positive for L4-tdTomato in the adult DRG explant cultures (Figure 23B). When focusing on axons laying in close vicinity to L4-tdTomato expressing glial cells in these two culture systems, granular RFP signals were occasionally found to overlap with Tuj1-stained axons (bottom panel in Figure 23A and C). Schwann cell protrusions often run along or wind themselves around axons. Therefore, it could not be concluded with certainty that these RFP-positive dots were present inside the axoplasm even if the subtracted axon-only image strongly suggested this interpretation. Furthermore, it was unclear if ribosome transfer from glial cells to axons occurred *in vitro* at all. To overcome this limitation, the expression pattern and localization of tdTomato-tagged ribosomes in cells and axons of the peripheral nervous system was studied *in vivo* in RiboTracker^{ho}-CNP-Cre^{+} mice, in the uninjured nerve and after sciatic nerve crush.

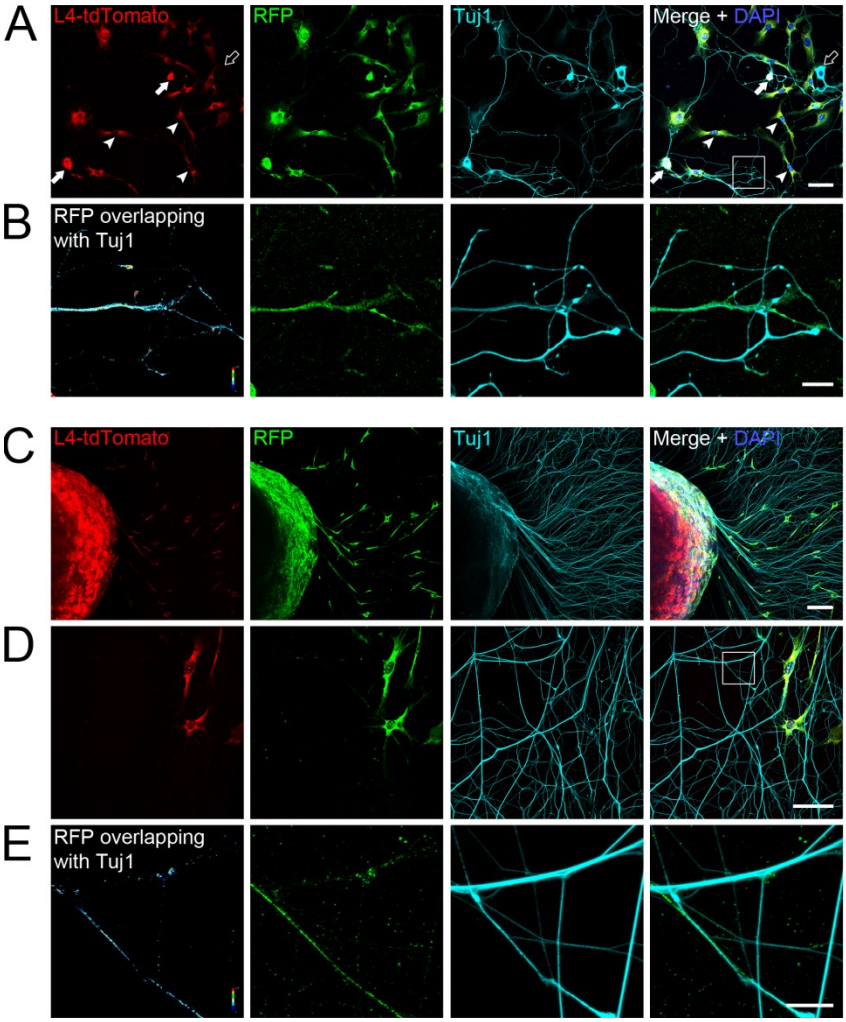

Figure 23: Expression pattern and localization of L4-tdTomato in RiboTracker^{ho}-CNP-Cre^{+} mice *in vitro*
(**A-E**) ICC for RFP (red), Tuj1 (cyan), and DAPI (blue) on cultures of dissociated sensory neurons (**A**, **B**) and DRG explants (**C-E**) prepared from adult RiboTracker^{ho}-CNP-Cre^{+} mice. L4-tdTomato is expressed in Schwann cells (arrowheads in A; C) and some (filled arrows in A; C), but not all sensory neurons (unfilled arrow in A). Higher magnifications show punctate pattern of RFP-labeled ribosomes in some axons (B, E). The extracted axon-only signals in the panels on the right confirmed the partial overlap of the RFP and β-III-tubulin signals. Scale bars: 50 µm (A, D); 10 µm (B, E); 100 µm (C).

3.5.2 Axonal L4-tdTomato originates from Schwann cells in the sciatic nerve *in vivo*

Sections of DRGs from RiboTracker^{ho}-CNP-Cre^{+} mice confirmed the glial expression of the transgene but also showed some positive neurons. Satellite glial cells that surrounded the neuronal cell bodies in the DRG contained RFP-stained L4-tdTomato in a ribosome-specific subcellular distribution (Figure 24A). Additionally, expression of tagged RPL4 was also detected in some neuronal cell bodies as observed in the *in vitro* data. Large sensory neurons, marked with the anti-NF200 antibody, did not express tdTomato-tagged RPL4 (Figure 24A and top panel in Figure 24B). Instead, L4-tdTomato was present in some small-diameter neurons corresponding to the subpopulation of CGRP- or IB4-positive cells (middle and bottom panel in Figure 24B).

In the sciatic nerve, the anti-RFP antibody strongly labeled Schwann cells but almost no axonally localized signals were detected after post-processing the overview images of unlesioned peripheral fibers (Figure 24C). However, one day after sciatic nerve crush and in comparison to the unlesioned control, a notably increased amount of axon-specific RFP immunoreactivity was found at the proximal (Figure 24D) and distal site of the injury (Figure 24E).

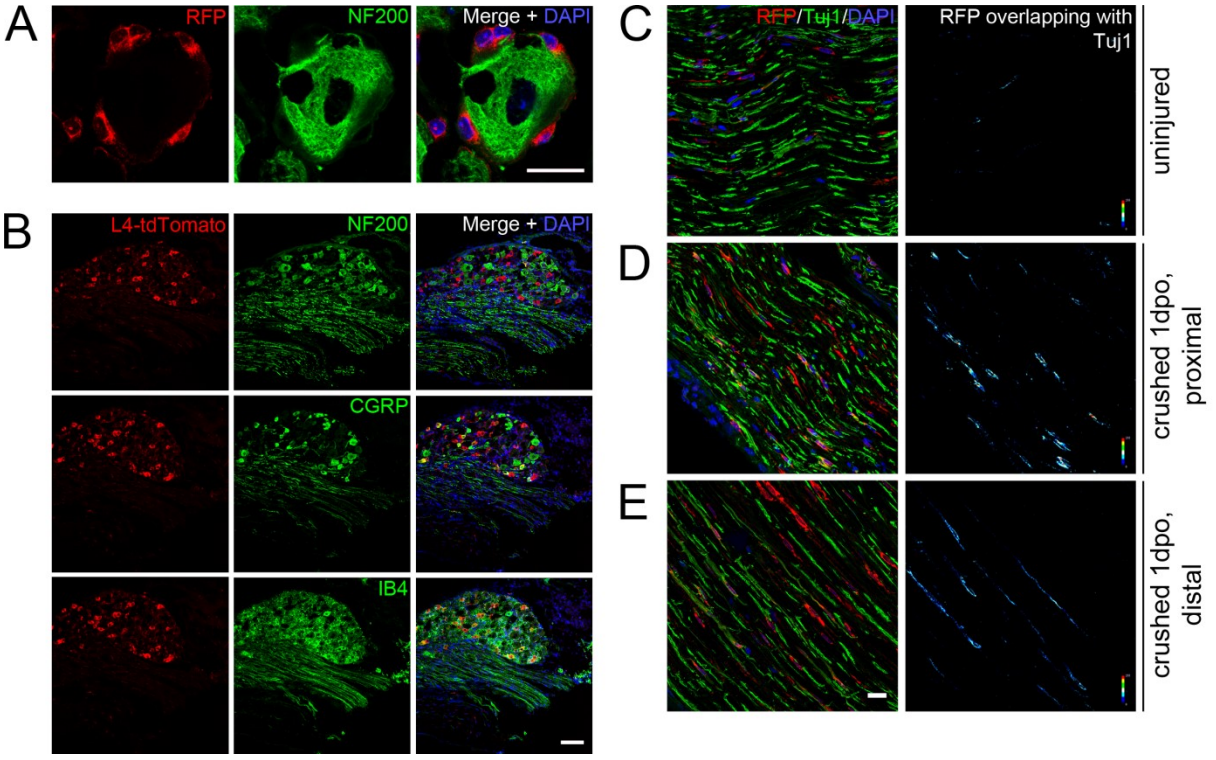

Figure 24: Expression pattern and localization of L4-tdTomato in the PNS of RiboTracker^{ho}-CNP-Cre^{+} mice *in vivo*

(**A**, **B**) IHC of adult DRG sections from RiboTracker^{ho}-CNP-Cre^{+} mouse with different markers for neuronal subpopulations (green). L4-tdTomato was stained with anti-RFP antibody (red) and found to be expressed in satellite glial cells adjacent to DRG neurons. Highest signals were detected in nucleoli and the cytoplasm (**A**). L4-tdTomato signals (red) were also present in a few DRG neurons (**B**) some of which belong to the subpopulation of CGRP- or IB4-positive neurons. Almost no NF200-positive neurons expressed L4-tdTomato. (**C-E**) Longitudinal sections of sciatic nerves from adult RiboTracker^{ho}-CNP-Cre^{+} mice were stained for RFP (red), Tuj1 (green), and DAPI (blue). The panels on the right show the overlap between RFP and β-III-tubulin as an intensity spectrum (RG2B algorithm). Schwann cells in the sciatic nerve showed strong RFP signals. One day after sciatic nerve crush, an increased proportion of axonally localized RFP signals was found proximally (**D**) and distally to the injury site (**E**) in comparison to the uninjured control (**C**). Scale bars: 20 µm (A, E); 100 µm (B).

In order to confirm the intra-axonal localization of the RFP-stained L4-tdTomato in sciatic nerve fibers, orthogonal projections of Remak fibers, which showed highest intensities of extracted axon-only signals, were analyzed. In the uninjured condition (Figure 25A), very few RFP signals were found to overlap with the staining of the axonal β-III-tubulin (panel of subtracted axon-only signal on the right and arrow in xz projection 2) and many labeled ribosomes were located outside of axons (xz projections 1 and 3). When comparing this higher magnification of the unlesioned sciatic nerve section (Figure 25A) with images of crushed fibers (Figure 25B, C), the injury-induced increase of tdTomato-tagged ribosomes in axons was more pronounced than expected from the previously shown overview pictures (Figure 24C-E). Remak fibers at both sides of the crush site showed a punctate pattern of

axonally localized RFP signals in the post-processed axon-only channel (right panel in Figure 25B and C). Orthogonal projections of signals that represented foci of high intensity in the spectral images (arrows) confirmed the localization of the RFP-stained ribosomes inside the axoplasm. Taken together, these data indicate that axonally localized ribosomes of the sciatic nerve originate from adjacent Schwann cells.

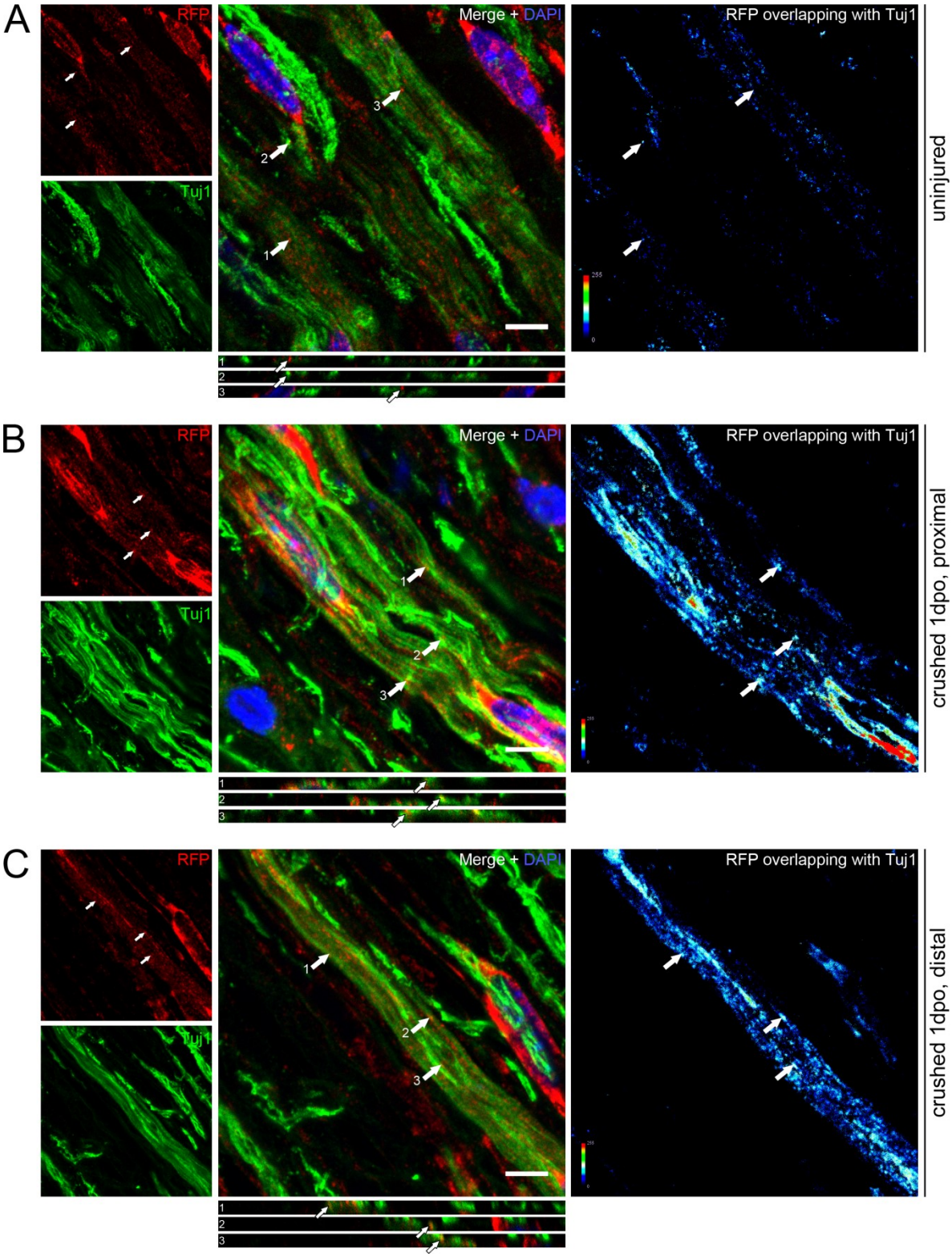

Figure 25: Localization of glially expressed L4-tdTomato in peripheral axons *in vivo*
(**A-C**) IHC for RFP (red), Tuj1 (green), and DAPI (blue) on longitudinal sections of sciatic nerves from adult RiboTracker^{ho}-CNP-Cre^{+} mice. The panels on the right show the overlap between RFP and Tuj1 as an intensity spectrum (RG2B algorithm). Orthogonal xz projections were constructed from 17 (**A**), 18 (**B**) or 20 (**C**) optical sections taken at 0.08 µm z-step intervals. In Remak fibers of the uninjured sciatic nerve, only few RFP signals overlapped with Tuj1-positive axons (arrow 2 in **A**). One day after sciatic nerve crush, more RFP signals were found to overlap with Tuj1 staining in Remak fibers proximal (arrows in **B**) and distal to the injury site (arrows in **C**).Scale bars: 5 µm (A-C).

4. Discussion

Over the last decades, many studies led to the now generally accepted conclusion that proteins are synthesized locally in axons (Koenig and Giuditta, 1999; Alvarez et al., 2000; Giuditta et al., 2002; 2008). This mechanism provides the axon with a certain independency from the cell body and allows a fast and local reaction to incidents in the periphery. For instance, local protein synthesis in PNS axons is important for growth cone guidance in response to external cues, retrograde signaling, and the formation of a new growth cone after injury (Wu et al., 2005; Vogelaar et al., 2009; Ben-Yaakov et al., 2012). Many transcripts have been identified in the axonal compartment (Andreassi et al., 2010; Gumy et al., 2014) and mRNAs were shown to be anterogradely transported in RNP complexes. RBPs present within these particles recognize axonal localization signals in the 3'UTR of the mRNA, stabilize the mRNA, and mediate the interaction with molecular motors (Sotelo-Silveira et al., 2006; Yoo et al., 2010). Axonal ribosomes are also assumed to originate from the neuronal cell body and to be axonally transported in RNPs by microtubule-based transport (Sotelo-Silveira et al., 2006; Kun et al., 2007). However, conclusive evidence is lacking since studies provide only static data (IHC or EM) for the presence of ribosomes in axons (Koenig and Martin, 1996; Koenig et al., 2000; Kun et al., 2007).

Recently, work from the group of Jan van Minnen challenged the prevalent view since Schwann cell-derived, labeled ribosomes were found in injured and regenerating axons *in vivo*. Results from IHC and EM analyses proposed the transfer of ribosomes in RVs from glia to axons to occur across the myelin sheath via cytoplasmic connections, such as Schmidt-Lanterman incisures. Based on their findings, Court et al. (2008; 2011) hypothesized that both neurons and Schwann cells provide the axonal compartment with ribosomes for local protein synthesis. Especially after injury or in cases of neuropathies such as ALS or CMT, the delivery of ribosomes from glial cells in particular was supposed to account for the increase of axonal ribosome, hence being important for successful nerve regeneration (Court et al., 2008; 2011; Verheijen et al., 2011; 2014).

These recent studies employed *Wld*^{s} mice, injection of viruses, and transplantation of nerve grafts repopulated by Schwann cells that expressed tagged ribosomes to show the glia-to-axon transfer of ribosomes. Since histological and EM analysis methods were applied, the neuronal cell body could not be excluded as additional source of ribosomes (Court et al., 2008; 2011). Moreover, these methods created a more or less artificial situation and did not fully represent the physiological *in vivo* condition.

The aim of the present study was to show that axonally localized ribosomes originate from the neuronal cell body *in vivo*. Here, endogenous ribosomes were visualized by the anti-RPL26 antibody and two tools were developed to specifically label neuronal ribosomes *in vivo*.

4.1 Labeling of ribosomes

In order to analyze the localization of endogenous ribosomes, the anti-RPL26 antibody was evaluated as ribosomal marker (Figure 8). RPL26 signals were found in the cell body and dendrites of cultured hippocampal neurons. The subcellular localization of RPL26 signals corresponded to other studies showing a similar staining pattern of ribosomal proteins (Tiedge and Brosius, 1996) and was in agreement with the known local protein synthesis by dendritically localized ribosomes (Bodian, 1965; Steward and Levy, 1982; Feig and Lipton, 1993; Kang and Schuman, 1996). Furthermore, the anti-RPL26 antibody was found to be more specific than the human-anti-ribosomal P antigen used in other studies (Court et al., 2008; Calliari et al., 2014). Based on these results, it was concluded that the anti-RPL26 antibody represented a reliable marker for endogenous ribosomes.

To enable the study of the neuronal origin of axonal ribosomes, fluorescently-labeled ribosomal proteins were expressed in a neuron-specific manner. RPL4 was selected for tagging because of its position within the large ribosomal subunit. Long helices and the C-terminus of RPL4 extend above or are located close to the surface of the ribosome (Klinge et al., 2011). Based on this configuration, the addition of a tag on the carboxyl-terminus was expected not to interfere with the ribosomal subunit. In addition, Court et al. (2008; 2011) used RPL4 tagged with eGFP and found no impairment of ribosomal function.

4.1.1 Recombinant AAVs express L4-eGFP

As a tool to label neuronal ribosomes, recombinant AAVs encoding eGFP-tagged RPL4 were generated. Due to the cell type-specific tropism of the rAAV serotype 1/2 (Bartlett et al., 1998; Mason et al., 2010), a neuron-restricted expression was achieved as confirmed by *in vitro* experiments (Figure 14). The fusion construct L4-eGFP (provided by Jan van Minnen, Court et al., 2008) has previously been used as ribosomal marker (Court et al., 2008) and was additionally validated by microscopic analyses in the present study. The subcellular localization of eGFP-tagged RPL4 in nucleoli, cytoplasm, and dendrites is similar to that of RPL26 and previously described other ribosomal constructs, such as eGFP-tagged RPL10a (Heiman et al., 2008; Cook-Snyder et al., 2015). Hence, rAAV-L4-eGFP represents a reliable tool to tag ribosomes specifically in neurons and was envisaged to demonstrate the axonal transport of soma-derived ribosomes.

4.1.2 RiboTracker mice as tool to tag ribosomes in a cell type-specific manner

The major tool to label ribosomes that was developed in the present study was the transgenic RiboTracker mouse.

When the generation of the RiboTracker mouse started in 2011, some reports of genetically-tagged ribosomes had already been published. However, none of these approaches were appropriate to address the questions of the present study. Heiman et al. (2008) expressed eGFP-tagged RPL10a in a cell type-specific manner for affinity purification of polysomal mRNAs (translating ribosome affinity purification, TRAP). Their application focused on the analysis of translation profiles of distinct cell populations. However, the use of bacterial artificial chromosome (BAC) transgenic mice made their approach very time-consuming because new transgenic mouse lines needed to be constructed for each cell lineage of interest. Alternatively, it would be better to profit by the broad spectrum of available Cre driver lines. This strategy was pursued by Sanz and colleagues (2009) who created the RiboTag knock-in mouse. Cre-mediated recombination led to the expression of the epitope-tagged $RPL22^{HA}$ instead of the endogenous ribosomal protein L22 (RPL22). However, the hemagglutinin (HA) tag cannot be visualized directly and is used primarily for biochemical applications such as the immunoprecipitation of tagged ribosomes from whole brain homogenates in order to isolate associated transcripts from the cell types of interest. In addition to the aforementioned transgenic mice, other technologies have been developed to tag ribosomal proteins in yeast (Halbeisen et al., 2009) or human cell lines (Gallo et al., 2011). Again, these studies aimed to isolate ribosomes and associated mRNAs by affinity purification.

In order to express fluorescently-labeled ribosomes in a cell type-specific manner, the RiboTracker mouse line was created. It combines the advantages of both previously described transgenic mouse lines. First, the use of the fluorescent tag tdTomato enables direct visualization of labeled ribosomes. It might even allow live animal imaging studies as tdTomato's fluorescence is reported to be brighter than eGFP (Shaner et al., 2004). Second, the targeting construct contains a floxed stop cassette preceding the fusion construct of L4-tdTomato, so that Cre driver lines can be used to accomplish a cell type-specific expression.

The RiboTracker mouse is a transgenic animal in which the L4-tdTomato is expressed from the *Rosa26* locus in addition to the endogenous ribosomal protein L4. It should be noted that endogenous RPL4 and tdTomato-tagged L4 coexist in cells, hence, theoretically not all ribosomes within a Cre-expressing cell are labeled.

During our studies on the RiboTracker line, Zhou et al. (2013) published a new TRAP allele for the expression of eGFP-tagged RPL10a that is almost identical to the setup of the RiboTracker mouse. Analogously, the fusion construct was expressed from the *Rosa26* locus under the CAG promoter and lineage selectivity was achieved by Cre-mediated excision of a floxed stop cassette in the Rosa26^{fsTRAP} allele. Still, the application was different because Zhou et al. (2013) used their transgenic mouse for transcriptional profiling.
Taken together, the RiboTracker line expands the pool of available transgenic mice expressing labeled ribosomes by applying another ribosomal protein and a red-fluorescent tag. More importantly, the present study is the first to use transgenic mice for visualization of axonal ribosomes and the subsequent investigation of their cellular origin.

In the RiboTracker mice, L4-tdTomato was found in dendrites of hippocampal neurons after neuron-specific Cre-mediated recombination (Figure 19). These results parallel the subcellular distribution of eGFP-L10a in CA1 neurons (Cook-Snyder et al., 2015), and both are in agreement with previous studies that report a somatodendritic localization of ribosomes in neurons (Bodian, 1965; Steward and Levy, 1982; Ostroff et al., 2002).
Unfortunately, it was not possible to check for colocalization of L4-tdTomato and other ribosomal markers because the antibodies tested for RPL4 and ribosomal protein S6 (RPS6) did not work for immunostainings (data not shown). Only the anti-RPL26 antibody yielded reliable signals (granular distribution, Figure 8-10). However, since the anti-RFP antibody, which is necessary to enhance the axonal L4-tdTomato signal, the anti-RPL26 antibody originated from the same species, it was technically impossible to perform co-stainings. Immunoblot analyses with an anti-RPL4 antibody allowed the successful detection of the fusion construct together with the endogenous RPL4 (Figure 16). Other verification experiments, like the analysis of L4-tdTomato in polysomal fractions by sucrose density gradient centrifugation are planned.
In summary, the tdTomato tag seemed not to interfere with the ribosomal function of the RPL4, since it displayed a ribosome-specific localization. Therefore, it was concluded that L4-tdTomato is a useful construct to label ribosomes in the RiboTracker mouse.

4.2 Cultured peripheral and central neurons contain ribosomes in their axons and growth cones

In the first part of this work, various cell culture systems were investigated for the presence of axonal ribosomes. Beside the visualization of endogenous ribosomes with the anti-RPL26 antibody (Figure 8, 9), a neuron-specific tagging of ribosomes was achieved by crossing RiboTracker mice with Cre lines driven by either the CamKIIα or the Advillin promoter. The cell type-specificity was confirmed by colocalization of the fusion construct with neuronal markers both *in vitro* and *in vivo*. Glial cells never expressed L4-tdTomato in these neuron-specific lines (Figure 19-22). Alternatively, cells were transduced with the rAAV-L4-eGFP *in vitro* leading also to a neuronal expression of fluorescently tagged ribosomes (Figure 14).
In dissociated cultures of adult DRG neurons, granular stainings of RPL26 were found in axonal processes and a similar punctate pattern was observed for the RFP staining of neuronally-expressed L4-tdTomato. In addition, axons of virally-transduced cells displayed granular L4-eGFP signals. This distribution corresponds with the known axonal localization of RPL4 in dissociated sensory neurons (Zheng et al., 2001). Furthermore, the results are in accordance with previously published staining patterns for other ribosomal proteins, rRNAs, and translation initiation factors in DRG axons (Verma et al., 2005; Cox et al., 2008).

When analyzing DRG explants of different developmental stages, a punctate pattern of endogenous RPL26-positive ribosomes was again observed in their axons and growth cones. Similarly, axons of neonatal cortex explants showed strong immunoreactivity for RPL26 at levels comparable to peripheral cultures. This result was surprising because central axons were previously reported to contain only low amounts of ribosomes, if any (Knowles et al., 1996; Verma et al., 2005). However, Verma et al. (2005) used adult retinal explants that only grew a little bit when subjected to a previous conditioning lesion and other studies analyzed embryonic dissociated cortical neurons (Knowles et al., 1996). The culture system applied in the current study enabled the analysis of long axon tracts, which grew without the need of conditioning lesion and represented the morphology of *in vivo* central axons much better. Only recently, Taylor et al. (2013) demonstrated the presence of ribosomal RNA in hippocampal axons *in vitro* and molecular markers of translation, namely phosphorylated forms of the eukaryotic translation initiation factor 4E-binding protein 1 and RPS6, have been detected in these axons (Baleriola et al., 2014).
Growth cones of peripheral and central axons contained distinct RPL26 granules that mostly overlapped with □-III-tubulin-positive areas representing the axon shaft and the core of the growth cone structure. Filopodia consisting of F-actin were not visualized by the Tuj1 staining. Only occasionally, ribosomes were detected in the unlabeled, peripheral domain of the growth cone. The restricted localization of RPL26 to the growth cone palm matches the

distribution of RPS6, which has previously been observed to associate with the RNA binding protein HuD and GAP-43 mRNA in growth cones of differentiated pheochromocytoma (PC) 12 cells (Smith et al., 2004). Using EM analysis, Bassell et al. (1998) detected polyribosomes at the end of axons and in growth cones of cortical neurons *in vitro*. Likewise, most polyribosomes were situated in the central part of the growth cone and only rarely in the peripheral or filopodia area. The group of Christine Holt also reported the presences of ribosomes, mRNAs, and RBPs in growth cones and revealed that asymmetric protein translation occurs in response to guidance cues (Campbell and Holt, 2001; Leung et al., 2006; Yao et al., 2006). The present work supports the increasing evidence that local protein synthesis may also occur in axons of central neurons.

Improvements in the field of microscopy during the last decades led to new superresolution fluorescence microscopy techniques that overcome the diffraction barrier. In comparison to confocal microscopy, which has an optical resolution of 200-300 nm in the lateral direction and 500-700 nm in the axial direction, the spatial resolution of the recently developed microscopic techniques is increased by an order of magnitude (reviewed by Huang et al., 2009). Several forms of superresolution fluorescence microscopy, such as stimulated emission depletion (STED) microscopy, saturated structured-illumination microscopy (SSIM), stochastic optical reconstruction microscopy (STORM), or single-molecule localization microscopy (SMLM), allow the study of previously unresolved details of cellular and subcellular structures at a range of 10-100 nm. In the present study, SMLM was used to visualize the previously observed punctate pattern of axonally localized ribosomes with higher accuracy. SMLM revealed a very precise image of defined RPL26 clusters along the entire length of the analyzed axon segments. The distribution of the ribosomal signals had a regular appearance and no sites of dense aggregation were observed, neither in peripheral, nor in central axons. These findings contradict the results from Spillane et al. (2013), who demonstrated with traditional microscopy that the translational machinery accumulated at presumptive branching sites in axons of sensory neurons in culture. Defined by actin filament enrichments, regions of local protein synthesis are assumed to exist in axons where ribosomes, RNA-binding proteins and mitochondria are present (Spillane et al., 2013).
The actin network of different cell types has been studied recently with superresolution microscopy. Using STORM, a periodic cytoskeletal structure of actin, spectrin, and associated proteins was observed in axons but not in dendrites of rat hippocampal neurons (Xu et al., 2013). Ring-like structures of actin wrap around the circumference of axons along the axonal shafts. This highly regular pattern possessed a periodicity of around 190 nm. A similar periodicity of cytoskeleton elements has been described for ankyrin and spectrin in motoneuron axons in *Drosophila* (Pielage et al., 2008). The just recently published work from D'Este et al. (2016) completed the preceding studies by showing that the periodic

cytoskeleton lattice is present in virtually all neuron types *in vitro* and in sciatic nerve fibers. Assuming that the organization of the actin cytoskeleton defines the distribution of polyribosomes in axons, the periodicity of actin might be the reason for the equal distribution of RPL26 clusters observed in this study. Indeed, the nearest neighbor distances calculated for the majority of RPL26 clusters lay in the range of 100-200 nm and thus, match very well the spacing of actin (198 ± 26 nm) in axons of DRG neurons (D'Este et al., 2016). To pursue this hypothesis, it will be helpful to analyze co-stainings for RPL26 and cytoskeleton elements with superresolution fluorescence microscopy in further studies.

In addition, the new superresolution microscopic techniques allow addressing further questions related to local protein translation and the subcellular distribution of proteins. For instance, it would be interesting to visualize more precisely protein interaction and displacement processes occurring during growth cone turning. It has previously been shown that *β-actin* mRNA is translated asymmetrically depending on the gradient of the attractive guidance cue netrin-1 (Leung et al., 2006). Similarly, a relocation of the translational machinery is expected to take place. The superresolution microscopy represents an optimal tool to visualize the influence of guidance molecules on localization of proteins and the translational machinery at the subcellular level.

Taken together, confocal and superresolution microscopy revealed that ribosomes are present in axons and growth cones of PNS and CNS explant cultures. Further, evidence was provided that the granular distribution of RPL26 might be achieved by an interaction with the axonal actin cytoskeleton.

In contrast to the results obtained from the RPL26 staining, unexpectedly, the axons and growth cones of PNS and CNS explant cultures of neuronal RiboTracker-Cre did not contain labeled ribosomes, even though L4-tdTomato was expressed in the neuronal cell bodies. The absence of axonally localized L4-tdTomato indicates that tagged ribosomes are not transported from the cell body to the periphery. Instead, it can be speculated that axonally localized ribosomes originate exclusively from glial cells, which did not express L4-tdTomato in the RiboTracker-CamKIIα- and -Advillin-Cre lines. In order to shed more light on this possibility, the complementary experiment was performed and RiboTracker mice were crossed with a glially expressed Cre driver.

Indeed, focusing on axons of cultured sensory neurons isolated from RiboTracker-CNP-Cre mice, punctate RFP signals were found to overlap with some □-III-tubulin-positive fibers, also occasionally in explant cultures (Figure 23). Because tagged ribosomes, when restricted to neurons, were not present in axons of explant cultures, it can be speculated that the ribosomes in the CNP-Cre line are transferred from glial cells to axons *in vitro*. In this regard, it should be noted that L4-tdTomato expressing glial cells were located close to RFP-positive

axons. Reports about cocultures of peripheral neurons and Schwann cells provide evidence that intercellular communication and interaction is maintained to a certain level *in vitro*. For example, the presence of Schwann cells in a culture of motor neurons has been shown to enhance neuronal viability and axon growth, and even myelination occurred *in vitro* (Honkanen et al., 2007; Hyung et al., 2015). However, other studies suggest that SCs do not myelinated DRG axons *in vitro* (Heinen et al., 2008). Nevertheless, additional studies are needed to pursue the hypothesis of ribosome transfer from glia to axon in culture and to visualize possible routes of transportation. Furthermore, it should be considered that Schwann cells often possess cytoplasmic protrusions filled with ribosomes (Love and Shah, 2015) that grow along or wrap around axons. It might be important to unravel glial and neuronal processes *in vitro* by using the anti-Tuj1 antibody together with a glial marker, such as glial fibrillary acidic protein (GFAP) or S100□.

In fact, dissociated neurons from all Cre lines contained tdTomato-tagged ribosomes in their axons, although in the neuronal RiboTracker-Cre lines, axons originating from the explants did not. This discrepancy leads to the speculation that dissociated cell cultures display properties that do not correspond to other culture systems that are better representatives of the *in vivo* situation. First, the dissociated neurons are isolated from their normal tissue environment and the dissociation process probably re-sets cells to developmental stages where a growth program is re-started (Tahirovic and Bradke, 2009). Dissociated neurons are located in a different environment without any contact and with reduced signaling to neighboring cells. Moreover, dissociated sensory neurons display much shorter axons compared to explant cultures or tissue. Taken together, this strongly indicates that characteristics of neurons are most likely changed in dissociated culture systems and do not represent *in vivo* conditions. By comparing the expression of neurotrophin receptor tyrosine kinases in sensory neurons, which were either cultivated in wholemount explants or as dissociated culture, Genc et al. (2005) came to the same conclusion that the properties of dissociated neurons were altered. Consequently, it can be assumed that intracellular mechanism function differently or that diffusion may account for the axonal localization of ribosomes in these short axons of dissociated DRG neurons. In contrast, the neurons in the explant culture remain in their tissue environment and are not completely dedifferentiated. They are axotomized and therefore do not need to completely restart growth, but just have to regenerate their axons from the stump.

The RPL26 staining confirmed the presence of ribosomes also in axons of explant cultures. Even though RPL26 was not present in every axon of DRG explants, the number of RPL26 immunoreactive axons was much higher compared to RFP-positive neurites in cultures from RiboTracker-CNP-Cre mice. This could be explained by the fact that not every ribosome of a glial cell is labeled with tdTomato because endogenous untagged RPL4 is still expressed in

Cre-positive cells in the RiboTracker mouse. Consequently, there are more ribosomes expected to be present in the axon than visualized by the RFP staining. Supporting evidence for this assumption is also provided by previously mentioned studies that report the presence of other ribosomal subunits in axons of explant cultures (Verma et al., 2005; Cox et al., 2008). An alternative consideration might be that RPL26 has an extra-ribosomal function in axons. Many ribosomal proteins fulfill additional functions apart from the ribosomal complex as reviewed by Wool (1996) and more recently by Lindstrom (2009) and Warner and McIntosh (2009). However, it is not clear if ribosomal proteins in general and RPL26 in particular exist in a ribosome-independent manner in axons and what their extra-ribosomal actions might be. More investigations are necessary to clarify why the immunostaining of endogenous ribosomal proteins revealed a higher amount of axonal ribosomes *in vitro* than the transgenic approach labeling ribosomes with tdTomato.

The present analyses of various cell culture systems showed that ribosomes are present in axons and growth cones of PNS and CNS neurons *in vitro*. Furthermore, the results suggest that ribosomes in long axons form DRG explants are possibly transferred from glia and not transported from the cell body since neuronally expressed L4-tdTomato was not detected in the axonal compartment.

4.3 The amount of axonal ribosomes increases after injury in sciatic nerve fibers

To investigate the distribution of endogenous ribosomes *in vivo*, the anti-RPL26 antibody was applied to control and injured sciatic nerves. In uninjured axons, low amounts of RPL26-positive granular structures were observed. Sciatic nerve crush led to an increase of axonally localized RPL26 signals both proximal and distal to the lesion (Figure 10). This is in accordance with the upregulation of axonal ribosomes observed in literature (Court and Alvarez, 2005; Court et al., 2008). However, these previous studies were performed on sciatic nerve tissue one week after lesion. The results presented in this study suggest a rapid increase of axonal ribosomes occurring already during the first 24 h after injury. This is in line with the proteomics analyses carried out by Michaelevski et al. (2010) showing that 24 h after injury, extensive changes occur in the protein distribution within peripheral axons and that especially proteins involved in RNA binding and translation machineries are transported to the lesion site. *In vitro* analyses of nerve explants performed by Court et al. (2008) suggested a comparable time course with the highest amount of ribosome-containing axons being found at 18 h after desomatization.

Indeed, in order to form a new growth cone (Verma et al., 2005) and to synthesize proteins for a retrograde signaling complex (for review see Rishal and Fainzilber, 2010, 2014), local

protein translation takes place in axons very shortly after injury. Making use of the photoconvertible fluorescent reporter molecule Kaede, Vogelaar et al. (2009) demonstrated that protein synthesis was already increased during the first 30 minutes after axotomy in cultured DRG axons. Similarly, the formation of new growth cones was observed within 20 minutes after cut of axons *in vitro* (Verma et al., 2005). These studies, together with the *in vivo* data of the present work, illustrate how fast axons respond to injury events by recruiting ribosomes and by increasing the local protein synthesis in order to initiate regeneration.

The RPL26 immunofluorescence displayed the most prominent signal in Remak fibers. This particular type of axons comprise a group of C fibers that originate from small-diameter neurons in the dorsal root ganglia. They are unmyelinated and bundled by the cytoplasm of a non-myelinating Schwann cell. Certainly, glial cells are filled with ribosomes, thus a punctate pattern of RPL26 was found in close vicinity to C fiber axons. After injury, however, many RPL26 signals overlapped with the axon-specific □-III-tubulin and orthogonal projections demonstrated the intra-axonal localization of these ribosomes (Figure 10D, E).
In summary, IHC staining with the anti-RPL26 antibody confirmed the presence of ribosomes in axons *in vivo*, especially after injury, where increased amounts of axonal ribosome have been detected.

4.4 Neuronally-expressed tdTomato-tagged ribosomes are absent in peripheral axons

In the current study, sciatic nerve fibers were shown to contain ribosomes and their axonal level were found to increase after injury. With the help of the RiboTracker mouse line, the present study aimed to demonstrate the neuronal supply of axonal ribosomes *in vivo*.
In PNS neurons, both neuronal RiboTracker-Cre lines showed a comparable expression pattern that also matched previous reports about their respective promoter activity. Even though Casanova et al. (2001) did not describe Cre expression outside of the brain, other studies clearly demonstrated that CamKIIα is present in small-diameter and medium-sized cells of dorsal root ganglia (Bruggemann et al., 2000; Carlton, 2002). The Advillin-Cre mouse line was claimed to be expressed in all DRG neurons (Minett et al., 2012). In the present study, the majority of L4-tdTomato expressing cells in both lines belong to the subpopulation of small- to medium-diameter sensory neurons (Figure 21), which are usually involved in thermoception and nociception. Axons of these neuronal cells comprise lightly myelinated type Aδ and unmyelinated type C fibers, the last of which correspond to Remak fibers (Kandel et al., 2012; Purves et al., 2012). By IHC with the anti-RPL26 antibody, these axons have been shown to contain ribosomes. Strikingly, in neuronal RiboTracker-Cre lines, myelinated axons and unmyelinated Remak fibers of the sciatic nerve lacked any RFP

signals, although L4-tdTomato was expressed in the corresponding cell bodies. These observations are in line with the *in vitro* data discussed above. Moreover, sciatic nerve crush did not induce an increase in labeled axonal ribosomes. The absence of axonally localized L4-tdTomato indicates that tagged ribosomes are not transported from the cell body to the periphery.

In addition to experiments with neuronal RiboTracker-Cre lines, a pilot study with rAAVs was undertaken. Intrathecal injection of rAAV-eGFP by lumbar puncture resulted in transduction of cells in the spinal cord, but DRG neurons were not transduced (Figure 15 and data not shown). These results are in contrast to the report from Vulchanova et al. (2010) and might be attributed to the use of different concentrations of mannitol solution (12.5% in the present compared to 25% in the previous study).

In the course of the present study, results obtained from experiments with neuronal RiboTracker-Cre lines disproved the hypothesis of a neuronal source of axonal ribosomes. Hence, experiments with rAAV-L4-eGFP are expected to function as negative controls and could be pursued to test for a possible influence of the tdTomato tag.

4.5 Axonal ribosomes may derive exclusively from glial cells

Results obtained from RiboTracker-CamKIIα- and –Advillin-Cre lines *in vitro* and *in vivo* showed that axonal ribosomes do not originate from the cell body. To investigate if ribosomes are transferred from glial cells to axons, as proposed by Court et al. (2008) and supported by the present *in vitro* data, the RiboTracker-CNP-Cre mice were used for studying ribosome transfer *in vivo*.

In RiboTracker-CNP-Cre animals, glial cells in the PNS (satellite glia and Schwann cells) expressed the fusion construct L4-tdTomato *in vitro* and *in vivo* (Figure 23-25), in accordance with a previous publication of CNP in the neural crest-derived Schwann cell lineage (Toma et al., 2007) and in oligodendrocytes (Vogel and Thompson, 1988; Sprinkle, 1989; Chandross et al., 1999; Yuan et al., 2002). Therefore, it was unexpected to find some DRG neurons, mainly CGRP+ or IB4+ cells, positive for L4-tdTomato. The promoter might be leaky in this CNP-Cre line (Eva-Maria Krämer-Albers, personal communication). Alternatively, the CNP promoter may be already active in precursor cells, leading to the excision of the stop codon in both the neuronal and glial lineage. Most glial and neuronal cells of the peripheral nervous system derive from the neural crest (Le Douarin and Kalcheim, 1999). During embryogenesis, different waves of cell migration and division occur in order to establish the different cell types of the PNS. Maro et al. (2004) found that emigrating neural crest cells give rise to boundary cap (BC) cells that are present at the dorsal root entry zone between E10.5 and birth. BC cells are the precursor cells of all Schwann cells in the spinal root, a

subpopulation of neurons (mainly with nociceptive afferences) and satellite cells in the dorsal root ganglia. Strikingly, this BC cell progeny matches those peripheral cell types that were found to express L4-tdTomato in RiboTracker-CNP-Cre mice. Since CNP is expressed from onward embryonic day 10 (Yuan et al., 2002), it might very well be that boundary cap cells express the Cre recombinase during development leading to the excision of the stop cassette. Consequently, all descending cells, including this subpopulation of sensory neurons, are expected to express L4-tdTomato.
Even though the CNP-Cre line is not exclusively glia-specific, these mice were still used in the present study to label glial ribosomes and to subsequently investigate their transfer into axons. Since the DRG population in the RiboTracker-CNP-Cre mice matches the population in the neuronal RiboTracker-Cre lines, results that are different between neuron-specific and CNP promoter-induced Cre expression in RiboTracker mice can be traced back to the glial origin of labeled ribosomes.

The results from the *in vivo* analysis of peripheral axons are very consistent (schematically summarized in Figure 26) and point to a glial origin of axonal ribosomes. In sciatic nerve fibers of RiboTracker-CNP-Cre mice, the amount of axonally localized L4-tdTomato roughly corresponds to endogenous levels of ribosomal proteins observed by RPL26 staining. Additionally, the increase of axonal ribosomes after sciatic nerve crush is analogous when comparing Figure 9 and Figure 24, and most prominently visible in Remak fibers.
At first sight, there seems to be a discrepancy between these data and Court et al. (2008), who proposed trajectory for the transfer of ribosomes from glia to axons via Schmidt-Lanterman incisures, which are cytoplasmic bridges in the myelin sheath near the nodes of Ranvier. At second sight, this hypothesis can easily be extended to the non-myelinated Remak fibers, since their axoplasm is in very close proximity to the cytoplasm of the Schwann cell enwrapping it.

The finding that neuronally-expressed L4-tdTomato was not present in uninjured axons or in axons after crush strongly suggest that ribosomes of peripheral axons originate exclusively from adjacent glial cells and are not transported from the neuronal cell body to the axon. This hypothesis is further supported by the notion that increased ribosomal amounts of distal axons can only be accomplished by transfer from glia because the axonal transport mechanisms are interrupted at the lesion site.

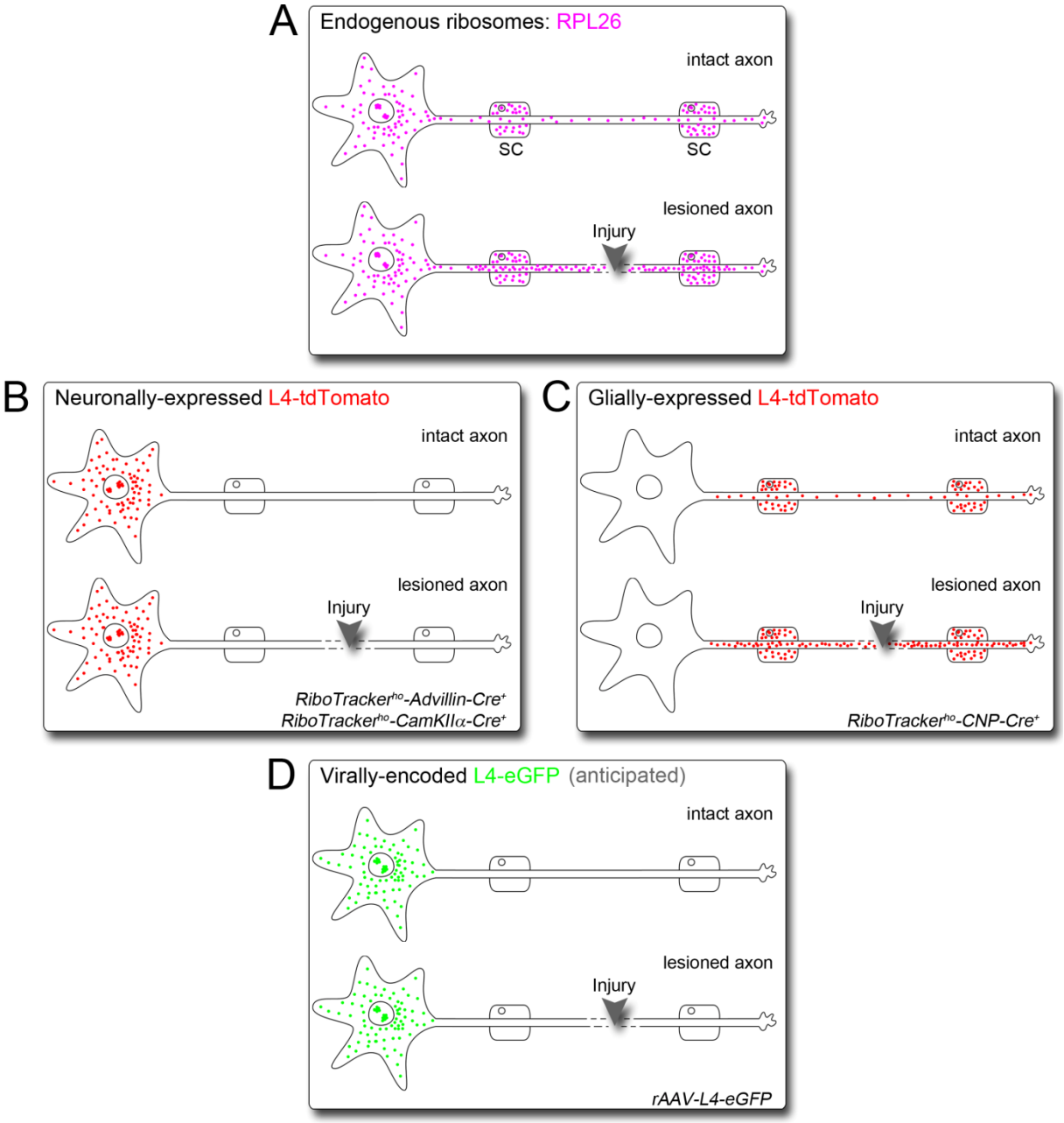

Figure 26: Summary of the generated tools and main results found in the PNS
(**A-D**) Schematic representation of the subcellular localization of endogenous (RPL26) and tagged ribosomes (L4-tdTomato or L4-eGFP) in intact and lesioned PNS axons based on the results of the present study. Abbreviation: SC: Schwann cell.

The possibility that the tdTomato tag was interfering with the loading of labeled ribosomes into RNPs for the axonal transport could not be ruled out. However, due to the observed ribosome-specific somatodendritic localization of L4-tdTomato in hippocampal neurons, it can be assumed that the tag is not interfering with intracellular transport mechanism. Furthermore, the present data showed that intercellular transfer of tagged ribosomes is not impaired. Additional studies are needed to confirm the aforementioned hypothesis of an exclusive transfer of axonal ribosomes from glial cells to the peripheral axon. For this purpose, the RiboTag mouse (Sanz et al., 2009) is a suitable tool because it can be combined with various Cre lines and the HA epitope represents an alternative to the tdTomato tag of the RiboTracker mouse. Ongoing experiments comprise the neuron-specific

expression of RPL22^{HA} with the expectation to observe once more a cell body-restricted localization of tagged ribosomes and no transport to peripheral axons. In parallel, RiboTag-Cre mice are crossed with RiboTracker animals. This experimental setup allows to analyze the distribution of two differently tagged ribosomal proteins in the same neuron and will lead to new insights into the subcellular distribution and transport of the translational machinery.
Furthermore, it will be necessary to confirm the results obtained from RiboTracker-CNP-Cre mice with another glia-specific Cre line, because of the neuronal leakage of the CNP-driven expression of Cre recombinase. Due to the fact that neurons and glial cells originate from common precursor cells, expression of Cre recombinase is also often detected in neuronal cells even if a generally considered glial-specific promoter was used as shown for the Plp-Cre mouse (Michalski et al., 2011). To circumvent this possible limitation, inducible Cre-lines, e.g. hGFAP-Cre-ER^{T2} mice (Ganat et al., 2006), can be used to drive Cre expression only in glial cells by applying tamoxifen at time points when the neuronal and glial lineages are separated.

Since the present data contradict the prevalent concept of ribosome trafficking, some general hypotheses and assumptions, as reviewed by Sotelo-Silveira et al. (2006), have to be reconsidered. First of all, most evidence for the axonal colocalisation of RNA and ribosomes in the axon is provided by *in vitro* data (Giuditta et al., 2008). The neuronal transport of RNPs has so far only been detected in dissociated cell cultures comprising growing, developing neurites (Knowles et al., 1996; Bassell et al., 1998) and in the dendritic domain of differentiated neurons (Kanai et al., 2004; Hirokawa, 2006; Martin and Zukin, 2006; Sossin and DesGroseillers, 2006), but not in mature axons (Sotelo-Silveira et al., 2006; Wang et al., 2007; Giuditta et al., 2008). However, there are some studies suggesting that RNPs may also account for the axonal supply ribosomes (Kun et al., 2007). Ribosomes have been detected in PARP domains together with myosin Va, β-actin mRNA, and its binding protein ZBP1 (Sotelo-Silveira et al., 2004; 2008). PARPs, containing high amounts of ribosomes, might represent the region of cell-to-cell transfer due to their close vicinity to the axonal membrane (Koenig and Martin, 1996; Koenig et al., 2000). Additionally, a gradient of ribosomal proteins to the axoplasm has been reported (Calliari et al., 2014). This might represent the small pool that is translationally active. If the ribosomes would originate from the neuronal cell body itself, one would expect to see the opposite (many ribosomes in the cytoplasm and few at the membrane). However, only rare granular signals of ribosomes were found that occasionally colocalized with one or the other component of RNPs in the axoplasm (Sotelo-Silveira et al., 2008; Calliari et al., 2014). No unequivocal evidence for the transport of ribosomes in axons has been provided so far and alternative interpretations are possible, particularly in the light of the present data.

Mallardo et al. (2003) showed the coexistence of two different classes of transport RNPs in whole brain homogenates. Large granules contained ribosomes, whereas the smaller RNA granules did not. In line with these findings, Elvira et al. (2006) additionally proposed the existence of different RNA granule populations. Since whole brain homogenates contain cell bodies, dendrites and axons, no conclusion could be drawn about the distribution of these subpopulations. Based upon the current results, it is tempting to speculate that axons contain the small ribosome-lacking particles and that in order to perform local protein synthesis, ribosomes are transferred from neighboring glial cells to the axons only when locally needed, for example in the case of injury. Possibly, it is too much effort for the neuron to provide the complete axon (up to 1 meter long in humans) with ribosomes, in view of the fact that ribosomes are only needed at sites of injury or other local stressors.

Taken together, the following hypothesis can be formulated for the axonal compartment of mammalian neurons: RNA is transported together with RBPs and motor proteins in granules from the cell body to the axon (reviewed by Gomes et al., 2014), but these granules do not contain ribosomes. Instead, ribosomes are transferred from adjacent glial cells to the axon where they predominantly localize to PARPs in order to translate the neuronal cell body-derived RNA.

4.6 Do central axons contain ribosomes *in vivo*?

Beside peripheral axons, the present study also comprised some preliminary experiments on CNS axons. As discussed earlier, central axons were found to contain ribosomes *in vitro*. By IHC with the anti-RPL26 antibody, ribosomes were not detected in the ascending fibers of the dorsal column *in vivo*. After spinal cord injury, some RPL26 signals were found to overlap with YFP-labeled axons. However, it is also possible that the colocalization is attributed to an overlap of glial cytoplasm with the axon region. More experiments, particularly orthogonal projections, are needed to investigate the subcellular localization of this RPL26 signals.
Based on the present data, no clear statement about the existence of ribosomes in central axons *in vivo* can be made. Likewise, this issue is still a major point of discussion in the neurobiological community since previous studies detected ribosomes only in the initial segment of CNS axons, but not in distal parts (Peters et al., 1968; Steward and Ribak, 1986). Recently, increasing evidence points to the presence of ribosomes in central axons, though mostly observed in injury- or disease-modified states. By using immuno-EM, Walker et al. (2012) detected ribosomes at nodes of Ranvier in CST axons *in vivo* when expressing eGFP-L10a in the corresponding neurons. Additionally, ribosomes were also found in regenerating growth cones within the spinal cord upon dorsal hemisection injuries. A glia-to-axon transfer of eGFP-labeled ribosomes was excluded based on the experimental setup

(Walker et al., 2012). It can be speculated, that differences in the supply of axonal ribosomes between CNS and PNS might exist. In addition, since the authors based their conclusions only on the eGFP-labeling in immuno-EM experiments and never demonstrated ribosomes as electron-dense granules within the CST, it has to be considered that probably only RPL10a is located in central axons but not the complete translational machinery. Kalinski et al. (2015) detected elements of the protein synthetic machinery in spinal cord axons that regenerated within a peripheral nerve graft. Peripheral axons of normal or crushed sciatic nerves served as reference. Unfortunately, the study did not provide information about the existence of ribosomes in uninjured CNS axons as spinal cord samples from control animals were not included (Kalinski et al., 2015). Recently, more conclusive evidence was provided by EM and IHC analyses of spinal cord sections of experimental autoimmune encephalomyelitis (EAE) mice (Shakhbazau et al., 2016). Free polyribosomes and RVs were detected in large axons in the dorsal column not until 12 days post EAE induction whereas control samples were negative. The amount of axonal ribosomes in the CNS was increasing in parallel with the EAE progression. Additionally, ribosomes were also found in a subpopulation of white matter axons in the brain of multiple sclerosis (MS) patients (Shakhbazau et al., 2016).
Taken together, these reports point to a pathology-related occurrence of ribosomes in central axons. Since a correlation between levels of protein synthesis machinery and the intrinsic growth capacity is hypothesized for axons (Verma et al., 2005), local protein translation might also be important for axonal regeneration processes in the CNS (Vogelaar et al., 2009).

Assuming that the amount of axonal ribosomes is increased after injury or in disease states not only in the PNS but also in the CNS, several questions arise. Where do ribosomes localized to central axons originate from? Do CNS glial cells play a supportive role by transferring ribosomes to axons just as it is assumed for the Schwann cells in the PNS?
There is evidence pointing to similar mechanism of ribosome transfers in CNS and PNS. For instance, Shakhbazau et al. (2016) reported a resemblance of polyribosomes in multi-membrane RVs detected in spinal cord axons to those seen in sciatic nerve fibers. Strikingly, also the ultrastructural localization of ribosomes in central axons, namely close to the axolemma or membranous structures as well as within small vesicles (Jin et al., 2016; Shakhbazau et al., 2016), is reminiscent of reports from EM studies performed on peripheral nerves (Court et al., 2008; Verheijen et al., 2014). To gain more insight into the probable transfer mechanism of ribosomes from glial cells to the axon, the RiboTracker-CNP-Cre mouse represents a suitable tool. Since the CNP promoter is active in Schwann cells and oligodendrocytes (Lappe-Siefke et al., 2003), not only peripheral axons, as mentioned earlier, but also CNS axons can be investigated for the presence of glia-derived, tdTomato-tagged ribosomes. On the other hand, it is also possible that central neurons provide their

axons with ribosomes. In order to address this question, RiboTracker mice crossed with CamKIIα- or NEX-Cre lines can be used. Their neuronal Cre promoter is active in cortical neurons (Casanova et al., 2001; Goebbels et al., 2006). Hence, CST axons can be analyzed for the presence of tdTomato-tagged ribosomes by IHC or immuno-EM. Findings from this two-sided approach will help to learn more about the routes and mechanism by which axonal ribosomes get to central axons.

Even if the data from the present study do not allow a clear statement about the existence of ribosomes in central axons, it still provides the tools to address this issue in further experiments.

4.7 Possible routes of transfer for ribosomes from glia cells to axons

Having shown that axonal ribosomes originate from glial cells, next, the question arises how this transfer is mediated. In the literature, different possibilities and routes of transfer are discussed which are outlined in the following.

4.7.1 Ribosome-containing vesicles

Several studies provide evidence for a vesicle-based transport of ribosomes from glial cells to the axon. Ribosome-containing vesicles were described in the axon-myelin sheath interface of vertebrate myelinated axons (Li et al., 2005; Kun et al., 2007). Court et al. (2008; 2011) hypothesized that these RVs are transferred via Schmidt-Lanterman incisures from the SC cytoplasm to the axon to support local protein translation. Recently, this model was further supported by two studies reporting the presence of RVs in peripheral axons that are affected by demyelination or neurodegenerative diseases, such as ALS, and contained increased levels of axonal ribosomes (Verheijen et al., 2014; Shakhbazau et al., 2016).

The present data change the point of view that the vesicle-based transfer of ribosomes from SCs to the axon represents an additional route beside the axonal transport from the neuronal cell body and further provide a model to study the glia-to-axon transfer of ribosomes while excluding the neuronal cytoplasm as additional source. If a vesicle-based transfer occurs, tdTomato-tagged ribosomes are expected to be found in RVs in axons of RiboTracker-CNP-Cre mice. To address this issue, immuno-EM with the anti-RFP antibody will be performed in further studies.

4.7.2 Exosomes

Even though Verheijen et al. (2014) argued that RVs detected in myelinated peripheral axons differ from exosomes due to their larger size and surrounding membranes, exosomes may represent an alternative vehicle for the transfer of ribosomes from SCs to the axoplasm.

Exosomes are large enough (40-100 nm in diameter) to carry a few ribosomes (Simons and Raposo, 2009), although the current literature does not provide evidence for a ribosomal cargo. Instead, mRNA, microRNA, and elongation factors were found among other proteins in exosomes from various cell types, including oligodendrocytes and Schwann cells (Kramer-Albers et al., 2007; Valadi et al., 2007; Skog et al., 2008; Pegtel et al., 2010; Lopez-Leal and Court, 2016). Therefore, exosomes are considered as potent means of transportation for intercellular communication and influencing, especially in the nervous system. Two recent studies illustrated the important role of neuron-glia communication via exosomes, leading to enhanced neuronal viability and increased regeneration capacity (Fruehbeis et al., 2013; Lopez-Verrilli et al., 2013).

Taken together, there is increasing evidence for an exosome-mediated glial support for neurons, especially for the axonal compartment. However, the underlying mechanisms are still unclear and further studies are necessary to learn more about this particular route of neuron-glia communication.

4.7.3 Direct cytoplasmic connections

In addition to a vesicle-based transport mechanism, it is conceivable that ribosomes are transferred via direct cytoplasmic contacts from glial cells to the axon. Transient structures of intercellular cytoplasmic connections, so-called tunneling nanotubes (TNTs), have been observed in various cell lines (e.g., PC12 and HEK293 cells) and in cultures of astrocytes and hippocampal neurons. TNTs contain F-actin and myosin Va and were shown to transfer endosome-related structures and mitochondria (Rustom et al., 2004; Zhu et al., 2005; Gurke et al., 2008; Wang and Gerdes, 2015). Since their formation occurred predominantly under stress conditions (experimentally induced by application of hydrogen peroxidase), TNTs might represent auxiliary routes of transport for the direct cell-to-cell support under pathological conditions (Zhu et al., 2005; Wang et al., 2011; Wang and Gerdes, 2015).

In the light of these reports, it can be speculated that TNTs may also form between glial cells and axons in order to increase the amount of axonal ribosomes after injury or in disease states as discussed above. However, the existence of TNTs in the CNS or PNS *in vivo* remains to be demonstrated.

In conclusion, a vesicle-mediated transfer of ribosomes, either via trans-endocytosis or via exosomes, is the most probable mechanism to occur between glial cells and the axon. The reports mentioned here provide first evidence, but additional studies are necessary to reveal the underlying mechanisms of the proposed intercellular transport of organelles and molecules.

4.8 Do glial cells transfer ribosomes together with RNA to the axon?

Polyribosomes are often associated with mRNAs and, at least for the dendritic compartment, it was shown that transcripts and ribosomes are transported together in RNPs (Krichevsky and Kosik, 2001; Elvira et al., 2006). Hence, the question arises if RNA is also transferred together with ribosomes from glial cells to axons. As outlined in the introduction, most axonal mRNAs certainly originate from the neuronal cell body, but some reports propose surrounding glial cells as supplemental source (for review see Sotelo et al., 2014). Singer and Green (1968) were the first to consider a glia-to-axon transfer of RNA and subsequent autoradiographic studies supported their hypothesis (Gambetti et al., 1973; Benech et al., 1982; Rapallino et al., 1988). In addition, Sotelo's group found that axonal mRNA levels are upregulated after injury and argued that this increase was possibly based on the horizontal transfer of RNA from adjacent SCs as shown for the transcript of *NF-L* (Sotelo-Silveira et al., 2000). Using bromouridine (BrU) to label newly-synthesized RNA, they proposed a myosin Va-dependent transfer mechanism that might occur along the same routes (Schmidt-Lanterman incisures, nodes of Ranvier) as discussed above for the trafficking of ribosomes (Sotelo et al., 2013; Canclini et al., 2014). Partial colocalization of BrU signals with ribosomes provides supporting evidence for this and indicates that at least in some instances, RNAs and translational machinery are probably transferred together (Sotelo et al., 2013). More investigations are needed to clarify if the glia-to-axon transfer of ribosomes and RNAs occurs in a combined or separated way. To address this question, the RiboTracker mouse can be useful because the tdTomato tag facilitates the isolation of ribosomes and enables the subsequent analysis of bound or co-transferred RNA.

4.9 Functional relevance of ribosome transfer and outlook

In the present work, an increased amount of SC-derived ribosomes was observed in the injured sciatic nerve. These data encourage the assumption that glial cells support axons in cases of injury or disease by supplying ribosomes for local protein synthesis (Court et al., 2008; 2011; Verheijen et al., 2011; 2014; Shakhbazau et al., 2016). In order to confirm that glia-derived ribosomes account for the increased axonal levels also in the context of diseases, RiboTracker-CNP-Cre mice could be analyzed in combination with a peripheral demyelination model or EAE as reported by Shakhbazau et al. (2016). Alternatively, mice homozygous for the CNP-Cre allele can be used, since these animals develop a phenotype of axonal degeneration at around 6-7 months of age (Lappe-Siefke et al., 2003). Furthermore, immuno-EM analyses or *in vivo* imaging studies with confocal or two-photon

microscopy on RiboTracker-CNP-Cre mice might lead to new insights into the transfer routes and mechanisms.

Regenerating axons contain all important components (mRNAs, rRNAs, ribosomal proteins, and even endoplasmic reticulum and Golgi proteins) to synthesizes proteins independently from the cell body (Zheng et al., 2001; Verma et al., 2005; Willis et al., 2007; Merianda et al., 2009; Gumy et al., 2011). Especially cytoskeletal, heat shock, and integral membrane proteins were found to be translated in the regenerating axon (Zheng et al., 2001; Willis et al., 2005; Willis and Twiss, 2006; Vogelaar et al., 2009; Gumy et al., 2010). Furthermore, local protein synthesis has been shown to be necessary for the formation and the structural integrity of a new growth cone which is an essential step for the successful regeneration of the axon (Zheng et al., 2001; Vogelaar et al., 2009). Therefore, it is obvious that the ribosome supply from SC to axons is important to assure local protein synthesis and finally regeneration.
When Schwann cells are missing, regeneration has been shown to fail (Chen et al., 2005). It is believed that other supportive molecules, such as cytokines, neurotrophins, cell adhesion molecules, and extracellular matrix proteins (reviewed by Fu and Gordon, 1997) are exchanged via the glia-axon connection. Furthermore, glial cells provide metabolic support for the axonal compartment (Nave and Trapp, 2008) and SC mitochondrial dysfunction was shown to affect axonal survival (Viader et al., 2011). Still, it can be speculated that ribosome transfer represents one mechanism of action among others to enhance regeneration. Its therapeutic application in neurodegenerative pathologies (ALS, CMT) or demyelinating diseases, such as MS, is thought to be promising, as outlined by recent experiments of Schwann cell therapy. For example, Shakhbazau et al. (2014) have shown that the injection of SCs improved the sensory recovery after sciatic nerve transection. Since preclinical studies did not indicate any safety concerns, transplantation of Schwann cells is on the way to become a clinic application for the treatment of SCI (Guest et al., 2013).
In the future, it is conceivable that the administration of glia-derived exosomes might be an alternative to the injection of whole Schwann cells. SC exosomes have been observed to support the regeneration of sciatic nerves after injury (Lopez-Verrilli et al., 2013), and oligodendrocyte-derived exosomes were reported to influence neurons in multiple ways (Frohlich et al., 2014). For the moment, it is unclear how exosomes exert their positive effects on neurons and axons and it can only be speculated that the transfer of RNAs or ribosomes might be of significance for this.

Assuming that glial cells are the source of axonal ribosomes, future research should focus on the investigation of the transfer mechanisms since its manipulation might represent a way to

stimulate regeneration in axons. This approach would be of great therapeutic use for patients with CNS injuries or neurodegenerative diseases.

4.10 Summary

Initially, the present study aimed to show that axonal ribosomes originate from the neuronal cell body. To address this issue, two genetic approaches were applied to label ribosomes in neurons only. One tool represents a recombinant adeno-associated virus with a tropism for neurons that encodes the ribosomal protein L4 fused with eGFP. Secondly, the transgenic RiboTracker mouse was developed to express tdTomato-tagged RPL4 in combination with neuronal Cre driver lines. Subsequent analyses of axons of explant cultures *in vitro* and sciatic nerve fibers under control and injury conditions *in vivo* showed the absence of L4-tdTomato in axons when expressed in neurons via the CamKIIα or Advillin promoter. These findings suggest that axonal ribosomes are not transported from the neuronal cell body.

Paralleling experiments with rAAV-L4-eGFP supported the *in vitro* data from neuronal RiboTracker-Cre mice. Based on the prior *in vivo* results, however, studies with rAAVs were not continued.

In contrast, when neighboring Schwann cells contained tagged ribosomes in RiboTracker-CNP-Cre mice, low levels of L4-tdTomato were detected in axons and these were found to be strongly increased after injury. This increase overlapped with observations made for endogenous ribosomes stained with the anti-RPL26 antibody.

Finally, these results led to the conclusion that a glia-to-axon transfer of ribosomes occurs *in vivo* and that axonal ribosomes originate exclusively from Schwann cells in the PNS. Accordingly, in the light of the present study, the scheme shown in the introduction (Figure 4) must be updated to the following model (Figure 27):

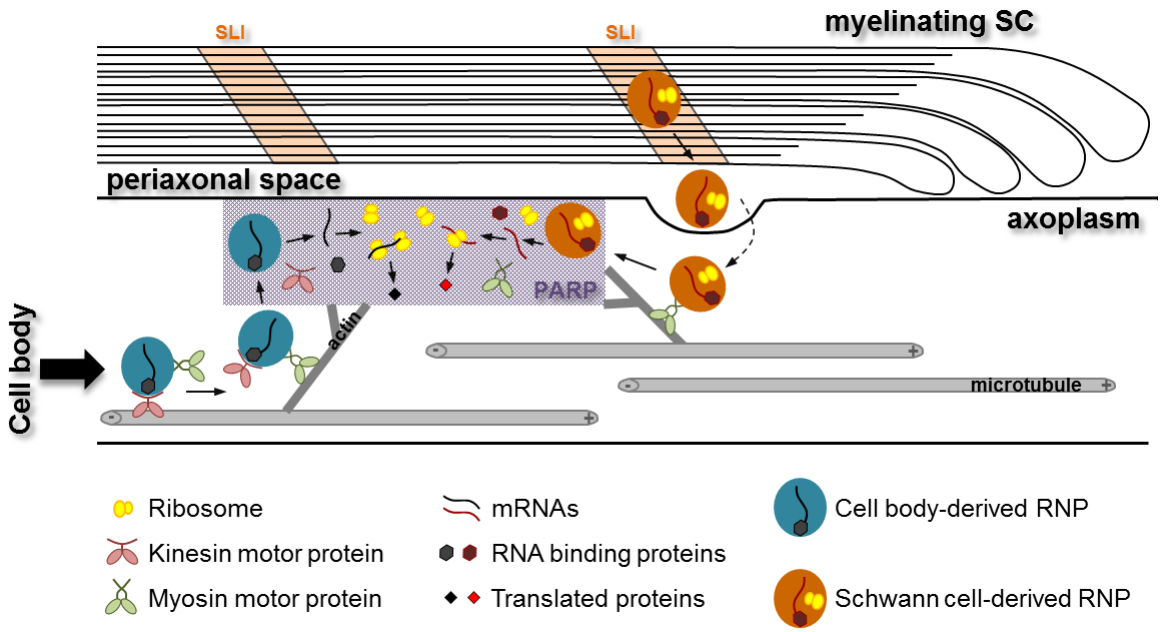

Figure 27: Model showing two possible routes for the axonal delivery of ribosomes and mRNAs
Results from the present study led to the assumption that the neuronal cell body supplies the axonal compartment only with ribonucleoprotein particles (RNPs) that contain mRNAs and their binding proteins, but no ribosomes. Instead, axonal ribosomes are believed to derive exclusively from adjacent Schwann cells (SC), probably also in tandem with glial transcripts. Within the axon, periaxoplasmic ribosomal plaques (PARPs) are likely to represent the sites of local protein translation where neuronal mRNAs encounter glia-derived ribosomes.

Taken together, the results of the present work challenge the prevalent concept that ribosomes are transported from the soma to the axon. Instead, evidence is provided for glial cells to be the exclusive source of axonal ribosomes in the peripheral nervous system. Further investigations are needed to understand the underlying mechanisms of the intercellular ribosome transfer and its possible contribution to regeneration processes.

5. References

Aakalu G, Smith WB, Nguyen N, Jiang C, Schuman EM (2001) Dynamic visualization of local protein synthesis in hippocampal neurons. Neuron 30:489-502.

Alberts B, Johnson A, Lewis J, Raff M, Roberts K, Walter P (2002) Molecular Biology of the Cell, 4th Edition. New York: Garland Science.

Alvarez J, Giuditta A, Koenig E (2000) Protein synthesis in axons and terminals: significance for maintenance, plasticity and regulation of phenotype. With a critique of slow transport theory. Prog Neurobiol 62:1-62.

Andreassi C, Zimmermann C, Mitter R, Fusco S, De Vita S, Saiardi A, Riccio A (2010) An NGF-responsive element targets myo-inositol monophosphatase-1 mRNA to sympathetic neuron axons. Nat Neurosci 13:291-301.

Antar LN, Li C, Zhang H, Carroll RC, Bassell GJ (2006) Local functions for FMRP in axon growth cone motility and activity-dependent regulation of filopodia and spine synapses. Mol Cell Neurosci 32:37-48.

Aronov S, Aranda G, Behar L, Ginzburg I (2001) Axonal tau mRNA localization coincides with tau protein in living neuronal cells and depends on axonal targeting signal. J Neurosci 21:6577-6587.

Aronov S, Aranda G, Behar L, Ginzburg I (2002) Visualization of translated tau protein in the axons of neuronal P19 cells and characterization of tau RNP granules. J Cell Sci 115:3817-3827.

Aschrafi A, Natera-Naranjo O, Gioio AE, Kaplan BB (2010) Regulation of axonal trafficking of cytochrome c oxidase IV mRNA. Mol Cell Neurosci 43:422-430.

Baas PW, Deitch JS, Black MM, Banker GA (1988) Polarity orientation of microtubules in hippocampal neurons: uniformity in the axon and nonuniformity in the dendrite. Proc Natl Acad Sci U S A 85:8335-8339.

Baleriola J, Walker CA, Jean YY, Crary JF, Troy CM, Nagy PL, Hengst U (2014) Axonally synthesized ATF4 transmits a neurodegenerative signal across brain regions. Cell 158:1159-1172.

Bartlett JS, Samulski RJ, McCown TJ (1998) Selective and rapid uptake of adeno-associated virus type 2 in brain. Hum Gene Ther 9:1181-1186.

Bassell GJ, Singer RH, Kosik KS (1994) Association of poly(A) mRNA with microtubules in cultured neurons. Neuron 12:571-582.

Bassell GJ, Zhang H, Byrd AL, Femino AM, Singer RH, Taneja KL, Lifshitz LM, Herman IM, Kosik KS (1998) Sorting of beta-actin mRNA and protein to neurites and growth cones in culture. J Neurosci 18:251-265.

Belgardt BF, Husch A, Rother E, Ernst MB, Wunderlich FT, Hampel B, Klöckener T, Alessi D, Kloppenburg P, Brüning JC (2008) PDK1 Deficiency in POMC-Expressing Cells Reveals FOXO1-Dependent and -Independent Pathways in Control of Energy Homeostasis and Stress Response. Cell Metabolism 7:291-301.

Ben-Yaakov K, Dagan SY, Segal-Ruder Y, Shalem O, Vuppalanchi D, Willis DE, Yudin D, Rishal I, Rother F, Bader M, Blesch A, Pilpel Y, Twiss JL, Fainzilber M (2012) Axonal transcription factors signal retrogradely in lesioned peripheral nerve. The EMBO Journal 31:1350-1363.

Benech C, Sotelo JR, Jr., Menendez J, Correa-Luna R (1982) Autoradiographic study of RNA and protein synthesis in sectioned peripheral nerves. Exp Neurol 76:72-82.

Bleher R, Martin R (2001) Ribosomes in the squid giant axon. Neuroscience 107:527-534.

Bodian D (1965) A Suggestive Relationship of Nerve Cell Rna with Specific Synaptic Sites. Proc Natl Acad Sci U S A 53:418-425.

Bradshaw KD, Emptage NJ, Bliss TV (2003) A role for dendritic protein synthesis in hippocampal late LTP. Eur J Neurosci 18:3150-3152.

Brandt N, Franke K, Rasin MR, Baumgart J, Vogt J, Khrulev S, Hassel B, Pohl EE, Sestan N, Nitsch R, Schumacher S (2007) The neural EGF family member CALEB/NGC mediates dendritic tree and spine complexity. EMBO J 26:2371-2386.

Brewer GJ, Torricelli JR (2007) Isolation and culture of adult neurons and neurospheres. Nature Protocols 2:1490-1498.

Brittis PA, Lu Q, Flanagan JG (2002) Axonal protein synthesis provides a mechanism for localized regulation at an intermediate target. Cell 110:223-235.

Bruggemann I, Schulz S, Wiborny D, Hollt V (2000) Colocalization of the mu-opioid receptor and calcium/calmodulin-dependent kinase II in distinct pain-processing brain regions. Brain Res Mol Brain Res 85:239-250.

Brunet I, Weinl C, Piper M, Trembleau A, Volovitch M, Harris W, Prochiantz A, Holt C (2005) The transcription factor Engrailed-2 guides retinal axons. Nature 438:94-98.

Bullock SL (2011) Messengers, motors and mysteries: sorting of eukaryotic mRNAs by cytoskeletal transport. Biochemical Society transactions 39:1161-1165.

Bunge MB (1973) Fine structure of nerve fibers and growth cones of isolated sympathetic neurons in culture. J Cell Biol 56:713-735.

Burton PR (1988) Dendrites of mitral cell neurons contain microtubules of opposite polarity. Brain Res 473:107-115.

Cajigas IJ, Tushev G, Will TJ, tom Dieck S, Fuerst N, Schuman EM (2012) The local transcriptome in the synaptic neuropil revealed by deep sequencing and high-resolution imaging. Neuron 74:453-466.

Calliari A, Farias J, Puppo A, Canclini L, Mercer JA, Munroe D, Sotelo JR, Sotelo-Silveira JR (2014) Myosin Va associates with mRNA in ribonucleoprotein particles present in myelinated peripheral axons and in the central nervous system. Dev Neurobiol 74:382-396.

Campbell DS, Holt CE (2001) Chemotropic responses of retinal growth cones mediated by rapid local protein synthesis and degradation. Neuron 32:1013-1026.

Canclini L, Wallrabe H, Di Paolo A, Kun A, Calliari A, Sotelo-Silveira JR, Sotelo JR (2014) Association of Myosin Va and Schwann cells-derived RNA in mammal myelinated axons, analyzed by immunocytochemistry and confocal FRET microscopy. Methods 66:153-161.

Capano CP, Giuditta A, Castigli E, Kaplan BB (1987) Occurrence and sequence complexity of polyadenylated RNA in squid axoplasm. J Neurochem 49:698-704.

Carlton SM (2002) Localization of CaMKIIalpha in rat primary sensory neurons: increase in inflammation. Brain Res 947:252-259.

Carter LM, Starkey ML, Akrimi SF, Davies M, McMahon SB, Bradbury EJ (2008) The yellow fluorescent protein (YFP-H) mouse reveals neuroprotection as a novel mechanism underlying chondroitinase ABC-mediated repair after spinal cord injury. J Neurosci 28:14107-14120.

Casanova E, Fehsenfeld S, Mantamadiotis T, Lemberger T, Greiner E, Stewart AF, Schutz G (2001) A CamKIIalpha iCre BAC allows brain-specific gene inactivation. Genesis 31:37-42.

Chandross KJ, Cohen RI, Paras P, Jr., Gravel M, Braun PE, Hudson LD (1999) Identification and characterization of early glial progenitors using a transgenic selection strategy. J Neurosci 19:759-774.

Chen YY, McDonald D, Cheng C, Magnowski B, Durand J, Zochodne DW (2005) Axon and Schwann cell partnership during nerve regrowth. J Neuropathol Exp Neurol 64:613-622.

Cook-Snyder DR, Jones A, Reijmers LG (2015) A retrograde adeno-associated virus for collecting ribosome-bound mRNA from anatomically defined projection neurons. Front Mol Neurosci 8:56.

Cook KB, Kazan H, Zuberi K, Morris Q, Hughes TR (2011) RBPDB: a database of RNA-binding specificities. Nucleic Acids Res 39:D301-308.

Court FA, Alvarez J (2005) Local regulation of the axonal phenotype, a case of merotrophism. Biol Res 38:365-374.

Court FA, Hendriks WT, MacGillavry HD, Alvarez J, van Minnen J (2008) Schwann cell to axon transfer of ribosomes: toward a novel understanding of the role of glia in the nervous system. J Neurosci 28:11024-11029.

Court FA, Midha R, Cisterna BA, Grochmal J, Shakhbazau A, Hendriks WT, Van Minnen J (2011) Morphological evidence for a transport of ribosomes from Schwann cells to regenerating axons. Glia 59:1529-1539.

Cox LJ, Hengst U, Gurskaya NG, Lukyanov KA, Jaffrey SR (2008) Intra-axonal translation and retrograde trafficking of CREB promotes neuronal survival. Nat Cell Biol 10:149-159.

Crino P, Khodakhah K, Becker K, Ginsberg S, Hemby S, Eberwine J (1998) Presence and phosphorylation of transcription factors in developing dendrites. Proc Natl Acad Sci U S A 95:2313-2318.

D'Este E, Kamin D, Velte C, Gottfert F, Simons M, Hell SW (2016) Subcortical cytoskeleton periodicity throughout the nervous system. Scientific reports 6:22741.

Davidovic L, Jaglin XH, Lepagnol-Bestel AM, Tremblay S, Simonneau M, Bardoni B, Khandjian EW (2007) The fragile X mental retardation protein is a molecular adaptor between the neurospecific KIF3C kinesin and dendritic RNA granules. Hum Mol Genet 16:3047-3058.

Dehmelt L, Halpain S (2005) The MAP2/Tau family of microtubule-associated proteins. Genome biology 6:204.

Dictenberg JB, Swanger SA, Antar LN, Singer RH, Bassell GJ (2008) A direct role for FMRP in activity-dependent dendritic mRNA transport links filopodial-spine morphogenesis to fragile X syndrome. Dev Cell 14:926-939.

Donnelly CJ, Fainzilber M, Twiss JL (2010) Subcellular communication through RNA transport and localized protein synthesis. Traffic 11:1498-1505.

Donnelly CJ, Willis DE, Xu M, Tep C, Jiang C, Yoo S, Schanen NC, Kirn-Safran CB, van Minnen J, English A, Yoon SO, Bassell GJ, Twiss JL (2011) Limited availability of ZBP1 restricts axonal mRNA localization and nerve regeneration capacity. The EMBO Journal.

Edstrom JE, Eichner D, Edstrom A (1962) The ribonucleic acid of axons and myelin sheaths from Mauthner neurons. Biochim Biophys Acta 61:178-184.

Elvira G, Wasiak S, Blandford V, Tong XK, Serrano A, Fan X, del Rayo Sanchez-Carbente M, Servant F, Bell AW, Boismenu D, Lacaille JC, McPherson PS, DesGroseillers L, Sossin WS (2006) Characterization of an RNA granule from developing brain. Mol Cell Proteomics 5:635-651.

Eng H, Lund K, Campenot RB (1999) Synthesis of beta-tubulin, actin, and other proteins in axons of sympathetic neurons in compartmented cultures. J Neurosci 19:1-9.

Feig S, Lipton P (1993) Pairing the cholinergic agonist carbachol with patterned Schaffer collateral stimulation initiates protein synthesis in hippocampal CA1 pyramidal cell dendrites via a muscarinic, NMDA-dependent mechanism. J Neurosci 13:1010-1021.

Feng G, Mellor RH, Bernstein M, Keller-Peck C, Nguyen QT, Wallace M, Nerbonne JM, Lichtman JW, Sanes JR (2000) Imaging neuronal subsets in transgenic mice expressing multiple spectral variants of GFP. Neuron 28:41-51.

Forgue ST, Dahl JL (1978) The turnover rate of tubulin in rat brain. J Neurochem 31:1289-1297.

Frohlich D, Kuo WP, Fruhbeis C, Sun JJ, Zehendner CM, Luhmann HJ, Pinto S, Toedling J, Trotter J, Kramer-Albers EM (2014) Multifaceted effects of oligodendroglial exosomes on neurons: impact on neuronal firing rate, signal transduction and gene regulation. Philosophical transactions of the Royal Society of London Series B, Biological sciences 369.

Fromont-Racine M, Senger B, Saveanu C, Fasiolo F (2003) Ribosome assembly in eukaryotes. Gene 313:17-42.

Fruehbeis C, Froehlich D, Kuo WP, Amphornrat J, Thilemann S, Saab AS, Kirchhoff F, Mobius W, Goebbels S, Nave KA, Schneider A, Simons M, Klugmann M, Trotter J, Kraemer-Albers EM (2013) Neurotransmitter-triggered transfer of exosomes mediates oligodendrocyte-neuron communication. PLoS Biol 11:e1001604.

Fu SY, Gordon T (1997) The cellular and molecular basis of peripheral nerve regeneration. Molecular neurobiology 14:67-116.

Gallo S, Beugnet A, Biffo S (2011) Tagging of functional ribosomes in living cells by HaloTag(R) technology. In Vitro Cell Dev Biol Anim 47:132-138.

Gambetti P, Autilio-Gambetti L, Shafer B, Pfaff LD (1973) Quantitative autoradiographic study of labeled RNA in rabbit optic nerve after intraocular injection of (3H)uridine. J Cell Biol 59:677-684.

Ganat YM, Silbereis J, Cave C, Ngu H, Anderson GM, Ohkubo Y, Ment LR, Vaccarino FM (2006) Early postnatal astroglial cells produce multilineage precursors and neural stem cells in vivo. J Neurosci 26:8609-8621.

Genc B, Ulupinar E, Erzurumlu RS (2005) Differential Trk expression in explant and dissociated trigeminal ganglion cell cultures. J Neurobiol 64:145-156.

Gioio AE, Chun JT, Crispino M, Capano CP, Giuditta A, Kaplan BB (1994) Kinesin mRNA is present in the squid giant axon. J Neurochem 63:13-18.

Gioio AE, Eyman M, Zhang H, Lavina ZS, Giuditta A, Kaplan BB (2001) Local synthesis of nuclear-encoded mitochondrial proteins in the presynaptic nerve terminal. J Neurosci Res 64:447-453.

Giuditta A, Cupello A, Lazzarini G (1980) Ribosomal RNA in the axoplasm of the squid giant axon. J Neurochem 34:1757-1760.

Giuditta A, Kaplan BB, van Minnen J, Alvarez J, Koenig E (2002) Axonal and presynaptic protein synthesis: new insights into the biology of the neuron. Trends Neurosci 25:400-404.

Giuditta A, Chun JT, Eyman M, Cefaliello C, Bruno AP, Crispino M (2008) Local gene expression in axons and nerve endings: the glia-neuron unit. Physiol Rev 88:515-555.

Giuditta A, Menichini E, Perrone Capano C, Langella M, Martin R, Castigli E, Kaplan BB (1991) Active polysomes in the axoplasm of the squid giant axon. J Neurosci Res 28:18-28.

Goebbels S, Bormuth I, Bode U, Hermanson O, Schwab MH, Nave KA (2006) Genetic targeting of principal neurons in neocortex and hippocampus of NEX-Cre mice. Genesis 44:611-621.

Gomes C, Merianda TT, Lee SJ, Yoo S, Twiss JL (2014) Molecular determinants of the axonal mRNA transcriptome. Dev Neurobiol 74:218-232.

Grull F, Kirchgessner M, Kaufmann R, Hausmann M, Kebschull U (2011) Accelerating Image Analysis for Localization Microscopy with FPGAs. In: Field Programmable Logic and Applications (FPL), 2011 International Conference on, pp 1-5.

Guest J, Santamaria AJ, Benavides FD (2013) Clinical translation of autologous Schwann cell transplantation for the treatment of spinal cord injury. Current opinion in organ transplantation 18:682-689.

Gumy LF, Tan CL, Fawcett JW (2010) The role of local protein synthesis and degradation in axon regeneration. Exp Neurol 223:28-37.

Gumy LF, Katrukha EA, Kapitein LC, Hoogenraad CC (2014) New insights into mRNA trafficking in axons. Dev Neurobiol 74:233-244.

Gumy LF, Yeo GS, Tung YC, Zivraj KH, Willis D, Coppola G, Lam BY, Twiss JL, Holt CE, Fawcett JW (2011) Transcriptome analysis of embryonic and adult sensory axons reveals changes in mRNA repertoire localization. RNA 17:85-98.

Gurke S, Barroso JF, Gerdes HH (2008) The art of cellular communication: tunneling nanotubes bridge the divide. Histochem Cell Biol 129:539-550.

Halbeisen RE, Scherrer T, Gerber AP (2009) Affinity purification of ribosomes to access the translatome. Methods 48:306-310.

Hanz S, Perlson E, Willis D, Zheng JQ, Massarwa R, Huerta JJ, Koltzenburg M, Kohler M, van-Minnen J, Twiss JL, Fainzilber M (2003) Axoplasmic importins enable retrograde injury signaling in lesioned nerve. Neuron 40:1095-1104.

Hasegawa H, Abbott S, Han BX, Qi Y, Wang F (2007) Analyzing somatosensory axon projections with the sensory neuron-specific Advillin gene. J Neurosci 27:14404-14414.

Heiman M, Schaefer A, Gong S, Peterson JD, Day M, Ramsey KE, Suarez-Farinas M, Schwarz C, Stephan DA, Surmeier DJ, Greengard P, Heintz N (2008) A translational profiling approach for the molecular characterization of CNS cell types. Cell 135:738-748.

Heinen A, Kremer D, Gottle P, Kruse F, Hasse B, Lehmann H, Hartung HP, Kury P (2008) The cyclin-dependent kinase inhibitor p57kip2 is a negative regulator of Schwann cell differentiation and in vitro myelination. Proc Natl Acad Sci U S A 105:8748-8753.

Hengst U, Deglincerti A, Kim HJ, Jeon NL, Jaffrey SR (2009) Axonal elongation triggered by stimulus-induced local translation of a polarity complex protein. Nat Cell Biol 11:1024-1030.

Hillefors M, Gioio AE, Mameza MG, Kaplan BB (2007) Axon viability and mitochondrial function are dependent on local protein synthesis in sympathetic neurons. Cellular and molecular neurobiology 27:701-716.

Hirokawa N (2006) mRNA transport in dendrites: RNA granules, motors, and tracks. J Neurosci 26:7139-7142.

Hirokawa N, Niwa S, Tanaka Y (2010) Molecular motors in neurons: transport mechanisms and roles in brain function, development, and disease. Neuron 68:610-638.

Holt CE, Bullock SL (2009) Subcellular mRNA localization in animal cells and why it matters. Science 326:1212-1216.

Honkanen H, Lahti O, Nissinen M, Myllyla RM, Kangas S, Paivalainen S, Alanne MH, Peltonen S, Peltonen J, Heape AM (2007) Isolation, purification and expansion of myelination-competent, neonatal mouse Schwann cells. Eur J Neurosci 26:953-964.

Huang B, Bates M, Zhuang X (2009) Super-resolution fluorescence microscopy. Annual review of biochemistry 78:993-1016.

Huber KM, Kayser MS, Bear MF (2000) Role for rapid dendritic protein synthesis in hippocampal mGluR-dependent long-term depression. Science 288:1254-1257.

Huttelmaier S, Zenklusen D, Lederer M, Dictenberg J, Lorenz M, Meng X, Bassell GJ, Condeelis J, Singer RH (2005) Spatial regulation of beta-actin translation by Src-dependent phosphorylation of ZBP1. Nature 438:512-515.

Hyung S, Yoon Lee B, Park JC, Kim J, Hur EM, Francis Suh JK (2015) Coculture of Primary Motor Neurons and Schwann Cells as a Model for In Vitro Myelination. Scientific reports 5:15122.

Jin LQ, Pennise C, Rodemer W, Jahn K, Selzer M (2016) Protein Synthetic Machinery and mRNA in Regenerating Tips of Spinal Cord Axons in Lamprey. J Comp Neurol.

Jung H, Yoon BC, Holt CE (2012) Axonal mRNA localization and local protein synthesis in nervous system assembly, maintenance and repair. Nat Rev Neurosci 13:308-324.

Kaga Y, Shoemaker WJ, Furusho M, Bryant M, Rosenbluth J, Pfeiffer SE, Oh L, Rasband M, Lappe-Siefke C, Yu K, Ornitz DM, Nave KA, Bansal R (2006) Mice with conditional inactivation of fibroblast growth factor receptor-2 signaling in oligodendrocytes have normal myelin but display dramatic hyperactivity when combined with Cnp1 inactivation. J Neurosci 26:12339-12350.

Kalinski AL, Sachdeva R, Gomes C, Lee SJ, Shah Z, Houle JD, Twiss JL (2015) mRNAs and Protein Synthetic Machinery Localize into Regenerating Spinal Cord Axons When They Are Provided a Substrate That Supports Growth. J Neurosci 35:10357-10370.

Kanai Y, Dohmae N, Hirokawa N (2004) Kinesin transports RNA: isolation and characterization of an RNA-transporting granule. Neuron 43:513-525.

Kandel E, Schwartz J, Jessell T, Siegelbaum S, Hudspeth AJ (2012) Principles of Neural Science, 5th Edition: McGraw Hill Professional.

Kang H, Schuman EM (1996) A requirement for local protein synthesis in neurotrophin-induced hippocampal synaptic plasticity. Science 273:1402-1406.

Kapitein LC, Hoogenraad CC (2011) Which way to go? Cytoskeletal organization and polarized transport in neurons. Mol Cell Neurosci 46:9-20.

Kapitein LC, Schlager MA, Kuijpers M, Wulf PS, van Spronsen M, MacKintosh FC, Hoogenraad CC (2010) Mixed microtubules steer dynein-driven cargo transport into dendrites. Curr Biol 20:290-299.

Kaplan BB, Gioio AE, Capano CP, Crispino M, Giuditta A (1992) beta-Actin and beta-Tubulin are components of a heterogeneous mRNA population present in the squid giant axon. Mol Cell Neurosci 3:133-144.

Kislauskis EH, Zhu X, Singer RH (1994) Sequences responsible for intracellular localization of beta-actin messenger RNA also affect cell phenotype. J Cell Biol 127:441-451.

Kleiman R, Banker G, Steward O (1994) Development of subcellular mRNA compartmentation in hippocampal neurons in culture. J Neurosci 14:1130-1140.

Klinge S, Voigts-Hoffmann F, Leibundgut M, Arpagaus S, Ban N (2011) Crystal structure of the eukaryotic 60S ribosomal subunit in complex with initiation factor 6. Science 334:941-948.

Knott AB, Perkins G, Schwarzenbacher R, Bossy-Wetzel E (2008) Mitochondrial fragmentation in neurodegeneration. Nat Rev Neurosci 9:505-518.

Knowles RB, Sabry JH, Martone ME, Deerinck TJ, Ellisman MH, Bassell GJ, Kosik KS (1996) Translocation of RNA granules in living neurons. J Neurosci 16:7812-7820.

Koenig E (1965) Synthetic mechanisms in the axon. II. Rna in myelin-free axons of the cat. J Neurochem 12:357-361.

Koenig E (1979) Ribosomal RNA in Mauthner axon: implications for a protein synthesizing machinery in the myelinated axon. Brain Res 174:95-107.

Koenig E (1991) Evaluation of local synthesis of axonal proteins in the goldfish Mauthner cell axon and axons of dorsal and ventral roots of the rat in vitro. Mol Cell Neurosci 2:384-394.

Koenig E, Adams P (1982) Local protein synthesizing activity in axonal fields regenerating in vitro. J Neurochem 39:386-400.

Koenig E, Martin R (1996) Cortical plaque-like structures identify ribosome-containing domains in the Mauthner cell axon. J Neurosci 16:1400-1411.

Koenig E, Giuditta A (1999) Protein-synthesizing machinery in the axon compartment. Neuroscience 89:5-15.

Koenig E, Martin R, Titmus M, Sotelo-Silveira JR (2000) Cryptic peripheral ribosomal domains distributed intermittently along mammalian myelinated axons. J Neurosci 20:8390-8400.

Kramer-Albers EM, Bretz N, Tenzer S, Winterstein C, Mobius W, Berger H, Nave KA, Schild H, Trotter J (2007) Oligodendrocytes secrete exosomes containing major myelin and stress-protective proteins: Trophic support for axons? Proteomics Clinical applications 1:1446-1461.

Kressler D, Hurt E, Bassler J (2010) Driving ribosome assembly. Biochim Biophys Acta 1803:673-683.

Krichevsky AM, Kosik KS (2001) Neuronal RNA granules: a link between RNA localization and stimulation-dependent translation. Neuron 32:683-696.

Kun A, Otero L, Sotelo-Silveira JR, Sotelo JR (2007) Ribosomal distributions in axons of mammalian myelinated fibers. J Neurosci Res 85:2087-2098.

Kundel M, Jones KJ, Shin CY, Wells DG (2009) Cytoplasmic polyadenylation element-binding protein regulates neurotrophin-3-dependent beta-catenin mRNA translation in developing hippocampal neurons. J Neurosci 29:13630-13639.

Lappe-Siefke C, Goebbels S, Gravel M, Nicksch E, Lee J, Braun PE, Griffiths IR, Nave KA (2003) Disruption of Cnp1 uncouples oligodendroglial functions in axonal support and myelination. Nature genetics 33:366-374.

Lasek RJ, Garner JA, Brady ST (1984) Axonal transport of the cytoplasmic matrix. J Cell Biol 99:212s-221s.

Le Douarin NM, Kalcheim C (1999) The Neural Crest, 2nd Edition. New York: Cambridge University Press.

Leung KM, van Horck FP, Lin AC, Allison R, Standart N, Holt CE (2006) Asymmetrical beta-actin mRNA translation in growth cones mediates attractive turning to netrin-1. Nat Neurosci 9:1247-1256.

Li YC, Li YN, Cheng CX, Sakamoto H, Kawate T, Shimada O, Atsumi S (2005) Subsurface cisterna-lined axonal invaginations and double-walled vesicles at the axonal-myelin sheath interface. Neuroscience research 53:298-303.

Lindstrom MS (2009) Emerging functions of ribosomal proteins in gene-specific transcription and translation. Biochem Biophys Res Commun 379:167-170.

Liu Y, Shi J, Lu CC, Wang ZB, Lyuksyutova AI, Song XJ, Zou Y (2005) Ryk-mediated Wnt repulsion regulates posterior-directed growth of corticospinal tract. Nat Neurosci 8:1151-1159.

Lopez-Leal R, Court FA (2016) Schwann Cell Exosomes Mediate Neuron-Glia Communication and Enhance Axonal Regeneration. Cellular and molecular neurobiology.

Lopez-Verrilli MA, Picou F, Court FA (2013) Schwann cell-derived exosomes enhance axonal regeneration in the peripheral nervous system. Glia 61:1795-1806.

Love JM, Shah SB (2015) Ribosomal trafficking is reduced in Schwann cells following induction of myelination. Front Cell Neurosci 9:306.

Lu R, Schmidtko A (2013) Direct intrathecal drug delivery in mice for detecting in vivo effects of cGMP on pain processing. Methods Mol Biol 1020:215-221.

Ma TC, Willis DE (2015) What makes a RAG regeneration associated? Front Mol Neurosci 8:43.

Mallardo M, Deitinghoff A, Muller J, Goetze B, Macchi P, Peters C, Kiebler MA (2003) Isolation and characterization of Staufen-containing ribonucleoprotein particles from rat brain. Proc Natl Acad Sci U S A 100:2100-2105.

Maro GS, Vermeren M, Voiculescu O, Melton L, Cohen J, Charnay P, Topilko P (2004) Neural crest boundary cap cells constitute a source of neuronal and glial cells of the PNS. Nat Neurosci 7:930-938.

Martin KC, Zukin RS (2006) RNA trafficking and local protein synthesis in dendrites: an overview. J Neurosci 26:7131-7134.

Martin R, Fritz W, Giuditta A (1989) Visualization of polyribosomes in the postsynaptic area of the squid giant synapse by electron spectroscopic imaging. J Neurocytol 18:11-18.

Mason MRJ, Ehlert EME, Eggers R, Pool CW, Hermening S, Huseinovic A, Timmermans E, Blits B, Verhaagen J (2010) Comparison of AAV Serotypes for Gene Delivery to Dorsal Root Ganglion Neurons. Molecular Therapy 18:715-724.

McClure C, Cole KL, Wulff P, Klugmann M, Murray AJ (2011) Production and titering of recombinant adeno-associated viral vectors. J Vis Exp:e3348.

Merianda TT, Lin AC, Lam JS, Vuppalanchi D, Willis DE, Karin N, Holt CE, Twiss JL (2009) A functional equivalent of endoplasmic reticulum and Golgi in axons for secretion of locally synthesized proteins. Mol Cell Neurosci 40:128-142.

Meyer M, de Angelis MH, Wurst W, Kuhn R (2010) Gene targeting by homologous recombination in mouse zygotes mediated by zinc-finger nucleases. Proc Natl Acad Sci U S A 107:15022-15026.

Michaelevski I, Segal-Ruder Y, Rozenbaum M, Medzihradszky KF, Shalem O, Coppola G, Horn-Saban S, Ben-Yaakov K, Dagan SY, Rishal I, Geschwind DH, Pilpel Y, Burlingame AL, Fainzilber M (2010) Signaling to transcription networks in the neuronal retrograde injury response. Sci Signal 3:ra53.

Michalski JP, Anderson C, Beauvais A, De Repentigny Y, Kothary R (2011) The proteolipid protein promoter drives expression outside of the oligodendrocyte lineage during embryonic and early postnatal development. PLoS One 6:e19772.

Minett MS, Nassar MA, Clark AK, Passmore G, Dickenson AH, Wang F, Malcangio M, Wood JN (2012) Distinct Nav1.7-dependent pain sensations require different sets of sensory and sympathetic neurons. Nat Commun 3:791.

Morfini GA, Burns MR, Stenoien DL, Brady ST (2012) Chapter 8 - Axonal Transport. In: Basic Neurochemistry (Eighth Edition) (Price STBJSWAL, ed), pp 146-164. New York: Academic Press.

Muslimov IA, Titmus M, Koenig E, Tiedge H (2002) Transport of Neuronal BC1 RNA in Mauthner Axons. J Neurosci 22:4293-4301.

Nalavadi VC, Griffin LE, Picard-Fraser P, Swanson AM, Takumi T, Bassell GJ (2012) Regulation of zipcode binding protein 1 transport dynamics in axons by myosin Va. J Neurosci 32:15133-15141.

Nave KA, Trapp BD (2008) Axon-glial signaling and the glial support of axon function. Annu Rev Neurosci 31:535-561.

Niquille M, Garel S, Mann F, Hornung JP, Otsmane B, Chevalley S, Parras C, Guillemot F, Gaspar P, Yanagawa Y, Lebrand C (2009) Transient neuronal populations are required to guide callosal axons: a role for semaphorin 3C. PLoS Biol 7:e1000230.

Ohara R, Fujita Y, Hata K, Nakagawa M, Yamashita T (2011) Axotomy induces axonogenesis in hippocampal neurons through STAT3. Cell death & disease 2:e175.

Ohashi S, Koike K, Omori A, Ichinose S, Ohara S, Kobayashi S, Sato TA, Anzai K (2002) Identification of mRNA/protein (mRNP) complexes containing Puralpha, mStaufen, fragile X protein, and myosin Va and their association with rough endoplasmic reticulum equipped with a kinesin motor. J Biol Chem 277:37804-37810.

Olink-Coux M, Hollenbeck PJ (1996) Localization and active transport of mRNA in axons of sympathetic neurons in culture. J Neurosci 16:1346-1358.

Ostroff LE, Fiala JC, Allwardt B, Harris KM (2002) Polyribosomes redistribute from dendritic shafts into spines with enlarged synapses during LTP in developing rat hippocampal slices. Neuron 35:535-545.

Pegtel DM, Cosmopoulos K, Thorley-Lawson DA, van Eijndhoven MA, Hopmans ES, Lindenberg JL, de Gruijl TD, Wurdinger T, Middeldorp JM (2010) Functional delivery of viral miRNAs via exosomes. Proc Natl Acad Sci U S A 107:6328-6333.

Perlson E, Hanz S, Ben-Yaakov K, Segal-Ruder Y, Seger R, Fainzilber M (2005) Vimentin-dependent spatial translocation of an activated MAP kinase in injured nerve. Neuron 45:715-726.

Peters A, Proskauer CC, Kaiserman-Abramof IR (1968) The small pyramidal neuron of the rat cerebral cortex. The axon hillock and initial segment. J Cell Biol 39:604-619.

Pettitt SJ, Liang Q, Rairdan XY, Moran JL, Prosser HM, Beier DR, Lloyd KC, Bradley A, Skarnes WC (2009) Agouti C57BL/6N embryonic stem cells for mouse genetic resources. Nat Methods 6:493-495.

Pielage J, Cheng L, Fetter RD, Carlton PM, Sedat JW, Davis GW (2008) A presynaptic giant ankyrin stabilizes the NMJ through regulation of presynaptic microtubules and transsynaptic cell adhesion. Neuron 58:195-209.

Piper M, Anderson R, Dwivedy A, Weinl C, van Horck F, Leung KM, Cogill E, Holt C (2006) Signaling mechanisms underlying Slit2-induced collapse of Xenopus retinal growth cones. Neuron 49:215-228.

Poon MM, Choi SH, Jamieson CA, Geschwind DH, Martin KC (2006) Identification of process-localized mRNAs from cultured rodent hippocampal neurons. J Neurosci 26:13390-13399.

Purves D, Augustine GJ, Fitzpatrick D, Hall WC, LaMantia AS, White LE (2012) Neuroscience, 5th Edition: Sinauer Associates, Inc.

Rapallino MV, Cupello A, Giuditta A (1988) Axoplasmic RNA species synthesized in the isolated squid giant axon. Neurochem Res 13:625-631.

Rishal I, Fainzilber M (2010) Retrograde signaling in axonal regeneration. Exp Neurol 223:5-10.

Rishal I, Fainzilber M (2014) Axon-soma communication in neuronal injury. Nat Rev Neurosci 15:32-42.

Rossoll W, Jablonka S, Andreassi C, Kroning AK, Karle K, Monani UR, Sendtner M (2003) Smn, the spinal muscular atrophy-determining gene product, modulates axon growth and localization of beta-actin mRNA in growth cones of motoneurons. J Cell Biol 163:801-812.

Rustom A, Saffrich R, Markovic I, Walther P, Gerdes HH (2004) Nanotubular highways for intercellular organelle transport. Science 303:1007-1010.

Sanz E, Yang L, Su T, Morris DR, McKnight GS, Amieux PS (2009) Cell-type-specific isolation of ribosome-associated mRNA from complex tissues. Proceedings of the National Academy of Sciences 106:13939-13944.

Shakhbazau A, Mohanty C, Kumar R, Midha R (2014) Sensory recovery after cell therapy in peripheral nerve repair: effects of naive and skin precursor-derived Schwann cells. Journal of neurosurgery 121:423-431.

Shakhbazau A, Schenk GJ, Hay C, Kawasoe J, Klaver R, Yong VW, Geurts JJ, van Minnen J (2016) Demyelination induces transport of ribosome-containing vesicles from glia to axons: evidence from animal models and MS patient brains. Molecular biology reports.

Shaner NC, Campbell RE, Steinbach PA, Giepmans BN, Palmer AE, Tsien RY (2004) Improved monomeric red, orange and yellow fluorescent proteins derived from Discosoma sp. red fluorescent protein. Nat Biotechnol 22:1567-1572.

Simons M, Raposo G (2009) Exosomes--vesicular carriers for intercellular communication. Curr Opin Cell Biol 21:575-581.

Singer M, Green MR (1968) Autoradiographic studies of uridine incorporation in peripheral nerve of the newt, Triturus. Journal of morphology 124:321-344.

Skog J, Wurdinger T, van Rijn S, Meijer DH, Gainche L, Sena-Esteves M, Curry WT, Jr., Carter BS, Krichevsky AM, Breakefield XO (2008) Glioblastoma microvesicles transport RNA and proteins that promote tumour growth and provide diagnostic biomarkers. Nat Cell Biol 10:1470-1476.

Smith CL, Afroz R, Bassell GJ, Furneaux HM, Perrone-Bizzozero NI, Burry RW (2004) GAP-43 mRNA in growth cones is associated with HuD and ribosomes. J Neurobiol 61:222-235.

Song AH, Wang D, Chen G, Li Y, Luo J, Duan S, Poo MM (2009) A selective filter for cytoplasmic transport at the axon initial segment. Cell 136:1148-1160.

Sossin WS, DesGroseillers L (2006) Intracellular trafficking of RNA in neurons. Traffic 7:1581-1589.

Sotelo-Silveira J, Crispino M, Puppo A, Sotelo JR, Koenig E (2008) Myelinated axons contain beta-actin mRNA and ZBP-1 in periaxoplasmic ribosomal plaques and depend on cyclic AMP and F-actin integrity for in vitro translation. J Neurochem 104:545-557.

Sotelo-Silveira JR, Calliari A, Cardenas M, Koenig E, Sotelo JR (2004) Myosin Va and kinesin II motor proteins are concentrated in ribosomal domains (periaxoplasmic ribosomal plaques) of myelinated axons. J Neurobiol 60:187-196.

Sotelo-Silveira JR, Calliari A, Kun A, Koenig E, Sotelo JR (2006) RNA trafficking in axons. Traffic 7:508-515.

Sotelo-Silveira JR, Calliari A, Kun A, Benech JC, Sanguinetti C, Chalar C, Sotelo JR (2000) Neurofilament mRNAs are present and translated in the normal and severed sciatic nerve. J Neurosci Res 62:65-74.

Sotelo JR, Canclini L, Kun A, Sotelo-Silveira JR, Xu L, Wallrabe H, Calliari A, Rosso G, Cal K, Mercer JA (2013) Myosin-Va-dependent cell-to-cell transfer of RNA from Schwann cells to axons. PLoS One 8:e61905.

Sotelo JR, Canclini L, Kun A, Sotelo-Silveira JR, Calliari A, Cal K, Bresque M, Dipaolo A, Farias J, Mercer JA (2014) Glia to axon RNA transfer. Dev Neurobiol 74:292-302.

Spillane M, Ketschek A, Merianda TT, Twiss JL, Gallo G (2013) Mitochondria Coordinate Sites of Axon Branching through Localized Intra-axonal Protein Synthesis. Cell Rep 5:1564-1575.

Spillane M, Ketschek A, Donnelly CJ, Pacheco A, Twiss JL, Gallo G (2012) Nerve growth factor-induced formation of axonal filopodia and collateral branches involves the intra-axonal synthesis of regulators of the actin-nucleating arp2/3 complex. J Neurosci 32:17671-17689.

Sprinkle TJ (1989) 2',3'-cyclic nucleotide 3'-phosphodiesterase, an oligodendrocyte-Schwann cell and myelin-associated enzyme of the nervous system. Critical reviews in neurobiology 4:235-301.

Steward O, Levy WB (1982) Preferential localization of polyribosomes under the base of dendritic spines in granule cells of the dentate gyrus. J Neurosci 2:284-291.

Steward O, Ribak CE (1986) Polyribosomes associated with synaptic specializations on axon initial segments: localization of protein-synthetic machinery at inhibitory synapses. J Neurosci 6:3079-3085.

Steward O, Reeves TM (1988) Protein-synthetic machinery beneath postsynaptic sites on CNS neurons: association between polyribosomes and other organelles at the synaptic site. J Neurosci 8:176-184.

Steward O, Schuman EM (2001) Protein synthesis at synaptic sites on dendrites. Annu Rev Neurosci 24:299-325.

Steward O, Falk PM, Torre ER (1996) Ultrastructural basis for gene expression at the synapse: synapse-associated polyribosome complexes. J Neurocytol 25:717-734.

Steward O, Wallace CS, Lyford GL, Worley PF (1998) Synaptic activation causes the mRNA for the IEG Arc to localize selectively near activated postsynaptic sites on dendrites. Neuron 21:741-751.

Szczurek AT, Prakash K, Lee HK, Zurek-Biesiada DJ, Best G, Hagmann M, Dobrucki JW, Cremer C, Birk U (2014) Single molecule localization microscopy of the distribution of chromatin using Hoechst and DAPI fluorescent probes. Nucleus 5:331-340.

Tahirovic S, Bradke F (2009) Neuronal polarity. Cold Spring Harb Perspect Biol 1:a001644.

Taylor AM, Wu J, Tai HC, Schuman EM (2013) Axonal translation of beta-catenin regulates synaptic vesicle dynamics. J Neurosci 33:5584-5589.

Taylor AM, Berchtold NC, Perreau VM, Tu CH, Li Jeon N, Cotman CW (2009) Axonal mRNA in uninjured and regenerating cortical mammalian axons. J Neurosci 29:4697-4707.

Tcherkezian J, Brittis PA, Thomas F, Roux PP, Flanagan JG (2010) Transmembrane receptor DCC associates with protein synthesis machinery and regulates translation. Cell 141:632-644.

Tennyson VM (1970) The fine structure of the axon and growth cone of the dorsal root neuroblast of the rabbit embryo. J Cell Biol 44:62-79.

Thomson E, Ferreira-Cerca S, Hurt E (2013) Eukaryotic ribosome biogenesis at a glance. J Cell Sci 126:4815-4821.

Tiedge H, Brosius J (1996) Translational machinery in dendrites of hippocampal neurons in culture. J Neurosci 16:7171-7181.

Tiruchinapalli DM, Oleynikov Y, Kelic S, Shenoy SM, Hartley A, Stanton PK, Singer RH, Bassell GJ (2003) Activity-dependent trafficking and dynamic localization of zipcode binding protein 1 and beta-actin mRNA in dendrites and spines of hippocampal neurons. J Neurosci 23:3251-3261.

Toma JS, McPhail LT, Ramer MS (2007) Differential RIP antigen (CNPase) expression in peripheral ensheathing glia. Brain Res 1137:1-10.

Tschochner H, Hurt E (2003) Pre-ribosomes on the road from the nucleolus to the cytoplasm. Trends Cell Biol 13:255-263.

Valadi H, Ekstrom K, Bossios A, Sjostrand M, Lee JJ, Lotvall JO (2007) Exosome-mediated transfer of mRNAs and microRNAs is a novel mechanism of genetic exchange between cells. Nat Cell Biol 9:654-659.

Verheijen MH, Lammens M, Ceuterick-de Groote C, Timmerman V, De Jonghe P, King RH, Smit AB, van Minnen J (2011) Increased axonal ribosome numbers in CMT diseases. Journal of the peripheral nervous system : JPNS 16:71-73.

Verheijen MH, Peviani M, Hendricusdottir R, Bell EM, Lammens M, Smit AB, Bendotti C, van Minnen J (2014) Increased axonal ribosome numbers is an early event in the pathogenesis of amyotrophic lateral sclerosis. PLoS One 9:e87255.

Verma P, Chierzi S, Codd AM, Campbell DS, Meyer RL, Holt CE, Fawcett JW (2005) Axonal protein synthesis and degradation are necessary for efficient growth cone regeneration. J Neurosci 25:331-342.

Viader A, Golden JP, Baloh RH, Schmidt RE, Hunter DA, Milbrandt J (2011) Schwann cell mitochondrial metabolism supports long-term axonal survival and peripheral nerve function. J Neurosci 31:10128-10140.

Vogel US, Thompson RJ (1988) Molecular structure, localization, and possible functions of the myelin-associated enzyme 2',3'-cyclic nucleotide 3'-phosphodiesterase. J Neurochem 50:1667-1677.

Vogelaar CF, Fawcett JW (2008) Axonal mRNA in regeneration. In: Neural Degeneration and Repair (Müller HW, ed), pp 135–151. Weinheim: WILEY-VCH Verlag GmbH & Co. KGaA.

Vogelaar CF, Vrinten DH, Hoekman MF, Brakkee JH, Burbach JP, Hamers FP (2004) Sciatic nerve regeneration in mice and rats: recovery of sensory innervation is followed by a slowly retreating neuropathic pain-like syndrome. Brain Res 1027:67-72.

Vogelaar CF, Gervasi NM, Gumy LF, Story DJ, Raha-Chowdhury R, Leung K-M, Holt CE, Fawcett JW (2009) Axonal mRNAs: Characterisation and role in the growth and regeneration of dorsal root ganglion axons and growth cones. Molecular and Cellular Neuroscience 42:102-115.

Vogelaar CF, Konig B, Krafft S, Estrada V, Brazda N, Ziegler B, Faissner A, Muller HW (2015) Pharmacological Suppression of CNS Scarring by Deferoxamine Reduces Lesion Volume and Increases Regeneration in an In Vitro Model for Astroglial-Fibrotic Scarring and in Rat Spinal Cord Injury In Vivo. PLoS One 10:e0134371.

Vulchanova L, Schuster DJ, Belur LR, Riedl MS, Podetz-Pedersen KM, Kitto KF, Wilcox GL, McIvor RS, Fairbanks CA (2010) Differential adeno-associated virus mediated gene transfer to sensory neurons following intrathecal delivery by direct lumbar puncture. Mol Pain 6:31.

Walker BA, Hengst U, Kim HJ, Jeon NL, Schmidt EF, Heintz N, Milner TA, Jaffrey SR (2012) Reprogramming axonal behavior by axon-specific viral transduction. Gene Therapy.

Wang W, van Niekerk E, Willis DE, Twiss JL (2007) RNA transport and localized protein synthesis in neurological disorders and neural repair. Dev Neurobiol 67:1166-1182.

Wang X, Gerdes HH (2015) Transfer of mitochondria via tunneling nanotubes rescues apoptotic PC12 cells. Cell death and differentiation 22:1181-1191.

Wang Y, Cui J, Sun X, Zhang Y (2011) Tunneling-nanotube development in astrocytes depends on p53 activation. Cell death and differentiation 18:732-742.

Warner JR, McIntosh KB (2009) How common are extraribosomal functions of ribosomal proteins? Mol Cell 34:3-11.

Willis D, Li KW, Zheng JQ, Chang JH, Smit A, Kelly T, Merianda TT, Sylvester J, van Minnen J, Twiss JL (2005) Differential transport and local translation of cytoskeletal, injury-response, and neurodegeneration protein mRNAs in axons. J Neurosci 25:778-791.

Willis DE, Twiss JL (2006) The evolving roles of axonally synthesized proteins in regeneration. Curr Opin Neurobiol 16:111-118.

Willis DE, van Niekerk EA, Sasaki Y, Mesngon M, Merianda TT, Williams GG, Kendall M, Smith DS, Bassell GJ, Twiss JL (2007) Extracellular stimuli specifically regulate localized levels of individual neuronal mRNAs. J Cell Biol 178:965-980.

Willis DE, Xu M, Donnelly CJ, Tep C, Kendall M, Erenstheyn M, English AW, Schanen NC, Kirn-Safran CB, Yoon SO, Bassell GJ, Twiss JL (2011) Axonal Localization of transgene mRNA in mature PNS and CNS neurons. J Neurosci 31:14481-14487.

Wizenmann A, Brunet I, Lam JSY, Sonnier L, Beurdeley M, Zarbalis K, Weisenhorn-Vogt D, Weinl C, Dwivedy A, Joliot A, Wurst W, Holt C, Prochiantz A (2009) Extracellular Engrailed Participates in the Topographic Guidance of Retinal Axons In Vivo. Neuron 64:355-366.

Wool IG (1996) Extraribosomal functions of ribosomal proteins. Trends Biochem Sci 21:164-165.

Wu KY, Hengst U, Cox LJ, Macosko EZ, Jeromin A, Urquhart ER, Jaffrey SR (2005) Local translation of RhoA regulates growth cone collapse. Nature 436:1020-1024.

Xing L, Bassell GJ (2013) mRNA localization: an orchestration of assembly, traffic and synthesis. Traffic 14:2-14.

Xu K, Zhong G, Zhuang X (2013) Actin, spectrin, and associated proteins form a periodic cytoskeletal structure in axons. Science 339:452-456.

Yamada KM, Spooner BS, Wessells NK (1971) Ultrastructure and function of growth cones and axons of cultured nerve cells. J Cell Biol 49:614-635.

Yao J, Sasaki Y, Wen Z, Bassell GJ, Zheng JQ (2006) An essential role for beta-actin mRNA localization and translation in Ca2+-dependent growth cone guidance. Nat Neurosci 9:1265-1273.

Yoo S, van Niekerk EA, Merianda TT, Twiss JL (2010) Dynamics of axonal mRNA transport and implications for peripheral nerve regeneration. Exp Neurol 223:19-27.

Yoo S, Kim HH, Kim P, Donnelly CJ, Kalinski AL, Vuppalanchi D, Park M, Lee SJ, Merianda TT, Perrone-Bizzozero NI, Twiss JL (2013) A HuD-ZBP1 ribonucleoprotein complex localizes GAP-43 mRNA into axons through its 3' untranslated region AU-rich regulatory element. J Neurochem 126:792-804.

Yoon BC, Jung H, Dwivedy A, O'Hare CM, Zivraj KH, Holt CE (2012) Local translation of extranuclear lamin B promotes axon maintenance. Cell 148:752-764.

Yuan X, Chittajallu R, Belachew S, Anderson S, McBain CJ, Gallo V (2002) Expression of the green fluorescent protein in the oligodendrocyte lineage: a transgenic mouse for developmental and physiological studies. J Neurosci Res 70:529-545.

Zelena J (1970) Ribosome-like particles in myelinated axons of the rat. Brain Res 24:359-363.

Zhang HL, Singer RH, Bassell GJ (1999) Neurotrophin regulation of beta-actin mRNA and protein localization within growth cones. J Cell Biol 147:59-70.

Zhang HL, Eom T, Oleynikov Y, Shenoy SM, Liebelt DA, Dictenberg JB, Singer RH, Bassell GJ (2001) Neurotrophin-induced transport of a beta-actin mRNP complex increases beta-actin levels and stimulates growth cone motility. Neuron 31:261-275.

Zheng JQ, Kelly TK, Chang B, Ryazantsev S, Rajasekaran AK, Martin KC, Twiss JL (2001) A functional role for intra-axonal protein synthesis during axonal regeneration from adult sensory neurons. J Neurosci 21:9291-9303.

Zhong J, Zhang T, Bloch LM (2006) Dendritic mRNAs encode diversified functionalities in hippocampal pyramidal neurons. BMC Neurosci 7:17.

Zhou P, Zhang Y, Ma Q, Gu F, Day DS, He A, Zhou B, Li J, Stevens SM, Romo D, Pu WT (2013) Interrogating translational efficiency and lineage-specific transcriptomes using ribosome affinity purification. Proc Natl Acad Sci U S A 110:15395-15400.

Zhu D, Tan KS, Zhang X, Sun AY, Sun GY, Lee JC (2005) Hydrogen peroxide alters membrane and cytoskeleton properties and increases intercellular connections in astrocytes. J Cell Sci 118:3695-3703.

Zivraj KH, Tung YC, Piper M, Gumy L, Fawcett JW, Yeo GS, Holt CE (2010) Subcellular profiling reveals distinct and developmentally regulated repertoire of growth cone mRNAs. J Neurosci 30:15464-15478.

Zurborg S, Piszczek A, Martinez C, Hublitz P, Al Banchaabouchi M, Moreira P, Perlas E, Heppenstall PA (2011) Generation and characterization of an Advillin-Cre driver mouse line. Mol Pain 7:66.

Acknowledgments

For data protection reasons the acknowledgements are not included in the online version.

Curriculum vitae

For data protection reasons the curriculum vitae is not included in the online version.

Parts of this PhD thesis will be published in upcoming papers.

Publications

Müller K, Schnatz A, van Minnen J, Vogelaar CF (in prep.) *The origin of axonal ribosomes.*